

Universiteit
Leiden
The Netherlands

Mapping the maze: advancing atrial fibrillation models and therapies

Harlaar, N.

Citation
Harlaar, N. (2026, January 29). *Mapping the maze: advancing atrial fibrillation models and therapies*. Retrieved from https://hdl.handle.net/1887/4288215

Version:	Publisher's Version
License:	Licence agreement concerning inclusion of doctoral thesis in the Institutional Repository of the University of Leiden
Downloaded from:	https://hdl.handle.net/1887/4288215

Note: To cite this publication please use the final published version (if applicable).

Mapping the Maze

Advancing Atrial Fibrillation Models and Therapies

Niels Harlaar

Colophon

Cover: Hubble UDF (NASA/ESA) with Heart Shaped Nebula (DALL-E 2)
Interior photos, illustrations and lay-out: Niels Harlaar

The studies described in this thesis were conducted at the Department of Cardiology and the Department of Cardiothoracic Surgery of the Leiden University Medical Centre, Leiden, The Netherlands

Financial support for this thesis by Proefdiervrij and ABN AMRO is gratefully acknowledged.

© 2026 Niels Harlaar, Leiden, The Netherlands.
All rights reserved. No part of this book may be reproduced or transmitted, in any form or by any means, without prior permission of the author.

Mapping the Maze

Advancing Atrial Fibrillation Models and Therapies

Proefschrift

ter verkrijging van
de graad van doctor aan de Universiteit Leiden,
op gezag van rector magnificus prof. dr. S. de Rijcke,
volgens het besluit van het college voor promoties
te verdedigen op donderdag 29 januari 2026
klokke 16:00 uur

door

Niels Harlaar

geboren te Alkmaar
in 1995

Promotor:

Prof. dr. D.A. Pijnappels

Co-promotores:

Dr. A.A.F. de Vries

Dr. T.J. van Brakel

Leden promotiecommissie:

Prof. dr. R.J.M. Klautz

Prof. dr. M.R.M. Jongbloed

Prof. dr. L. Dekker (Catharina Ziekenhuis, Eindhoven)

Dr. H. Devalla (Amsterdam UMC, Amsterdam)

“Extraordinary claims require extraordinary evidence.”

— Carl Sagan

Thesis outline

1 General introduction and outline 8

Part One - Outcomes of thoracoscopic ablation in long-standing persistent atrial fibrillation

2 Clamping versus nonclamping thoracoscopic box ablation in long-standing persistent atrial fibrillation 24
J Thorac Cardiovasc Surg. 2020;160:399-405

3 Long-term follow-up of thoracoscopic ablation in long-standing persistent atrial fibrillation 42
Interact Cardiovasc Thorac Surg. 2022;34:990-998

Part Two - Development of clinically relevant human in vitro models of atrial fibrillation

4 Excised human atrial tissue-based models for investigating atrial electrophysiology 68

5 Conditional immortalization of human atrial myocytes for the generation of in vitro models of atrial fibrillation 88
Nat Biomed Eng. 2022;6:389-402

6 Summary, discussion and future perspectives 166
Adapted from Cardiovasc Res. 2022;118:e105-e107

Nederlandse samenvatting 184

List of publications 189

List of abbreviations 190

Contributing authors 192

Dankwoord 195

Curriculum vitae 196

Chapter 1



General introduction

General introduction

Atrial fibrillation in the clinic

Atrial fibrillation (AF) is the most common cardiac arrhythmia and an important contributor of morbidity, mortality and healthcare costs in the western world. The current prevalence of AF is estimated to be 2-4% in the adult population (1) and is expected to more than double in the coming decades as the result of population ageing (2, 3). It was recently estimated that 1 in 3 Europeans will develop AF in their lifetimes (4, 5). Individuals developing AF can (initially) remain asymptomatic, however symptoms including palpitations, dyspnoea and fatigue are common, frequently resulting in impaired quality of life (6). Additionally, the presence of AF is associated with serious complications, including a 4- to 5-fold increased risk of stroke (7, 8), increased risk of heart failure (9, 10) and 1.5- to 3.5-fold increase in all-cause mortality (5, 11, 12). Overall, it is estimated that up to 2.6% of total healthcare costs in European countries can be attributed to the management of AF and its complications (13, 14).

Presence of AF is characterised by rapid and chaotic electrical activation of the atria and is the result of a complex interaction of triggers, perpetuators and an atrial substrate (15). The most important risk factor for developing AF is age, however other factors include hypertension, heart failure, diabetes mellitus, coronary artery disease, obesity, smoking, valve disease, chronic kidney disease and more (6, 16). The pathophysiology behind the manifestation of AF remains a heavily studied topic, as the understanding of the multiform mechanisms leading to its initiation, maintenance and termination remains incomplete (17). Generally, initiation of AF is the result of rapid electrical activation that originates from the pulmonary veins, although such ectopic activity can also arise from other locations within the atria (15). This rapid electrical activation can result in the induction of re-entrant electrical activity, sustaining the arrhythmia. The stability and longevity of this re-entrant activity is in turn influenced by the severity of the atrial substrate. In clinical practise, AF is classified based on its duration, being paroxysmal when lasting <7 days, persistent when continuously present >7 days, and long-standing persistent when continuing >1 year (6). In tandem with the chronicity, the underlying mechanism driving AF generally changes, shifting from an incidental trigger-based tachyarrhythmia, to stable re-entry sustained by heavy structural and electrical remodelling of the atria (15). The progression of AF can be driven by progressive atrial remodelling due to (untreated) comorbidities, however the

presence of AF itself can also lead to remodelling in a phenomenon called "AF begets AF" (18).

The current treatment strategy for individuals with AF, based on the AF-CARE pathway, comprises a combination of stroke risk reduction, symptom management and comorbidity treatment optimalization (6). Stroke prevention in the form of anticoagulation therapy is applied in individuals with an increased risk of stroke based on additional risk factors besides AF, commonly calculated using the CHA2DS2-VA score (6, 19). This has shown to be effective in reducing thromboembolic events, however comes with an increased risk of (major) bleeding (20, 21). In addition to stroke risk reduction, pharmacological "rate control" is frequently applied to limit the ventricular rate, with the aim of preventing tachycardia-induced cardiomyopathy and to reduce symptoms. When symptoms persist, "rhythm control" can be pursued to restore and maintain sinus rhythm, typically performed in conjunction with rate control and anticoagulation therapy. Acute restoration of sinus rhythm through electrical or pharmacological cardioversion is very effective, although limited by the need for a brief hospital admission each time and it having minimal effect on preventing AF recurrences (22, 23). Antiarrhythmic drug therapy can be used to maintain sinus rhythm, however, the efficacy is limited and is associated with significant side effects (24). Electrical isolation of the pulmonary veins, which is possible through various endovascular and surgical techniques, has shown to be effective in reducing the occurrence of AF (25), and has become an important modality in the treatment of symptomatic AF. Overall, the efficacy of these rhythm control therapies is higher in paroxysmal AF and have the benefit of slowing progression in this population (26). Additionally, there is a growing body of evidence supporting early rhythm control, suggesting a lower risk of adverse cardiovascular outcomes. Unfortunately, these treatment strategies are not effective in all patients and a large portion of patients will still progress to the persistent or long-standing persistent form of AF where restoration of sinus rhythm becomes more challenging.

Ablation of symptomatic long-standing persistent atrial fibrillation

Patients who have progressed to long-standing persistent AF (LSPAF) are particularly difficult to treat due to the extensive arrhythmogenic substrate present. Where in paroxysmal AF the majority of triggers can be localised to the pulmonary veins, triggers in LSPAF are also frequently located in other parts of the left and right atrium, particularly in the left atrial posterior wall and left atrial

appendage (15). As a result, minimally invasive catheter ablation of the pulmonary veins alone has shown poor outcomes in LSPAF, resulting in around 20-24% AF freedom after a single intervention and 41-47% AF freedom after multiple (up to 5) interventions at 5-year follow-up (27, 28). Performing more extensive endocardial ablation in this population, by for instance targeting complex fractionated electrograms and/or adding linear lesions to isolate the left atrial posterior wall or left atrial appendage, has thus far not yielded improved outcomes (29). This likely results from lesion transmurality and contiguity issues associated with the current point-by-point endocardial ablation techniques and technologies applied for linear lesions (30).

Conversely, surgical ablation using the Cox-maze IV technique, widely considered the gold standard for AF ablation, has shown to be effective in the LSPAF population with rates of AF freedom as high as 67% at 7-year follow-up (31). This technique, introduced in its current form in 2002, comprises an extensive set of lesions in the left and right atrium, including amputation of the left atrial appendage. The aim of this lesion set is prohibiting AF to establish and perpetuate, while allowing impulses from the sinus node to reach the atrioventricular node (32). The advantages of this surgical approach include better access to both the endo- and epicardial side of the atrial myocardium, elimination of the blood cooling effect and use of linear ablation tools and clamps, all aiding better lesion transmurality and contiguity. Despite the high efficacy, the applicability of the stand-alone Cox-maze IV is severely limited by its invasiveness, required expertise and need for cardiopulmonary bypass. As a result, the Cox-maze IV has a more prominent place as a concomitant procedure during cardiac surgery of patients with AF (33).

For stand-alone surgical ablation to serve as an alternative to catheter ablation in LSPAF, minimal invasiveness, ease of performing the procedure and high efficacy are important. With the advent of thoracoscopic surgery techniques, minimally invasive thoracoscopic ablation on the beating heart has become commonplace over the past decade. This has resulted in a wide array of minimally invasive thoracoscopic ablation devices and techniques applied in clinical practice to treat AF. The efficacy of these thoracoscopic ablation procedures, however, has (thus far) mostly been studied in patients with paroxysmal and early-persistent AF and not in the more difficult to treat LSPAF patients. As a result, literature on thoracoscopic ablation efficacy in LSPAF is sparse and has mostly been limited to short- to medium-term follow-up studies (34-36). In addition to the variability in devices and techniques in these studies, the modality of rhythm follow-up differs frequently, ranging from

incidental electrocardiography up to continuous rhythm analysis through implantable loop recorders. To provide more clarity on the applicability of thoracoscopic ablation as alternative to catheter ablation in LSPAF patients, more (preferably long-term) comparative data is needed on the different ablation techniques and rhythm follow-up strategies.

Preclinical research and models of atrial fibrillation

On the other side of the spectrum, development of novel therapeutics effectively targeting the underlying pathophysiology of AF has been arduous. In the last decade, no new antiarrhythmic drugs have been approved, and only a few compounds are currently in the pipeline (37, 38). One of the factors limiting preclinical safety and efficacy studies has been the lack of sufficient numbers of well-differentiated human atrial cardiomyocytes. Together with the (associated) absence of clinically relevant human-based in vitro models of AF, preclinical research into AF mechanisms and novel therapeutic strategies has been mainly limited to animal studies. Given the principal differences in (patho)physiology between humans and animals, these new therapeutics frequently fail due to limited efficacy or strong adverse effects in patients (39).

Replacing the animal-derived cells in the *in vitro* models of AF with human cells, aiming to increase the translational value, has been difficult. Despite good accessibility of the human heart during routine cardiac surgery, (atrial) cardiomyocytes isolated from surgical waste material rapidly dedifferentiate in culture and vary in terms of quality (40). Attempts to prolong the lifespan of these cells by saving the extracellular matrix and culturing cardiac tissue slices are promising (41), although still only applied on small scale, given that they are most commonly derived from scarcely available explanted human hearts.

Since the early 2010s, an alternative source of human atrial cardiomyocytes is provided by human pluripotent stem cells (hPSCs), where the development of differentiation protocols utilizing retinoic acid have allowed the creation of cardiomyocytes with atrial features (42, 43). However, in spite of certain attractive features and unique applications in personalized disease modelling, current hPSC-derived atrial cardiomyocytes (hPSC-AMs) are associated with laborious workflows, high phenotypic variation, and overall immaturity. Attempts to create in vitro models of human AF using hPSC-AMs have been reported (44, 45), however they were unable to represent the rapid activation frequencies of 6-8 Hz (46-48) seen during human AF.

The creation of permanent cardiac cell lines from primary material to create a standardised and unlimited source of cardiomyocytes has been pursued on several occasions. Currently, three cell lines are commercially available and frequently cited in literature (49). These include the H9c2 cell line, generated in 1976 through selective serial passage of embryonic BDIX rat heart tissue (50). These cells have a myoblast origin and display properties of both skeletal muscle and, to some extent, cardiac muscle (51). Two decades later, the HL-1 cell line was established (52), originating from adult mice where the expression of simian virus 40 large T antigen (SV40-LT) was targeted to atrial cardiomyocytes via the atrial natriuretic factor promoter. Later, the AC16 line was generated through the fusion of primary human ventricular cardiomyocytes with SV40-transformed human fibroblasts (53). Despite their widespread use and popularity in literature, these three cell lines show limited resemblance to mature cardiac cells (49), likely due to the fact that continuing proliferation inhibits differentiation in most cell types (54). To address this limitation, efforts to generate conditionally immortalized cardiomyocyte cell lines that can switch between proliferative and differentiated phenotypes have been undertaken (55-59). Among these conditionally immortalized lines, the iAM-1 line (59) demonstrated the most effective transition between a proliferative state and a differentiated phenotype. This cell line, functioning through doxycycline-induced expression of SV40-LT in neonatal rat atrial cardiomyocytes, could even be applied to model atrial arrhythmias in vitro. Although the aforementioned lines are of great value in reducing the need for animals in cardiovascular research, their differences with respect to human (patho)physiology remain significant, reducing their clinical relevance as previously mentioned. Successfully applying this technology to human atrial cardiomyocytes could lead to more accurate models for human heart diseases and reduce reliance on animal testing, ultimately accelerating the development of effective therapies, not just for atrial fibrillation, but for cardiovascular conditions in general.

Aims and outline of this thesis

Part One. Outcomes of thoracoscopic ablation in long-standing persistent atrial fibrillation

The first part of this thesis, is aimed at investigating the efficacy of thoracoscopic ablation in the LSPAF population as an intermediate option between minimally invasive (but limited efficacious) catheter ablation and highly effective (but highly invasive) surgical ablation. In chapter 2, the efficacy of the two most common ablation tools used for isolating the posterior left atrium during thoracoscopic ablation are compared on perioperative performance and short-term follow-up. In chapter 3, the long-term efficacy of thoracoscopic ablation in LSPAF is studied, including the role of catheter ablation in patients with recurrences. Also, recurrence rates characterized by incidental 24h-Holter monitoring and continuous rhythm monitoring using implantable loop recorders are compared.

Part Two. Development of clinically relevant human in vitro models of atrial fibrillation

The second part of this thesis is aimed at investigating the improvement of access to well-differentiated human atrial cardiomyocytes and to develop a clinically relevant in vitro model of AF. In chapter 4, the electrophysiological properties of excised human atrial tissue are studied, and the feasibility of creating culturable atrial tissue slices is assessed. In chapter 5, the conditional immortalization of human atrial cardiomyocytes is explored, including analysis of the success rate, extensive characterisation of the phenotype of these cells and their applicability for modelling AF in vitro.

Finally, in chapter 6 the main conclusions and their implications, as well as future perspectives, are discussed.

References

1. Benjamin EJ, Muntner P, Alonso A, Bittencourt MS, Callaway CW, Carson AP, et al. Heart Disease and Stroke Statistics-2019 Update A Report From the American Heart Association. Circulation. 2019;139(10):E56-E528.

2. Colilla S, Crow A, Petkun W, Singer DE, Simon T, Liu XC. Estimates of Current and Future Incidence and Prevalence of Atrial Fibrillation in the US Adult Population. Am J Cardiol. 2013;112(8):1142-7.

3. Krijthe BP, Kunst A, Benjamin EJ, Lip GYH, Franco OH, Hofman A, et al. Projections on the number of individuals with atrial fibrillation in the European Union, from 2000 to 2060. Eur Heart J. 2013;34(35):2746-51.

4. Staerk L, Wang BQ, Preis SR, Larson MG, Lubitz SA, Ellinor PT, et al. Lifetime risk of atrial fibrillation according to optimal, borderline, or elevated levels of risk factors: cohort study based on longitudinal data from the Framingham Heart Study. Bmj-Brit Med J. 2018;361.

5. Magnussen C, Niiranen TJ, Ojeda FM, Gianfagna F, Blankenberg S, Njolstad I, et al. Sex Differences and Similarities in Atrial Fibrillation Epidemiology, Risk Factors, and Mortality in Community Cohorts Results From the BiomarCaRE Consortium (Biomarker for Cardiovascular Risk Assessment in Europe). Circulation. 2017;136(17):1588-+.

6. Van Gelder IC, Rienstra M, Bunting KV, Casado-Arroyo R, Caso V, Crijns HJGM et al. 2024 ESC Guidelines for the management of atrial fibrillation developed in collaboration with the European Association for Cardio-Thoracic Surgery (EACTS). Eur Heart J. 2024;45(36):3314-3414

7. Wolf PA, Dawber TR, Thomas HE, Kannel WB. Epidemiologic Assessment of Chronic Atrial-Fibrillation and Risk of Stroke - Framingham Study. Neurology. 1978;28(10):973-7.

8. Andrew NE, Thrift AG, Cadilhac DA. The Prevalence, Impact and Economic Implications of Atrial Fibrillation in Stroke: What Progress Has Been Made? Neuroepidemiology. 2013;40(4):227-39.

9. Anter E, Jessup M, Callans DJ. Atrial Fibrillation and Heart Failure Treatment Considerations for a Dual Epidemic. Circulation. 2009;119(18):2516-25.

10. Kotecha D, Piccini JP. Atrial fibrillation in heart failure: what should we do? Eur Heart J. 2015;36(46):3250-U58.

11. Andersson T, Magnuson A, Bryngelsson IL, Frobert O, Henriksson KM, Edvardsson N, et al. All-cause mortality in 272 186 patients hospitalized with incident atrial fibrillation 1995-2008: a Swedish nationwide long-term case-control study. Eur Heart J. 2013;34(14):1061-7.

12. Benjamin EJ, Wolf PA, D'Agostino RB, Silbershatz H, Kannel WB, Levy D. Impact of atrial fibrillation on the risk of death. Circulation. 1998;98(10):946-52.

13. Ringborg A, Nieuwlaat R, Lindgren P, Jonsson B, Fidan D, Maggioni AP, et al. Costs of atrial fibrillation in five European countries: results from the Euro Heart Survey on atrial fibrillation. Europace. 2008;10(4):403-11.

14. Cotte FE, Chaize G, Gaudin AF, Samson A, Vainchtock A, Fauchier L. Burden of stroke and other cardiovascular complications in patients with atrial fibrillation hospitalized in France. Europace. 2016;18(4):501-7.

15. Lip GYH, Fauchier L, Freedman SB, Van Gelder I, Natale A, Gianni C, et al. Atrial fibrillation. Nat Rev Dis Primers. 2016;2.

16. Chung MK, Refaat M, Shen WK, Kutyifa V, Cha YM, Di Biase L, et al. Atrial Fibrillation JACC Council Perspectives. J Am Coll Cardiol. 2020;75(14):1689-713.

17. Nattel S, Heijman J, Zhou LP, Dobrev D. Molecular Basis of Atrial Fibrillation Pathophysiology and Therapy A Translational Perspective. Circ Res. 2020;127(1):51-72.

18. Wijffels MCEF, Kirchhof CJHJ, Dorland R, Allessie MA. Atrial-Fibrillation Begets Atrial-Fibrillation - a Study in Awake Chronically Instrumented Goats. Circulation. 1995;92(7):1954-68.

19. Lip GYH, Nieuwlaat R, Pisters R, Lane DA, Crijns HJGM. Refining Clinical Risk Stratification for Predicting Stroke and Thromboembolism in Atrial Fibrillation Using a Novel Risk Factor-Based Approach The Euro Heart Survey on Atrial Fibrillation. Chest. 2010;137(2):263-72.

20. Mcbride R. Stroke Prevention in Atrial-Fibrillation Study - Final Results. Circulation. 1991;84(2):527-39.

21. Connolly SJ, Ezekowitz MD, Yusuf S, Eikelboom J, Oldgren J, Parekh A, et al. Dabigatran versus Warfarin in Patients with Atrial Fibrillation. New Engl J Med. 2009;361(12):1139-51.

22. Fetsch T, Bauer P, Engberding R, Koch HP, Lukl J, et al. Prevention of atrial fibrillation after cardioversion: results of the PAFAC trial. Eur Heart J. 2004;25(16):1385-94.

23. Tieleman RG, Van Gelder IC, Crijns HJ, De Kam PJ, Van Den Berg MP, et al. Early recurrences of atrial fibrillation after electrical cardioversion: a result of fibrillation-induced electrical remodeling of the atria? J Am Coll Cardiol. 1998;31(1):167-73.

24. Zimetbaum P. Antiarrhythmic drug therapy for atrial fibrillation. Circulation. 2012;125(2):381-9.

25. Asad ZU, Yousif A, Khan MS, Al-Khatib SM, Stavrakis S. Catheter Ablation Versus Medical Therapy for Atrial Fibrillation A Systematic Review and Meta-Analysis of Randomized Controlled Trials. Circ-Arrhythmia Elec. 2019;12(9).

26. Camm AJ, Naccarelli GV, Mittal S, Crijns H, Hohnloser SH, Ma CS, et al. The Increasing Role of Rhythm Control in Patients With Atrial Fibrillation: JACC State-of-the-Art Review. J Am Coll Cardiol. 2022;79(19):1932-48.

27. Tilz RR, Rillig A, Thum AM, Arya A, Wohlmuth P, Metzner A, et al. Catheter ablation of long-standing persistent atrial fibrillation: 5-year outcomes of the Hamburg Sequential Ablation Strategy. J Am Coll Cardiol. 2012;60(19):1921-9.

28. Teunissen C, Kassenberg W, van der Heijden JF, Hassink RJ, van Driel VJHM, et al. Five-year efficacy of pulmonary vein antrum isolation as a primary ablation strategy for atrial fibrillation: a single-centre cohort study. Europace. 2016;18(9):1335-42.

29. Scott PA, Silberbauer J, Murgatroyd FD. The impact of adjunctive complex fractionated atrial electrogram ablation and linear lesions on outcomes in persistent atrial fibrillation: a meta-analysis. Europace. 2016;18(3):359-67.

30. McCarthy PM, Cox JL, Kislitsina ON, Kruse J, Churyla A, Malaisrie SC, et al. Surgery and Catheter Ablation for Atrial Fibrillation: History, Current Practice, and Future Directions. J Clin Med. 2022;11(1).

31. Lapenna E, De Bonis M, Giambuzzi I, Del Forno B, Ruggeri S, Cireddu M, et al. Long-term Outcomes of Stand-Alone Maze IV for Persistent or Long-standing Persistent Atrial Fibrillation. Ann Thorac Surg. 2020;109(1):124-31.

32. Ruaengsri C, Schill MR, Khiabani AJ, Schuessler RB, Melby SJ, Damiano RJ, Jr. The Cox-maze IV procedure in its second decade: still the gold standard? Eur J Cardiothorac Surg. 2018;53(suppl_1):i19-i25.

33. Ruaengsri C, Schill MR, Khiabani AJ, Schuessler RB, Melby SJ, Damiano RJ. The Cox-maze IV procedure in its second decade: still the gold standard? Eur J Cardio-Thorac. 2018;53:19-25.

34. Haldar S, Khan HR, Boyalla V, Kralj-Hans I, Jones S, Lord J, et al. Catheter ablation vs. thoracoscopic surgical ablation in long-standing persistent atrial fibrillation: CASA-AF randomized controlled trial. Eur Heart J. 2020;41(47):4471-80.

35. Ohtsuka T, Nonaka T, Hisagi M, Ninomiya M, Stewart JR. En Bloc Left Pulmonary Vein and Appendage Isolation in Thoracoscopic Surgery for Atrial Fibrillation. Annals of Thoracic Surgery. 2018;106(5):1340-8.

36. van Laar C, Bentala M, Weimar T, Doll N, Swaans MJ, Molhoek SG, et al. Thoracoscopic ablation for the treatment of atrial fibrillation: a systematic outcome analysis of a multicentre cohort. Europace. 2019;21(6):893-9.

37. Geng M, Lin A, Nguyen TP. Revisiting Antiarrhythmic Drug Therapy for Atrial Fibrillation: Reviewing Lessons Learned and Redefining Therapeutic Paradigms. Front Pharmacol. 2020;11.

38. Peyronnet R, Ravens U. Atria-selective antiarrhythmic drugs in need of alliance partners. Pharmacol Res. 2019;145.

39. Robinson NB, Krieger K, Khan FM, Huffman W, Chang M, Naik A, et al. The current state of animal models in research: A review. Int J Surg. 2019;72:9-13.

40. Voigt N, Pearman CM, Dobrev D, Dibb KM. Methods for isolating atrial cells from large mammals and humans. J Mol Cell Cardiol. 2015;86:187-98.

41. Amesz JH, de Groot NMS, Langmuur SJJ, el Azzouzi HE, Tiggeloven VPC, van Rooij MMMM, et al. Biomimetic cultivation of atrial tissue slices as novel platform for in-vitro atrial arrhythmia studies. Sci Rep-Uk. 2023;13(1).

42. Devalla HD, Schwach V, Ford JW, Milnes JT, El-Haou S, Jackson C, et al. Atrial-like cardiomyocytes from human pluripotent stem cells are a robust preclinical model for assessing atrial-selective pharmacology. EMBO Mol Med. 2015;7(4):394-410.

43. Zhang Q, Jiang J, Han P, Yuan Q, Zhang J, Zhang X, et al. Direct differentiation of atrial and ventricular myocytes from human embryonic stem cells by alternating retinoid signals. Cell Res. 2011;21(4):579-87.

44. Goldfracht I, Protze S, Shiti A, Setter N, Gruber A, Shaheen N, et al. Generating ring-shaped engineered heart tissues from ventricular and atrial human pluripotent stem cell-derived cardiomyocytes. Nat Commun. 2020;11(1):75.

45. Laksman Z, Wauchop M, Lin E, Protze S, Lee J, Yang W, et al. Modeling Atrial Fibrillation using Human Embryonic Stem Cell-Derived Atrial Tissue. Sci Rep. 2017;7(1):5268.

46. Sanders P, Berenfeld O, Hocini M, Jais P, Vaidyanathan R, Hsu LF, et al. Spectral analysis identifies sites of high-frequency activity maintaining atrial fibrillation in humans. Circulation. 2005;112(6):789-97.

47. Schuessler RB, Kay MW, Melby SJ, Branham BH, Boineau JP, Damiano RJ, Jr. Spatial and temporal stability of the dominant frequency of activation in human atrial fibrillation. J Electrocardiol. 2006;39(4 Suppl):S7-12.

48. Yoshida K, Ulfarsson M, Oral H, Crawford T, Good E, Jongnarangsin K, et al. Left atrial pressure and dominant frequency of atrial fibrillation in humans. Heart Rhythm. 2011;8(2):181-7.

49. Onodi Z, Visnovitz T, Kiss B, Hambalko S, Koncz A, Agg B, et al. Systematic transcriptomic and phenotypic characterization of human and murine cardiac myocyte cell lines and primary cardiomyocytes reveals serious limitations and low resemblances to adult cardiac phenotype. J Mol Cell Cardiol. 2022;165:19-30.

50. Kimes BW, Brandt BL. Properties of a clonal muscle cell line from rat heart. Exp Cell Res. 1976;98(2):367-81.

51. Hescheler J, Meyer R, Plant S, Krautwurst D, Rosenthal W, Schultz G. Morphological, biochemical, and electrophysiological characterization of a clonal cell (H9c2) line from rat heart. Circ Res. 1991;69(6):1476-86.

52. Claycomb WC, Lanson NA, Jr., Stallworth BS, Egeland DB, Delcarpio JB et al. HL-1 cells: a cardiac muscle cell line that contracts and retains phenotypic characteristics of the adult cardiomyocyte. Proc Natl Acad Sci U S A. 1998;95(6):2979-84.

53. Davidson MM, Nesti C, Palenzuela L, Walker WF, Hernandez E, Protas L, et al. Novel cell lines derived from adult human ventricular cardiomyocytes. J Mol Cell Cardiol. 2005;39(1):133-47.

54. Ruijtenberg S, van den Heuvel S. Coordinating cell proliferation and differentiation: Antagonism between cell cycle regulators and cell type-specific gene expression. Cell Cycle. 2016;15(2):196-212.

55. Jahn L, Sadoshima J, Greene A, Parker C, Morgan KG, Izumo S. Conditional differentiation of heart- and smooth muscle-derived cells transformed by a temperature-sensitive mutant of SV40 T antigen. J Cell Sci. 1996;109 (Pt 2):397-407.

56. Goldman BI, Amin KM, Kubo H, Singhal A, Wurzel J. Human myocardial cell lines generated with SV40 temperature-sensitive mutant tsA58. In Vitro Cell Dev Biol Anim. 2006;42(10):324-31.

57. Rybkin, II, Markham DW, Yan Z, Bassel-Duby R, Williams RS, Olson EN. Conditional expression of SV40 T-antigen in mouse cardiomyocytes facilitates an inducible switch from proliferation to differentiation. J Biol Chem. 2003;278(18):15927-34.

58. Zhang Y, Nuglozeh E, Toure F, Schmidt AM, Vunjak-Novakovic G. Controllable expansion of primary cardiomyocytes by reversible immortalization. Hum Gene Ther. 2009;20(12):1687-96.

59. Liu J, Volkers L, Jangsangthong W, Bart CI, Engels MC, Zhou G, et al. Generation and primary characterization of iAM-1, a versatile new line of conditionally immortalized atrial myocytes with preserved cardiomyogenic differentiation capacity. Cardiovasc Res. 2018;114(14):1848-59.

Part One

Outcomes of thoracoscopic ablation in long-standing persistent atrial fibrillation



Chapter 2



Clamping versus nonclamping thoracoscopic box ablation in long-standing persistent atrial fibrillation

J Thorac Cardiovasc Surg. 2020;160:399-405.

Niels Harlaar, Niels J. Verberkmoes, Pepijn H. van der Voort, Serge A. Trines, Stefan E. Verstraeten, Bart J. A. Mertens, Robert J. M. Klautz, Jerry Braun, Thomas J. van Brakel

Abstract

Objective: To compare clinical outcomes of clamping devices and linear nonclamping devices for isolation of the posterior left atrium (box) in thoracoscopic ablation of long-standing persistent atrial fibrillation.

Methods: Eighty patients who underwent thoracoscopic pulmonary vein and box isolation using a bipolar clamping device (42 patients) or bipolar nonclamping device (38 patients) to create the roof/inferior lesions for box isolation were included from 2 centres. Follow-up consisted of 24-hour Holter at regular intervals. Freedom from AF during 1-year follow-up and catheter repeat interventions were compared between groups.

Results: Acute intraoperative electrical isolation of the box compartment was significantly higher in the clamping group than in the nonclamping group (100% and 79%, respectively, $P < 0.01$). At 1-year follow-up, 91% of the clamping group and 79% of the nonclamping group were in sinus rhythm. During 1-year follow-up, recurrence rates did not significantly differ between the 2 groups ($P = 0.08$). Repeat catheter interventions were required in 10% of the clamping group and 21% of the nonclamping group ($P = 0.15$). Conduction gaps in the roof or inferior lesions were found in 1 patient (2%) in the clamping group versus 4 patients (11%) in the nonclamping group ($P = 0.13$).

Conclusions: Thoracoscopic pulmonary vein and box isolation are highly effective in restoring sinus rhythm in long-standing persistent atrial fibrillation on short-term follow-up. Comparison of clamping and nonclamping devices revealed lower rates of intraoperative exit block of the box in the nonclamping group. However, this did not translate into a significant difference in atrial fibrillation freedom at short-term (1-year) follow-up.

Introduction

Totally thoracoscopic ablation has been increasingly accepted for the treatment of patients with long-standing persistent atrial fibrillation (AF) because of its high efficacy compared with percutaneous ablation and minimally invasive character (1,2). The left atrial posterior wall has been suggested to play a major role in the initiation and the maintenance of AF, and therefore complete isolation of this area is desired (3). The most common lesion set consists of pulmonary vein (PV) antrum isolation combined with left atrial posterior wall (box) isolation. To create the box lesions, current thoracoscopic techniques mainly rely on 2 types of bipolar radiofrequency (RF) ablation devices, that is, ablation clamps and linear nonclamping devices. Thus far, no study has compared these devices in terms of their clinical efficacy. Histologic studies suggest that clamping devices create more durable lesions compared with nonclamping devices (4-6). Because durable isolation of the PVs and posterior wall is crucial for freedom from AF, we compared the 1-year outcomes of these 2 common devices in patients with long-standing persistent AF.

Materials and Methods

Patients and Data Collection

Consecutive patients with symptomatic long-standing persistent AF undergoing thoracoscopic ablation at the Leiden University Medical Centre (October 2009 to December 2016) and Catharina Hospital (December 2013 to November 2016) were included. Patients were refractory to 1 or more class I/III antiarrhythmic drugs or had failed catheter ablation. Clinical data were prospectively collected in the electronic patient information system of the Cardiothoracic Surgery/Cardiology departments of both hospitals and were retrospectively analysed. Definitions of long-standing persistent AF and clinical outcomes were based on the Heart Rhythm Society expert consensus statement on catheter and surgical ablation of AF (7). This study was conducted with approval of the institutional review boards of the Leiden University Medical Centre (LUMC, G17.101) and Catharina Hospital Eindhoven. Patient data in the LUMC were collected after written informed consent, whereas data in the Catharina Hospital were collected as part of a quality improvement initiative, waiving the need for individual informed consent. All data were handled in accordance with the European General Data Protection Regulation.

Surgical Techniques

In both thoracoscopic approaches, PV isolation was performed using ablation clamps, whereas isolation of the posterior left atrium (box) was performed using a clamping or a linear nonclamping device (**Figure 1**). In each of the 2 centres, one technique was performed exclusively. The clamping box lesion set was performed only in the Leiden University Medical Centre by 2 surgeons (J.B./T.J.v.B.), whereas the nonclamping box lesion set was performed in the Catharina Hospital by 1 surgeon (N.J.V.).

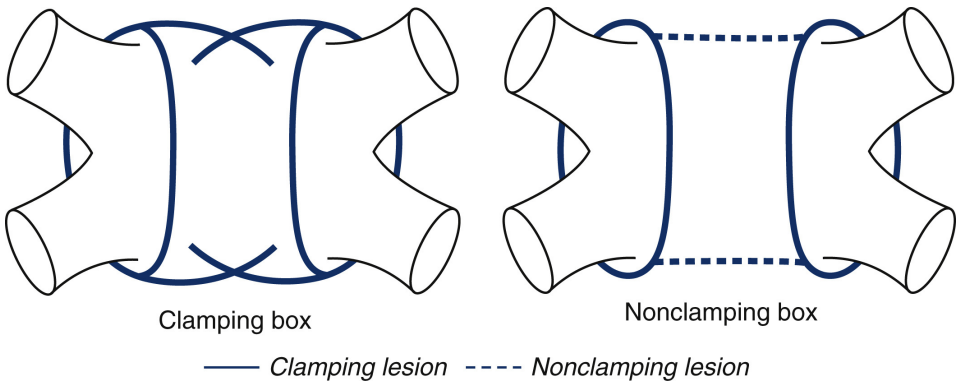


Figure 1. Schematic overview of the PV and box ablation lesions placed with clamping and nonclamping devices in the 2 groups. Solid lines represent lesions ablated with a clamping device, and dotted lines represent lesions placed with a nonclamping device.

The clamping box lesion set was created by using a single device, a bipolar saline-irrigated RF clamp (Cardioblate Gemini-s, Medtronic). Starting ablation from the left, the clamp was applied 4 times with the convexity of the clamp facing toward the atrial myocardium to apply left PV antrum lesions and 4 times with the concavity of the clamp facing toward the myocardium to create the roof/inferior lesions. This clamping across the left atrial posterior wall is shown in **Figure 2**. For each application, energy was delivered until impedance measurements indicated transmurality (based on the generator algorithm). Between applications, the ablation clamp was repositioned to ensure overlap of the lesions at the hinge point of the Gemini Clamp. The same lesions were repeated from the right side to create the right PV antrum lesion and to close the box. This procedure has been described previously in detail (8) and can also be seen in **Supplemental Video 1**.

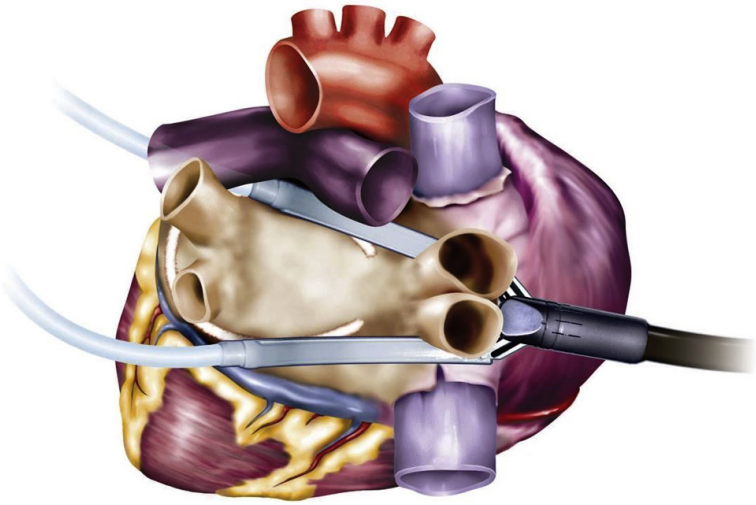


Figure 2. Illustration of the Gemini-s device clamping across the left atrial posterior wall to create the roof and inferior lesions in the clamping group.

The nonclamping box lesion set consisted of creating a circumferential right antral PV lesion using a nonirrigated bipolar RF clamp (EMR2, AtriCure). During a minimum of 5 applications, the clamp was repositioned each time when impedance measurements (based on the generator algorithm) indicated transmurality. Continuing on the right, starting from the PVs, the roof and inferior lesion were created using a linear nonclamping device (Coolrail Linear Pen, AtriCure) by overlapping an average of 20 lesions connecting with the left PV antrum thereby closing the box. Then, the left PV antrum was isolated using a bipolar RF clamp again (EML2, AtriCure). This procedure has also been described in detail (9) and can be seen in **Supplemental Video 2**.

In both techniques, electrical isolation of the PVs and box was confirmed after completion of the lesion set. Patients who did not achieve sinus rhythm during the procedure underwent electric cardioversion. Entrance block was defined as the absence of sharp electrograms in each of the PVs and box compared with baseline measurements (Cardioblate MAPS Device, Medtronic or Max 5 Pen, AtriCure). Exit block was defined as the absence of left atrial capture when pacing in all PVs and the box. In the event that entrance or exit block had not been achieved after lesion set completion, a series of additional RF applications were performed and entrance/exit block measurements were

repeated. Although additional RF applications entrance or exit block could not be achieved, it would be regarded as failed entrance/exit block.

Left atrial appendage (LAA) management varied between centres. Preoperatively, transesophageal echocardiography was used in all patients to exclude the presence of a left atrial thrombus. Management was performed by 60-mm stapler exclusion (Endo GIA Universal Stapler, Medtronic) or clip closure (AtriClip, AtriCure) when deemed feasible.

Antiarrhythmic drugs were started or continued after the procedure throughout the 3-month blanking period and discontinued after the first follow-up if the patient was in sinus rhythm. Oral anticoagulation was resumed until (a minimum of) 6 months after the procedure and discontinued, based on rhythm and CHA_2DS_2-VASc score (congestive heart failure, hypertension, age, diabetes, stroke, vascular disease and sex score), at the discretion of the cardiologist.

Follow-up

Follow-up consisted of 24-hour Holter monitoring at regular intervals (3, 6, and 12 months). Recurrence was defined as any episode of AF, atrial flutter (AFL), or atrial tachycardia (AT) lasting 30 seconds or more on 24-hour Holter, electrocardiography, or pacemaker/implantable cardioverter defibrillator interrogation after the 3-month blanking period. Patients were asked to visit the hospital in case of symptoms suggestive of arrhythmia for additional electrocardiography or 24-hour Holter monitoring. Patients with suspected reconnection due to the presence of AF/AFL/AT were invited for an endocardial electrophysiologic evaluation and ablation. All patients who completed the 1-year 24-hour Holter recording were included in the analysis.

Statistical Analysis

Categoric data are presented as counts and percentages, whereas numeric data are expressed as mean ± standard deviation for normally distributed data or as median [interquartile range] for non-normally distributed data. Numeric data were compared using the independent sample t test or Mann–Whitney U test, and categoric data were compared using the chi-square test or Fisher exact test. A mixed-effect logistic regression model was fitted to model the probability of atrial arrhythmia recurrence. Time and surgical technique effect were fitted as fixed effects. Time was included as a categoric covariate, contrasting follow-up moments at 6 and 12 months versus 3 months, to account for nonlinearity of effect at log-odds scale. Time points represented

rhythm status measured at the follow-up moment plus any recurrences detected in the preceding interval. A normally distributed within-person effect was added to the model to account for within-person correlation in longitudinally observed recurrence of atrial arrhythmias. Statistical analysis was performed using SPSS (v23.0, IBM), and graphs were plotted in GraphPad Prism (v7.0, GraphPad Software Inc).

Results

Baseline Demographics

Eighty patients with long-standing persistent AF underwent thoracoscopic ablation between 2009 and 2016. A total of 42 patients underwent box ablation using a clamping device, whereas 38 patients underwent nonclamping device box ablation. In the clamping group, mean age was 59 ± 8 years with a median duration of AF of 4 (2-6) years. Median left atrial volume index was 42 (38-52.3) mL/m^2, and 7 patients (17%) had previously undergone catheter ablation. In the nonclamping group mean age was 61 ± 9 years, median AF duration was 3 (2-7) years, median left atrial volume index was 36.5 (31.5-51.3) mL/m^2, and 12 patients (32%) previously underwent catheter ablation. During follow-up, 6 patients (14%) in the clamping group and 6 patients (16%) in the nonclamping group had continuous rhythm monitoring through an implanted device. Between the 2 groups, the median CHA_2DS_2-VASc score was significantly higher in the nonclamping group (1 [0-2], 2 [1-2], P = 0.01) as well as the body mass index (29.6 ± 4.3 vs 26.9 ± 3.1, P < 0.01). An overview of baseline characteristics is shown in **Table 1**.

Follow-up

At the end of the blanking period, 100% of patients in the clamping group and 95% of patients in the nonclamping group were in sinus rhythm, whereas at 1 year, 91% of patients in the clamping group and 79% of patients in the nonclamping group were free from atrial arrhythmias (**Figure 3**). After correction for time effect in random-effect logistic regression, we found no significant difference in AF/AFL/AT recurrence during 1-year follow-up between the 2 groups (F-test = 3.05, P = 0.08, **Table 2**). At 1 year, 12% of the clamping group and 16% of the nonclamping group were continuing to use antiarrhythmic drugs (P = 0.61). During the 1-year follow-up period, repeat catheter ablation was performed in 4 of 42 patients (10%) in the clamping box group and in 8 of 38 patients (21%) in the nonclamping box group (P = 0.15).

Table 1. Baseline clinical characteristics

Characteristic	Clamping box (n = 42)	Non-clamping box (n = 38)	
Age (years)	59 ± 8	61 ± 9	*P = 0.21*
Female	10 (24%)	11 (29%)	*P = 0.60*
Duration of AF (years)	4 [2-6]	3 [2-7]	*P = 0.64*
Left atrial volume index (ml/m^2)	42 [38-52.5]	36.5 [31.5-51.3]	*P = 0.05*
CHA_2DS_2-VASc score	1 [0-2]	2 [1-2]	*P = 0.01*
0	15 (36%)	6 (16%)	
1	15 (36%)	11 (29%)	
2	7 (16%)	12 (32%)	
≥ 3	5 (12%)	9 (24%)	
Body Mass Index (kg/m^2)	26.9 ± 3.1	29.6 ± 4.3	*P < 0.01*
Hypertension	17 (41%)	22 (58%)	*P = 0.12*
Diabetes mellitus	0 (0%)	2 (5%)	*P = 0.13*
Prior stroke	1 (2%)	4 (11%)	*P = 0.13*
Prior transient ischemic attack	2 (5%)	1 (3%)	*P = 0.62*
Prior catheter ablation	7 (17%)	12 (32%)	*P = 0.12*
Pacemaker/ICD monitoring	6 (14%)	6 (16%)	*P = 0.85*

Data are presented as *n* (%), mean ± SD or median [ICR]
AF: atrial fibrillation, ICD: implantable cardioverter defibrillator, ICR: interquartile range, SD: standard deviation

Catheter Repeat Ablations

During repeat catheter procedures, gaps in the lesion set were regularly found as source of recurrence. PV lesion gaps were found in 2 patients (5%) in the clamping group versus 3 patients (8%) in the nonclamping group (P = 0.56). Gaps in the roof or inferior box lesions were present in 1 patient (2%) in the clamping group versus 4 patients (11%) in the nonclamping group (P = 0.13). Cavotricuspid isthmus ablation for the presence of typical AFLs was performed in 1 patient in the clamping group and in 5 patients in the nonclamping group (P = 0.07). In both groups, 1 patient underwent posterior mitral isthmus ablation for the presence of a mitral isthmus dependent flutter. After repeat catheter ablation, all 4 patients in the clamping group regained sinus rhythm, whereas in the nonclamping group 4 of 8 patients returned to sinus rhythm, 2 of 8 patients

remained in AF, and 2 of 8 patients continued to experience AFLs. A complete overview is presented in **Table 3.**

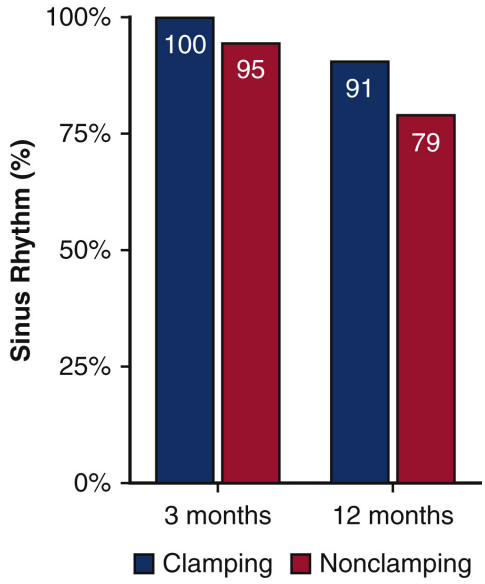


Figure 3. Percentage of patients in sinus rhythm after the blanking period (3 months) and at maximal (12 months) follow-up in the clamping and nonclamping box isolation groups.

Table 2. Mixed-effect logistic regression model of atrial arrhythmia recurrence including ablation technique and time effect

Variables	Estimate	SE	OR (95% CI)	P
Intercept	-4.497	0.838	0.011 (0.002-0.058)	0.000
Use of non-clamping technique*	0.971	0.556	2.640 (0.883-7.897)	0.082
Rhythm 6-months†	1.732	0.827	5.652 (1.108-28.822)	0.037
Rhythm 12-months†	2.312	0.804	10.099 (2.072-49.222)	0.004

*Reference = Use of clamping technique, †Reference = Rhythm 3-months
SE: standard error, OR: odds ratio, CI: confidence interval

Table 3. Characteristics of repeat catheter interventions

#	SVT type	Device of box isolation	Repeat intervention	Rhythm after
1	AF	Clamping	Reisolation of LPV/RPV/roof/inferior	SR
2	AF	Clamping	CFAE ablation + LAAI	SR
3	AF	Clamping	Reisolation of LPV + CFAE ablation + CTI	SR
4	AFL	Clamping	MI ablation	SR
5	AF/AFL	Non-clamping	CFAE ablation + CTI	AF
6	AF	Non-clamping	Reisolation of roof + CFAE ablation	SR
7	AFL	Non-clamping	CTI ablation	SR
8	AFL	Non-clamping	CTI ablation	AFL
9	AF/AFL	Non-clamping	Reisolation of RPV/roof/inferior + MI	SR
10	AFL	Non-clamping	CTI ablation	SR
11	AF/AFL	Non-clamping	Reisolation of LPV/roof/inferior + CTI	AF
12	AF	Non-clamping	Reisolation of RPV/roof + CFAE ablation	AF

AF: atrial fibrillation, AFL: atrial flutter, CFAE: complex fractionated atrial electrograms, CTI: cavotricuspid isthmus, LAAI: left atrial appendage isolation, LPV: left pulmonary veins, MI: mitral isthmus, RPV: right pulmonary veins, SR: sinus rhythm, SVT: supraventricular tachycardia

Discussion

This is the first study comparing outcomes of clamping and nonclamping devices for creation of the roof/inferior (box) lesions in addition to PV isolation in thoracoscopic long-standing persistent AF ablation. The main findings were 1) intraoperative electrical isolation of the clamping box lesions was significantly higher compared with the nonclamping box lesion (100% vs 79%, respectively); 2) repeat catheter interventions due to recurrence were required in 10% of the clamping group and 21% of the nonclamping group; and 3) resulting sinus rhythm rates at 1 year were 91% using clamping devices and 79% using nonclamping devices.

Thoracoscopic AF ablation has been established as a valuable therapy compared with catheter ablation in patients with long-standing persistent AF, in whom outcomes have generally been suboptimal and require multiple procedures to achieve sinus rhythm (10,11). The ablation outcomes in our

groups (91% and 79% freedom from AF at 1 year, on antiarrhythmic drugs) demonstrate that thoracoscopic ablation is effective in restoring sinus rhythm in long-standing persistent AF and are consistent with previous reports of thoracoscopic ablation in these populations (1,2).

In the 2 groups, we found that the acute electrical isolation of the box compartment as measured by exit block was significantly lower in the nonclamping group. However, this did not result in a significant difference in sinus rhythm rates during 1-year follow-up (P = 0.08). Because repeat procedures performed within the 1-year timeframe might influence the rates of sinus rhythm at 1 year, we also assed the frequency of repeat procedures and associated findings in both groups. Repeat procedures did not significantly differ between groups (10% in clamping vs 21% in nonclamping groups, P = 0.15), and neither did the amount of conduction gaps found in the box compartment (2% in clamping vs 11% in nonclamping groups, P = 0.13). However, in the present study, only part of the 2 groups were admitted for endocardial electrophysiologic testing, which likely underestimates the actual number of conduction gaps present. Bulava and colleagues (12) performed a staged hybrid procedure in a similar group with nonclamping roof/inferior lesions and found that 23% of the nonclamping box lesions versus 69% of the clamping PV lesions were electrically isolated 6 to 8 weeks after the surgical procedure.

The heterogeneity in acute lesion integrity can likely be attributed to a combination of factors. Mainly, thermal sinking proves to be a substantial obstacle when performing epicardial nonclamping ablation, as the endocardium is continuously cooled by circulating blood, thereby counteracting transmurality. Clamping devices are less affected by this phenomenon because of blood displacement between the 2 jaws. Moreover, epicardial fat presence significantly affects lesion transmurality, because fat is a poor conductor of energy (13,14). Particularly in chronic AF, epicardial fat volumes increase compared with both healthy patients and patients with paroxysmal AF (15), and thick epicardial fat pads have been described at the location of the roof lesion (16). With nonclamping devices, energy flows between the 2 electrodes of the device, possibly not reaching the endocardium when thick epicardial fat pads are present. This is in contrast to clamping devices, where energy flows from epicardium to endocardium, to the other endocardium and again to epicardium. Moreover, the need of nonclamping devices to overlap multiple applications to create linear lesions might prove to be a risk factor for the presence of conduction gaps.

The strategy toward LAA management was different in the 2 participating centres. Surgeons in the nonclamping group strived toward high LAA management rates, whereas surgeons in the clamping group were more conservative and managed the LAA on the basis of thromboembolic risk, LAA anatomy, and stapling safety. Which strategy is preferable remains under debate, because the risk–benefit ratio of empirical LAA exclusion is uncertain. Although not yet studied, safe closure of the LAA might be higher with the clip compared with stapling devices. Besides potentially reducing thromboembolic events, some electrophysiologic benefit might be expected when performing empirical LAA isolation as seen in percutaneous ablation studies (17). One patient in our group in whom the LAA was left *in situ* because of unfavourable anatomy for stapler excision required percutaneous electrical isolation of the LAA due to recurrence of AF. Whether there is an electrophysiologic benefit of empirical LAA isolation when performing thoracoscopic ablation remains to be determined.

Study Limitations

Several limitations of this study should be mentioned, which are mainly the relatively small group sizes and the nonmatched and nonrandomized retrospective nature. Because each centre performed 1 of the 2 techniques exclusively, differences in clinical baseline characteristics and risk factors (*e.g.* body mass index and CHA_2DS_2-VASc score), as well as clinical protocols and practice (*e.g.* follow-up patterns, medication regimens, and aggressiveness of treatment), could affect the clinical outcomes. These features prevent any definitive conclusions to be drawn regarding the efficacy of clamping and nonclamping box isolation. As mentioned earlier, the frequency of lesion gaps found during repeat procedures is likely underestimated because only part of the group underwent endocardial testing of the lesion integrity. Also, the 1-year freedom rates might be overestimated because some asymptomatic arrhythmia episodes may not have been detected by 24-hour Holter monitoring. Nonetheless, this study provides a first comparison of the efficacy of 2 types of ablation devices for box isolation currently used in clinical practice. Larger prospective studies with a longer rhythm follow-up should provide more definitive information on the ability of clamping and nonclamping devices to create continuous transmural roof/inferior lesions, as well as on their efficacy in treating long-standing persistent AF.

Conclusions

Thoracoscopic PV and box isolation following a structured approach and using intraoperative assessment of conduction block are highly effective in restoring sinus rhythm in long-standing persistent AF. Comparison of clamping and nonclamping devices for roof/inferior lesion ablation revealed lower rates of intraoperative conduction block in the nonclamping group. However, this did not translate into significant differences in AF freedom at short-term (1-year) follow-up in our groups.

References

1. van Laar, C., Kelder, J. & van Putte, B.P. The totally thoracoscopic maze procedure for the treatment of atrial fibrillation. Interact Cardiovasc Thorac Surg. 2017;24:102-111

2. Je, H.G., Shuman, D.J. & Ad, N. A systematic review of minimally invasive surgical treatment for atrial fibrillation: a comparison of the Cox-Maze procedure, beating-heart epicardial ablation, and the hybrid procedure on safety and efficacy. Eur J Cardiothorac Surg. 2015;48:531-540

3. Roberts-Thomson, K.C. et al. Anatomically determined functional conduction delay in the posterior left atrium relationship to structural heart disease. J Am Coll Cardiol. 2008;51:856-862

4. Watanabe, Y., Weimar, T., Kazui, T., Lee, U., Schuessler, R.B. & Damiano Jr., R.J. Epicardial ablation performance of a novel radiofrequency device on the beating heart in pigs. Ann Thorac Surg. 2014;97:673-678

5. Voeller, R.K., Zierer, A., Schuessler, R.B. & Damiano Jr., R.J. Performance of a novel dual-electrode bipolar radiofrequency ablation device: a chronic porcine study. Innovations (Phila). 2011;6:17-22

6. Lee, A.M., Aziz, A., Clark, K.L., Schuessler, R.B. & Damiano Jr., R.J. Chronic performance of a novel radiofrequency ablation device on the beating heart: limitations of conduction delay to assess transmurality. J Thorac Cardiovasc Surg. 2012;144:859-865

7. Calkins, H. et al. 2017 HRS/EHRA/ECAS/APHRS/SOLAECE expert consensus statement on catheter and surgical ablation of atrial fibrillation. Heart Rhythm. 2017;14:e275-e444

8. Compier, M.G. et al. Outcome of stand-alone thoracoscopic epicardial left atrial posterior box isolation with bipolar radiofrequency energy for longstanding persistent atrial fibrillation. Neth Heart J. 2016;24:143-151

9. van Laar, C., Geuzebroek, G.S., Hofman, F.N. & van Putte, B.P. The totally thoracoscopic left atrial maze procedure for the treatment of atrial fibrillation. Multimed Man Cardiothorac Surg. 2016; (Available at: https://mmcts.org/tutorial/99. Accessed July 27, 2018)

10. Tilz, R.R. et al. Catheter ablation of long-standing persistent atrial fibrillation: 5-year outcomes of the Hamburg sequential ablation strategy. J Am Coll Cardiol. 2012;60:1921-1929

11. Wang, J., Li, Y. & Shi, J. Minimally invasive surgical versus catheter ablation for the long-lasting persistent atrial fibrillation. PLoS One. 2011;6:e22122

12. Bulava, A., Mokracek, A., Hanis, J., Eisenberger, M., Kurfirst, V. & Dusek, L. Correlates of arrhythmia recurrence after hybrid epi- and endocardial radiofrequency ablation for persistent atrial fibrillation. Circ Arrhythm Electrophysiol. 2017;10:e005273

13. Suárez, A.G., Hornero, F. & Berjano, E.J. Mathematical modeling of epicardial RF ablation of atrial tissue with overlying epicardial fat. Open Biomed Eng J. 2010;4:47-55

14. Thomas, A.P., Guy, D.J., Boyd, A.C., Eipper, V.E., Ross, D.L. & Chard, R.B. Comparison of epicardial and endocardial linear ablation using handheld probes. Ann Thorac Surg. 2003;75:543-548

15. Gaeta, M. et al. Is epicardial fat depot associated with atrial fibrillation? A systematic review and meta-analysis. Europace. 2017;19:747-752

16. Osmancik, P., Budera, P., Zdarska, J., Herman, D., Petr, R. & Straka, Z. Electrophysiological findings after surgical thoracoscopic atrial fibrillation ablation. Heart Rhythm. 2016;13:1246-1252

17. Di Biase, L. et al. Left atrial appendage isolation in patients with longstanding persistent AF undergoing catheter ablation: BELIEF trial. J Am Coll Cardiol. 2016;68:1929-1940

Supplemental Information

Supplemental Video 1. Overview of the thoracoscopic PV and box isolation procedure using a clamping device to isolate the box. Video available at: doi.org/10.1016/j.jtcvs.2019.07.104

Supplemental Video 2. Overview of the thoracoscopic PV and box isolation procedure using a linear nonclamping device to isolate the box. Video available at: doi.org/10.1016/j.jtcvs.2019.07.104

Chapter 3



Long-term follow-up of thoracoscopic ablation in long-standing persistent atrial fibrillation

Interact Cardiovasc Thorac Surg. 2022;34:990-998.

Niels Harlaar, Maurice A. Oudeman, Serge A. Trines, Gijsbert S. de Ruiter, Bart J. Mertens, Muchtair Khan, Robert J. M. Klautz, Katja Zeppenfeld, Andrew Tjon, Jerry Braun, Thomas J. van Brakel

Abstract

Objective: Catheter ablation of long-standing persistent atrial fibrillation (LSPAF) remains challenging, with suboptimal success rates obtained following multiple procedures. Thoracoscopic ablation has shown effective at creating transmural lesions around the pulmonary veins and box; however, long-term rhythm follow-up data are lacking. This study aims, for the first time, to assess the long-term outcomes of thoracoscopic pulmonary vein and box ablation in LSPAF.

Methods: Rhythm follow-up consisted of continuous rhythm monitoring using implanted loop recorders or 24-h Holter recordings. Rhythm status and touch-up interventions were assessed up to 5 years.

Results: Seventy-seven patients with symptomatic LSPAF underwent thoracoscopic ablation in 2 centres. Freedom from atrial arrhythmias at 5 years was 50% following a single thoracoscopic procedure and 68% allowing endocardial touch-up procedures (performed in 21% of patients). The mean atrial fibrillation burden in patients with continuous monitoring was reduced from 100% preoperatively to 0.1% at the end of the blanking period and 8.0% during the second year. Antiarrhythmic drug use decreased from 49.4% preoperative to 12.1% and 14.3% at 2 and 5 years, respectively ($P < 0.001$). Continuous rhythm monitoring resulted in higher recurrence detection rates compared to 24-h Holter monitoring at 2-year follow-up (hazard ratio: 6.5, $P = 0.003$), with comparable recurrence rates at 5-year follow-up.

Conclusions: Thoracoscopic pulmonary vein and box isolation are effective in long-term restoration of sinus rhythm in LSPAF, especially when complemented by endocardial touch-up procedures, as demonstrated by the 68% freedom rate at 5 years. Continuous rhythm monitoring revealed earlier, but not more numerous documentation of recurrences at 5-year follow-up.

Introduction

Long-term rhythm control in long-standing persistent atrial fibrillation (LSPAF) remains challenging to achieve in clinical practice. Catheter ablation has shown modest rates of sinus rhythm in this population, despite repeated procedures (1-4). In addition to the pulmonary veins (PVs), the left atrial posterior wall has been identified as an important ablation target to isolate the arrhythmogenic substrate driving LSPAF (5,6). The creation of transmural long-lasting linear lesions isolating this region, however, has proven difficult through endocardial techniques alone (7). Epicardial surgical ablation devices have shown to be able to effectively create transmural linear atrial lesions in a minimally invasive setting (8,9). Despite totally thoracoscopic ablation becoming increasingly accepted for the treatment of symptomatic (long-standing) persistent atrial fibrillation (AF), long-term follow-up data remain sparse, particularly in the LSPAF population. In this study, we report long-term outcomes of thoracoscopic isolation of the PVs and the left atrial posterior wall in an LSPAF population.

Patients and Methods

Patient inclusion and data collection

Eighty consecutive patients with symptomatic LSPAF who underwent thoracoscopic ablation at the Leiden University Medical Centre (LUMC, 2009–2017) and OLVG (2012–2017) were screened for the inclusion in the long-term rhythm analysis. All patients with a rhythm follow-up beyond the blanking period (> 3 months) were included. LSPAF was defined as continuous AF with a duration longer than 12 months (10). All patients were symptomatic and refractory to 1 or more class I or III antiarrhythmic drugs (AADs) or had failed both AAD and catheter ablation. Clinical data in the electronic patient information system of the Cardiothoracic Surgery/Cardiology departments were retrospectively analysed.

Surgical procedure

The thoracoscopic ablation procedure was performed under general anaesthesia with a double-lumen endotracheal tube to facilitate single-lung ventilation. In both centres, the procedure was performed by 2 surgeons. Transoesophageal echocardiography was used to exclude the presence of a left atrial thrombus. Utilizing 3 bilateral ports (12, 12 and 5 mm) with 8–10 mmHg CO_2 insufflation, the pericardium was opened anterior to the phrenic nerve on

the right side. After dissecting the pericardial reflection, the superior and inferior guides of the Cardioblate Gemini-S (Medtronic) were introduced through the transverse and oblique sinuses. On the left, the pericardium was opened posterior to the phrenic nerve, where the guides were retrieved and subsequently attached to the bipolar irrigated radiofrequency clamp. The clamp was then positioned to encircle the left PVs and left atrial posterior wall as depicted in **Figure 1.** Ablation was performed for a minimum of 4 times with the convexity of the clamp facing towards the atrial myocardium to apply left PV antrum lesions, and for a minimum of 4 times with the concavity of the clamp facing towards the myocardium to create the roof- and inferior lesions. For each application, energy was delivered until impedance measurements indicated transmurality (based on the generator algorithm). Between applications, the ablation clamp was repositioned to ensure lesion continuity. The same lesions were repeated on the right side to create the right PV antrum lesion and to close the box around the left atrial posterior wall. For a schematic illustration of the lesion set, see **Supplemental Figure 1**.

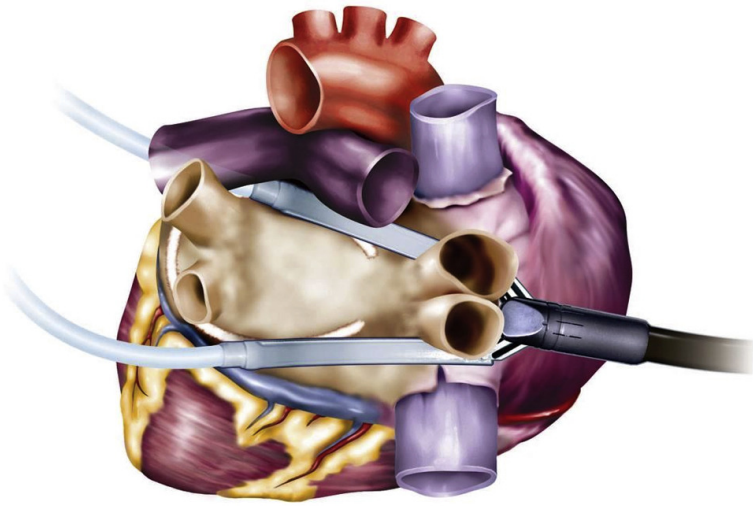


Figure 1. Positioning of the Gemini-S ablation device to isolate the pulmonary veins and left atrial posterior wall.

Following left and right lesion application, electrical isolation of the PVs and box was tested. Entrance block was defined as the absence of sharp electrograms in each of the PVs and box, when comparing sensed bipolar electrograms to baseline measurements (MAPS device, Medtronic). Electrical cardioversion was performed if sinus rhythm had not been achieved during the procedure. If

sinus rhythm was achieved, exit block was defined as absence of conducted atrial activity during pacing at 10 V, 2 ms pulse width in all PVs and the box. Visual confirmation of pacing viable myocardium was ensured to exclude false-positive exit block measurements. If entrance and/or exit block were absent following lesion set completion, a series of additional radiofrequency applications were performed, and entrance/exit block measurements were repeated. The absence of entrance and/or exit block despite additional radiofrequency applications was regarded as failed entrance/exit block.

At the end of the procedure, the left atrial appendage (LAA) was excluded using a 60 mm stapler (Endo GIA Universal Stapler, Medtronic or Powered Echelon), and was performed based on thromboembolic risk, appendage anatomy and stapling safety, as determined by the surgeon.

AADs were continued perioperatively. Patients not on an AAD received sotalol or amiodarone postoperatively, or in case of a contraindication for these drugs, a beta-blocker was started. AAD was used throughout the 3-month blanking period and discontinued after the first follow-up if the patient was in sinus rhythm. Oral anticoagulation was discontinued 2–3 days before surgery, was resumed until 6 months after the procedure and discontinued based on rhythm and CHA_2DS_2-VASc score, at the discretion of the cardiologist.

Follow-up

The follow-up procedure differed between the 2 centres. In the OLVG, follow-up of the first 3 years was performed based on rhythm monitored through a preoperatively implanted loop recorder (ILR; Reveal XT® or Linq®, Medtronic), with an additional 24-h Holter performed at 5 years. In the LUMC, standard follow-up consisted of 24-h Holter monitoring at 3 and 6 months, 1, 2 and 5 years. Failure was defined as any episode of AF, atrial flutter or atrial tachycardia lasting ≥ 30 s on 24-h Holter, electrocardiogram or ILR/pacemaker interrogation after a 3-month blanking period. Patients were asked to visit the hospital in case of symptoms suggestive of arrhythmia for additional electrocardiogram and/or 24-h Holter monitoring. Patients with suspected reconnection due to the presence of frequent symptomatic AF/atrial flutter/atrial tachycardia recurrences were invited for an endocardial electrophysiological evaluation and ablation.

Statistical analysis

Statistical analysis was performed using SPSS (v25, IBM Corporation) and graphs were plotted in GraphPad Prism (v8.1, GraphPad Software Inc.).

Categorical data are presented as counts and percentages, whereas numerical data are expressed as mean (standard deviation) for normally distributed data or as median [interquartile range] for non-normally distributed data. The normality of the data was assessed using the Shapiro–Wilk test. Numeric data were compared using the independent sample t-test or Mann–Whitney U test (for normally and non-normally distributed data, respectively), and categorical data were compared using the chi-squared test or Fisher's exact test in case of low expected counts. Arrhythmia burden between baseline and 2-year follow-up was compared using a paired samples t-test.

Freedom from first atrial arrhythmia recurrence was calculated using the Kaplan–Meier method. Graphs were truncated at 5 years to allow for sufficient numbers of patients at risk. Thoracoscopic-only freedom was the freedom from first atrial arrhythmia recurrence following thoracoscopic ablation only after the blanking period. Thoracoscopic + endocardial touch-up freedom was calculated from the last performed ablation procedure, being either the thoracoscopic procedure or an endocardial touch-up intervention.

Predictors of atrial arrhythmia recurrence following thoracoscopic ablation were identified using multivariable Cox regression analysis. Variates with a *P*-value smaller than 0.20 in the univariate analysis were included in the multivariable model. Hazard rates were calculated using Cox regression analysis. Due to the non-proportional hazards when comparing continuous and intermittent monitoring, landmark analysis was used to compare recurrence rates from baseline to medium-term (2 years) follow-up and from medium-term to long-term (5 years) follow-up. A P-value < 0.05 was considered significant.

Ethics statement

This study was conducted with the approval of both local institutional review boards (LUMC: G17.101-10/09/18; OLVG: WO19.105-18/09/19).

Results

Baseline demographics

Eighty patients with LSPAF underwent thoracoscopic ablation between 2009 and 2017. Seventy-six patients had a rhythm follow-up longer than 3 months and were included. One patient who died during the blanking period was included as an ablation failure. As a result, 77 patients were analysed in this study (flowchart: **Supplemental Figure 2**). Mean age was 58.9 ± 7.7 years, 22.1%

was female and median time since first AF diagnosis was 3.8 [1.9–6.3] years. The median left atrial volume index was 46 ± 13 ml/m^2 and 16% of patients had a history of prior catheter ablation. For an overview of baseline characteristics, see **Table 1**.

Perioperative data

The mean procedure time was 184 ± 60 min. In both centres, a downwards trend in procedure time indicative of a learning curve was observed over the course of the study (**Supplemental Figure 3**). The entrance block of the PVs and box was achieved in all patients. Following ablation, 32.5% of patients spontaneously converted to sinus rhythm. After electrical cardioversion in the remaining patients, 88.3% of patients were in sinus rhythm at the end of the procedure. Exit block of the PV and box compartments was confirmed in all patients, which were in sinus rhythm. The LAA was excluded in 66.2% of patients.

Safety

No conversion to median sternotomy was required. Video-assisted thoracoscopic reoperation was performed due to haemothorax in 5 patients and due to pericardial effusion/tamponade in 1 patient. In addition, transient phrenic nerve paresis with function recovery occurred in 2 patients and pacemaker implantation for sick sinus syndrome was performed in 2 patients. One patient with a contraindication to anticoagulation (and CHA_2DS_2-VASc of 3) had a cerebrovascular event at day 9 after surgery and died 54 days after surgery.

Long-term follow-up

The median follow-up duration was 3.0 [1.3–5.2] years. Freedom from atrial arrhythmias lasting ≥ 30 s following thoracoscopic ablation using the Kaplan–Meier method was 74.7% at 2 years [95% confidence interval (CI), 62.7–83.4] and 50.0% at 5 years (95% CI, 36.0–62.6). Catheter touch-up interventions due to symptomatic recurrences were performed in 20.8% of patients. Freedom from any atrial arrhythmia including catheter touch-up interventions was 92.3% at 2 years (95% CI, 82.1–96.8) and 68.0% at 5 years (95% CI, 50.9–80.2) following the last ablation procedure (**Figure 2**).

Actual rhythm status measured at the standard follow-up moments revealed sinus rhythm rates of 92.1%, 84.7%, 86.2% and 62.9% at 6 months, 1, 2 and 5 years, respectively. At 5-year follow-up, in addition to 62.9% of patients being

in sinus rhythm, 20.0% was in paroxysmal AF, 14.3% in persistent AF and 2.9% was experiencing atrial flutter. Sinus rhythm rates without use of AADs were 82.9%, 79.1%, 79.3% and 54.3% at 6 months, 1, 2 and 5 years, respectively (**Figure 3**).

AAD use decreased significantly following thoracoscopic ablation. Preoperatively, 49.4% of patients were taking AADs, compared to 11.8%, 8.3%, 12.1% and 14.3% at 6 months, 1, 2 and 5 years, respectively (all $P<0.001$ compared to preoperative AAD use). In particular, significant de-escalation of Amiodarone use was seen during follow-up (**Table 2**).

Table 1. Baseline clinical characteristics ($n = 77$).

Characteristic	Value
Age (years)	58.9 ± 7.7
Female	17 (22%)
Time since first AF diagnosis (years)	3.8 [1.9-6.3]
Left atrial volume index (ml/m^2)	46 ± 13
CHA_2DS_2-VASc score	1 [0-2]
0	24 (31%)
1	23 (30%)
≥2	30 (39%)
Body Mass Index (kg/m^2)	27.5 ± 3.7
Moderate mitral insufficiency	11 (14%)
Coronary artery disease	7 (9%)
Hypertension	39 (51%)
Diabetes mellitus	2 (3%)
Prior stroke/TIA	8 (10%)
Preoperative anticoagulation	75 (97%)
Preoperative antiarrhythmics	52 (68%)
Preoperative pacemaker/ICD	5 (7%)
Continuous rhythm monitoring	35 (46%)
Prior catheter ablation	12 (16%)
Pulmonary vein isolation	9 (12%)
AFL ablation	3 (4%)

Data are presented as *n* (%), mean ± SD or median [IQR].
AF: atrial fibrillation, AFL: atrial flutter, TIA: transient ischemic attack, SD: standard deviation, IQR: interquartile range, ICD: implantable cardiac defibrillator

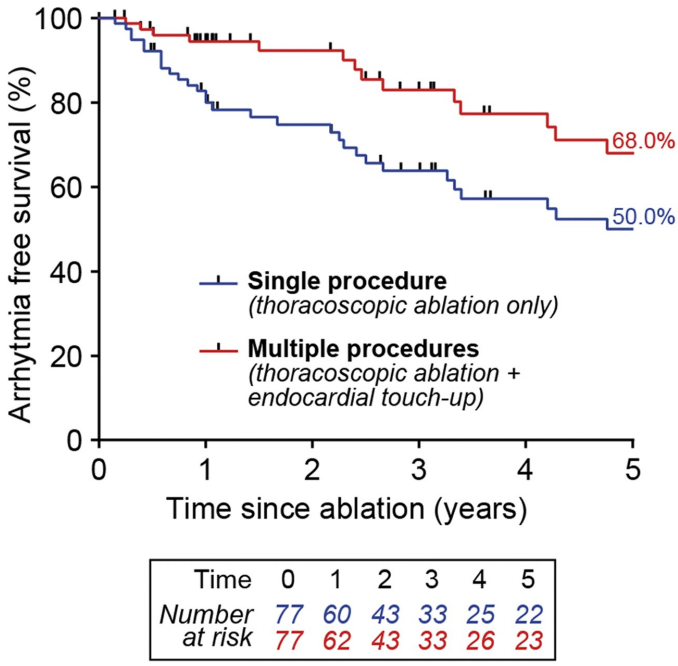


Figure 2. Freedom from all atrial arrhythmias after a single thoracoscopic ablation procedure only (single procedure freedom, blue line) or when allowing catheter touch-up procedures if required (multiple procedure freedom, measured from last procedure, red line).

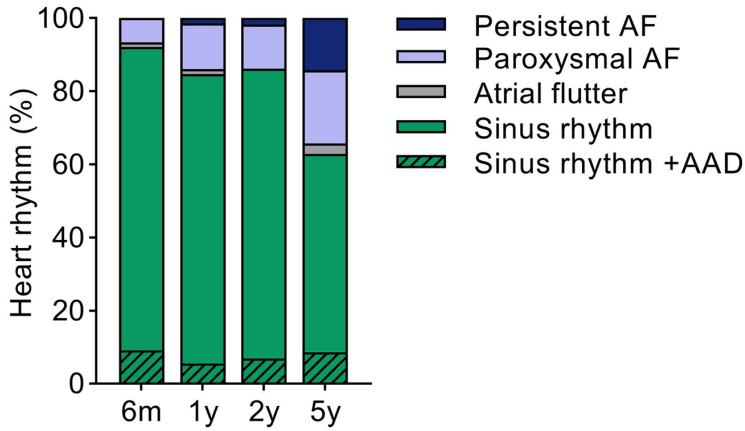


Figure 3. Rhythm status at 6 months and 1, 2 and 5 years following thoracoscopic ablation, including touch-up procedures and antiarrhythmic drug use. Patients at each timepoint are *n*=76, *n*=72, *n*=57 and *n*=35, respectively. AAD: antiarrhythmic drug; AF: atrial fibrillation.

Table 2. Antiarrhythmic drug (AAD) use during follow-up.					
	Preoperative (*n* = 77)	6 months (*n* = 76)	1 year (*n* = 72)	2 years (*n* = 58)	5 years (*n* = 35)
Total AAD use	49.4%	11.8%‡	8.3%‡	12.1%‡	14.3%‡
Flecainide	10.4%	7.9%	5.5%	6.9%	8.6%
Sotalol	19.5%	1.3%‡	2.8%†	3.4%†	5.7%
Amiodarone	19.5%	2.6%†	-‡	1.7%†	-†
P-value: * < 0.05, † < 0.01, ‡ < 0.001 (versus preoperative).					

Catheter touch-up procedures

Catheter touch-up procedures were performed in 16 (20.8%) of 77 patients. The mean time to first touch-up procedure was 2.0 ± 1.0 years. Three patients required a second catheter touch-up procedure after the first. Re-isolation of gaps found in the PV- and/or box lesions was performed in 7 patients. In the other 9 patients undergoing a touch-up procedure, the PV and box lesions were already durably isolated. Additional complex fractionated atrial electrograms ablation was performed in 5 patients. Ablation at the base of the stapled LAA was performed in 3 patients, whereas electrical isolation of the non-stapled LAA was performed in 2 patients. A cavo-tricuspid isthmus line was performed in 7 patients and a mitral isthmus line in 8 patients. For an overview of all touch-up procedures, see **Supplemental Table 1.**

Predictors of recurrence

Cox regression analysis of relevant clinical factors was performed to assess their impact on atrial arrhythmia recurrence. Multivariable analysis revealed left atrial volume index to be the only independent risk factor for first atrial arrhythmia recurrence following thoracoscopic ablation (hazard ratio: 1.05 for each ml/m^2 increase in left atrial volume index, 95% CI: 1.02–1.09, $P = 0.001$), as shown in **Supplemental Tables 2 and 3.**

Continuous versus intermittent rhythm monitoring

Implantable devices capable of continuous atrial rhythm sensing and detection of atrial arrhythmia episodes were present in 45.5% of patients (continuous group). The rest of the cohort relied on 24-h Holter recordings at various timepoints and presentation of symptomatic patients (intermittent group). Here, 91.7% of detected recurrences were due to patients presenting

outside standard follow-up moments. Comparison of atrial arrhythmia recurrences between the 2 groups revealed similar recurrence rates at 5-year follow-up (**Figure 4a**). However, landmark analysis at medium-term follow-up (2 years) revealed significantly higher recurrence rates in the continuous rhythm monitoring group in the first 2 years (**Figure 4b**).

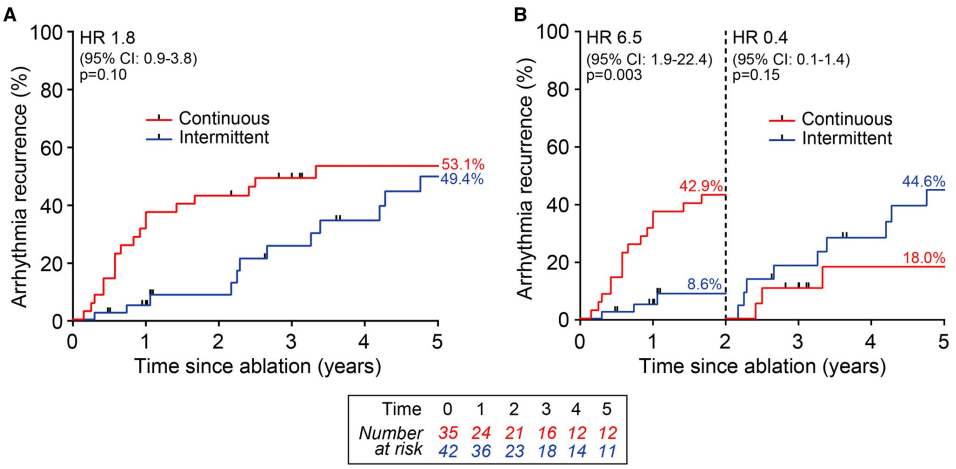


Figure 4. (a) Atrial arrhythmia recurrence after the thoracoscopic ablation procedure only, in intermittent (blue line) and continuous (red line) rhythm monitoring groups. **(b)** Landmark analysis of recurrence rates from baseline to medium-term (2 years) follow-up and from medium-term to long-term (5 years) follow-up between continuous and intermittent rhythm monitoring. CI: confidence interval; HR: hazard ratio.

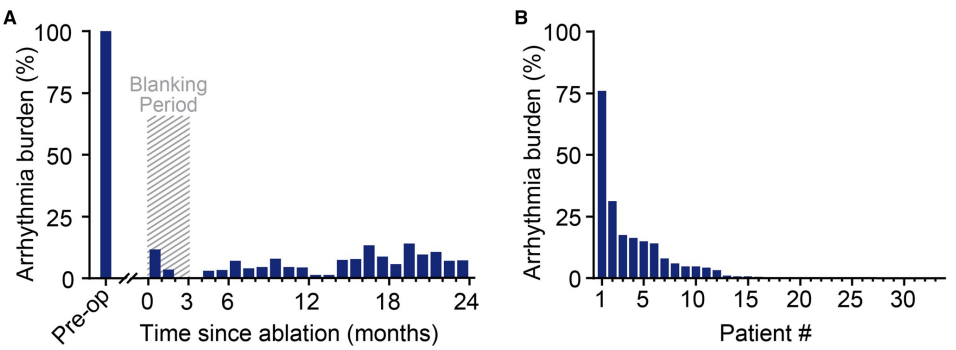


Figure 5. Atrial arrhythmia burden determined using continuous rhythm monitoring devices over the first 2 years following thoracoscopic ablation. **(a)** Changes in the average population burden following ablation. **(b)** Mean burden over the first 2 years following ablation per individual patient, ranked from highest to lowest.

Arrhythmia burden

In the month prior to thoracoscopic ablation, mean atrial arrhythmia burden was 100% (n=35). Following thoracoscopic ablation, the mean burden dropped to 0.1% at the end of the 3-month blanking period (**Figure 5a**). Over the first year, excluding the blanking period, the atrial arrhythmia burden was 4.2% on average. Two years following ablation, the average atrial burden decreased to 8.0% (P<0.001). During the 2 years following ablation, 48.5% of patients had an average burden <0.1% (**Figure 5b**). For an overview of individual patient burden development, see **Supplemental Figure 4**.

Discussion

This present study is the first to report long-term efficacy data of thoracoscopic ablation in an LSPAF cohort. Rhythm outcomes were studied for 77 LSPAF patients that underwent thoracoscopic ablation of the PVs and box using a clamping ablation device. The 5-year success rate (defined as freedom from any atrial arrhythmia ≥ 30 s) was 50% following a single thoracoscopic procedure and was 68% allowing endocardial touch-up procedures (performed in 20.8% of patients). The mean atrial arrhythmia burden was strongly reduced from 100% before ablation, to 0.1% at the end of the blanking period and 8.0% in the second year of follow-up. Comparison of recurrence rates between continuous and intermittent rhythm monitoring groups revealed similar recurrence rates at latest follow-up, but with earlier recurrence detection in patients with continuous rhythm monitoring.

Long-term rhythm control of LSPAF has been challenging to achieve in clinical practice, with electrical cardioversion and AAD therapy being poorly effective in this population (11). Catheter ablation targeting the arrhythmogenic substrate is frequently performed; however, long-term outcomes remain suboptimal. Tilz *et al.* (1) previously reported 20% freedom from atrial arrhythmias after 5 years following a single catheter ablation procedure, whereas freedom from AF was 38% after 1 or 2 procedures as compared to 45% after multiple (up to 5) procedures. Teunissen *et al.* (4) reported similar rates at 5-year follow-up, being 24% freedom following a single ablation procedure and 41% freedom following multiple procedures.

Conversely, surgical ablation using the Cox-maze IV technique, widely considered the gold standard for AF ablation, has shown high rates of long-term freedom in the LSPAF population. In the recent study of Lapenna *et al.* (12), 67%

of LSPAF patients remained free from recurrences 7 years following a stand-alone Cox-maze IV procedure. The group of Ad *et al.* (13) reported comparable rates at 5 years, with 59% of patients being free from atrial arrhythmia recurrences following a single stand-alone minimal access Cox-maze IV procedure. Nonetheless, despite being very efficacious, the invasiveness, required expertise and need for cardiopulmonary bypass of the stand-alone Cox-maze limits widespread applicability.

For surgical ablation to serve as an alternative to catheter ablation, minimal invasiveness, ease of performing the procedure and high efficacy are key. With the advent of thoracoscopic ablation techniques, minimally invasive 'beating heart' ablation using simple lesion sets has become commonplace over the past decade. In terms of efficacy, we show in this study for the first time that thoracoscopic ablation is effective in long-term sinus rhythm restoration in LSPAF, as demonstrated by the 68% freedom at 5 years (compared to 38–45% after multiple catheter ablation procedures and 59–67% after stand-alone Cox IV Maze). Particularly, we believe thoracoscopic ablation is effective in the LSPAF population when complemented by catheter touch-up procedures in patients with early recurrence, resulting in a 5-year success rate of 68% after 1 thoracoscopic procedure and a touch-up procedure in 21% of patients.

Literature on totally thoracoscopic ablation efficacy in LSPAF has thus far been limited to short- to medium-term follow-up studies. Haldar *et al.* (14) in the CASA-AF study reported 26% of patients being free from recurrence at 1-year follow-up, whereas Ohtsuka *et al.* (15) reported 47% freedom at 2-year follow-up and van Laar *et al.* (16) reported 54% freedom at 1.7-year follow-up. Although comparison of data between studies is difficult due to differences in patient characteristics and rhythm follow-up, the success rates we report at medium term (75% freedom at 2 years following thoracoscopic ablation only) appear to be higher than previously presented. Here, we believe differences in ablation technique might play a role, as the majority of previous studies have used non-clamping devices to electrically isolate the left atrial posterior wall. We previously reported (8) on the importance of creating the complete lesion set using clamping ablation devices as opposed to non-clamping devices, as the latter are known to deliver inferior lesion transmurality. To confirm whether a completely clamping lesion set is indeed the preferred method, large long-term comparative follow-up studies are needed.

Monitoring of the atrial rhythm following AF ablation has predominantly been performed by intermittent 24-h or 48-h Holter recordings in clinical practice.

Despite a trend in recent years towards longer recordings, ILRs have mostly been used in a research setting, where their high temporal data resolution allows for an accurate quantification of the arrhythmia burden. An interesting observation in this study is the notable decrease of an average 100% preoperative arrhythmia burden towards a 0.1% arrhythmia burden measured at the end of the blanking period. This suggests that the thoracoscopic substrate modification (with brief AAD therapy) is sufficient to, at least initially, convert all patients to a situation where they are nearly AF free. In that case, more extensive lesion sets or even hybrid procedures would not be needed to further improve initial success, but rather to prevent late recurrences. With 50% of the patients remaining free from recurrences at long-term follow-up after a single procedure, an initial strategy of a more aggressive ablation would not be the preferred approach, as it would result in overtreatment of a large percentage of patients. Still, the reported strategy of the current study may already overtreat patients, as 20–24% pulmonary vein isolation-alone responders have been reported in endocardial ablation studies (1-4).

Furthermore, another interesting observation of continuous rhythm monitoring is the earlier, but not more numerous documentation of recurrences. Since the intermittent group mostly relies on the presentation of patients with symptomatic recurrences (92% of recurrences were based on patients presenting outside standard follow-up moments), this would indicate that asymptomatic AF episodes as detected by continuous monitoring precede the symptomatic AF in these patients. Whether use of continuous rhythm monitoring would provide additional value in a clinical setting remains to be determined.

Although there are no large registries for minimally invasive surgical ablation that provide robust insight into the incidence of adverse events, data from smaller studies (16-18) show complication rates in the range of 7.8–23.0% per procedure (for reference, 14.3% in this study). This is higher than the complication rates for catheter ablation procedures which have been well studied and reported in worldwide surveys, and generally range between 3.9% and 12.6% (1,4,19,20). However, the treatment of patients with symptomatic LSPAF using endocardial techniques generally requires multiple procedures and thus the risks are cumulative. Therefore, the optimal balance between the number of procedures, efficacy and risks in the treatment of these patients needs to be determined. The data reported in this study show that thoracoscopic ablation may play a role in the treatment strategy of patients with LSPAF. Multicentre registries with larger patient groups, preferably

including quality of life measurements, are needed to answer the question whether the strong arrhythmia outcome is worth the cost in procedural complications. Finally, cardiologists and surgeons should discuss with their patients all pros and cons of a more invasive surgical procedure with an anticipated superior efficacy, but with a higher event rate, to achieve optimal shared decision-making.

Study limitations

The retrospective nature and small number of patients in this study influence the conclusions that can be drawn from the data. Actual AF freedom rates might be overestimated in this study as asymptomatic arrhythmia episodes may not have been detected by intermittent 24-h Holter monitoring. Particularly between 2 and 5 years, no systematic Holter monitoring was performed and detection of recurrence was mainly based on patients presenting to their physician. Due to limited battery capacity of ILRs, rhythm monitoring in the continuous group beyond 3 years relied on incidental 24-h Holter monitoring. The comparison of continuous and intermittent follow-up in relation to rhythm outcome may be limited by the majority of the patients in the continuous group (80%) being derived from 1 centre, possibly influencing outcomes by differences in clinical baseline characteristics and risk factors, and/or clinical protocols and practice. A comparison of baseline, procedural and follow-up characteristics between the 2 groups has been provided in **Supplemental Table 4.**

Conclusion

Thoracoscopic PV and box isolation is effective in long-term restoration of sinus rhythm in LSPAF, especially when the thoracoscopic procedure is complemented by an endocardial touch-up procedure in case of recurrence, as demonstrated by the 68% freedom rate at 5 years. Continuous rhythm monitoring revealed earlier, but not more numerous documentation of recurrences up to long-term follow-up.

References

1. Tilz, R.R. et al. Catheter ablation of long-standing persistent atrial fibrillation: 5-year outcomes of the Hamburg Sequential Ablation Strategy. J Am Coll Cardiol. 2012;60:1921-9.

2. Brooks, A.G. et al. Outcomes of long-standing persistent atrial fibrillation ablation: a systematic review. Heart Rhythm. 2010;7:835-46.

3. Clarnette, J.A. et al. Outcomes of persistent and long-standing persistent atrial fibrillation ablation: a systematic review and meta-analysis. Europace. 2018;20:f366-f76.

4. Teunissen, C. et al. Five-year efficacy of pulmonary vein antrum isolation as a primary ablation strategy for atrial fibrillation. Europace. 2016;18:1335-42.

5. Roberts, K.C. et al. Anatomically determined functional conduction delay in the posterior left atrium relationship to structural heart disease. J Am Coll Cardiol. 2008;51:856-62.

6. Thiyagarajah, A. et al. Feasibility, Safety, and Efficacy of Posterior Wall Isolation During Atrial Fibrillation Ablation: A Systematic Review and Meta-Analysis. Circ Arrhythm Electrophysiol. 2019;12:e007005.

7. Kumar, P. et al. Challenges and Outcomes of Posterior Wall Isolation for Ablation of Atrial Fibrillation. J Am Heart Assoc. 2016;5.

8. Harlaar, N. et al. Clamping versus nonclamping thoracoscopic box ablation in long-standing persistent atrial fibrillation. J Thorac Cardiovasc Surg. 2020;160:399-405.

9. Voeller, R.K., Zierer, A., Schuessler, R.B. & Damiano Jr., R.J. Performance of a novel dual-electrode bipolar radiofrequency ablation device: a chronic porcine study. Innovations (Phila). 2011;6:17-22.

10. Calkins, H. et al. 2017 HRS/EHRA/ECAS/APHRS/SOLAECE expert consensus statement on catheter and surgical ablation of atrial fibrillation. Heart Rhythm. 2017;14:e275-e444.

11. Burkhardt, J.D., Di Biase, L. & Natale, A. Long-standing persistent atrial fibrillation: the metastatic cancer of electrophysiology. J Am Coll Cardiol. 2012;60:1930-2.

12. Lapenna, E. et al. Long-term Outcomes of Stand-Alone Maze IV for Persistent or Long-standing Persistent Atrial Fibrillation. Ann Thorac Surg. 2020;109:124-31.

13. Ad, N., Holmes, S.D. & Friehling, T. Minimally Invasive Stand-Alone Cox Maze Procedure for Persistent and Long-Standing Persistent Atrial Fibrillation: Perioperative Safety and 5-Year Outcomes. Circ Arrhythm Electrophysiol. 2017;10.

14. Haldar, S. et al. Catheter ablation vs. thoracoscopic surgical ablation in long-standing persistent atrial fibrillation: CASA-AF randomized controlled trial. Eur Heart J. 2020.

15. Ohtsuka, T., Nonaka, T., Hisagi, M. & Ninomiya, M. En Bloc Left Pulmonary Vein and Appendage Isolation in Thoracoscopic Surgery for Atrial Fibrillation. Ann Thorac Surg. 2018;106:1340-47.

16. van Laar, C. et al. Thoracoscopic ablation for the treatment of atrial fibrillation: a systematic outcome analysis of a multicentre cohort. Europace. 2019;21:893-99.

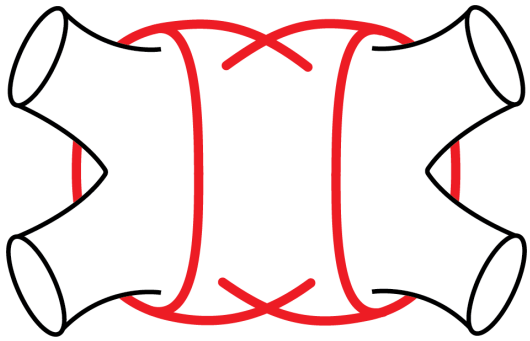
17. Boersma, L.V. et al. Atrial fibrillation catheter ablation versus surgical ablation treatment (FAST): a 2-center randomized clinical trial. Circulation. 2012;125:23-30.

18. Vos, L.M. et al. Totally thoracoscopic ablation for atrial fibrillation: a systematic safety analysis. Europace. 2018;20:1790-97.

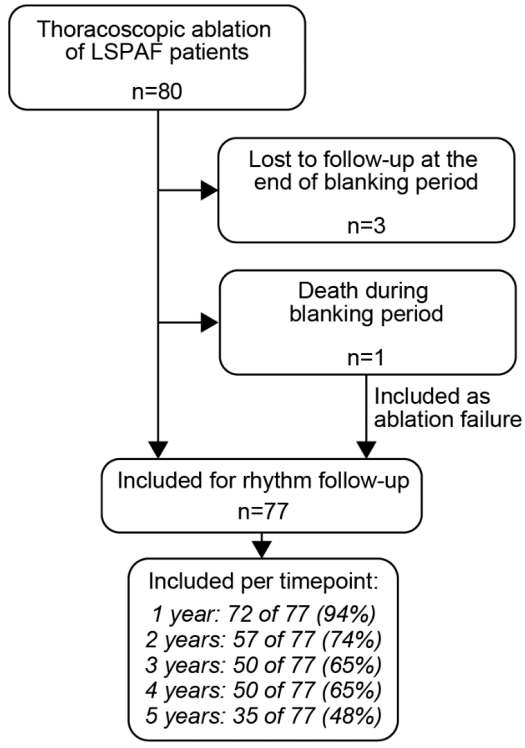
19. Steinbeck, G., Sinner, M.F., Lutz, M., Muller-Nurasyid, M., Kaab, S. & Reinecke, H. Incidence of complications related to catheter ablation of atrial fibrillation and atrial flutter: a nationwide in-hospital analysis of administrative data for Germany in 2014. Eur Heart J. 2018;39:4020-29.

20. Bertaglia, E. et al. Early complications of pulmonary vein catheter ablation for atrial fibrillation: a multicenter prospective registry on procedural safety. Heart Rhythm. 2007;4:1265-71.

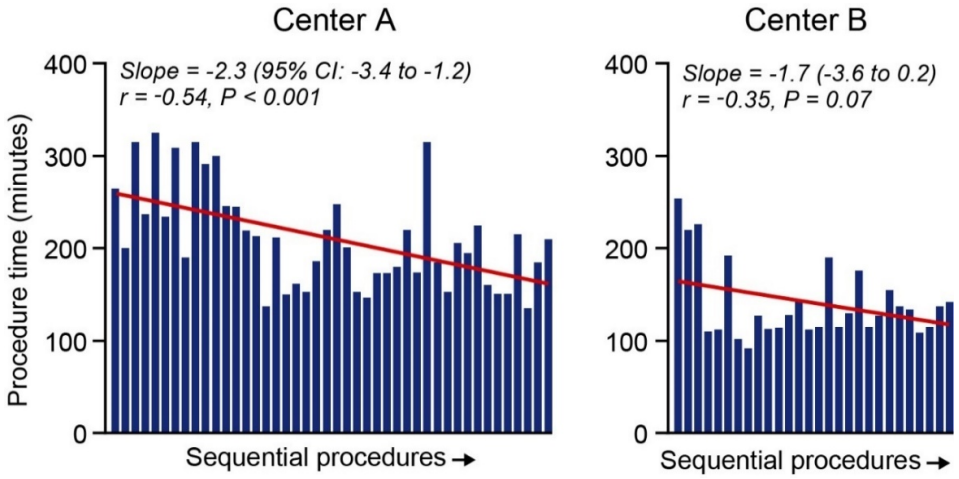
Supplemental information



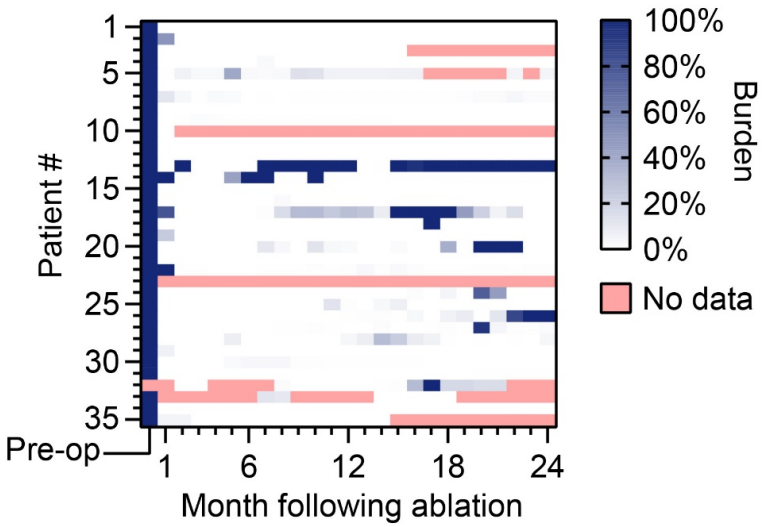
Supplemental Figure 1. Schematic of the Gemini-S lesion set used to isolate the pulmonary veins and left atrial posterior wall during thoracoscopic ablation.



Supplemental Figure 2. Flowchart depicting the selection of patients for the long-term rhythm analysis following ablation, as well as number included per timepoint.



Supplemental Figure 3. Sequential procedure times plotted of the two centers included in this study with interpolation of a linear standard curve (in red) to assess trend directionality. Respective mean decreases in procedure time of 2.3 and 1.7 minutes per procedure.



Supplemental Figure 4. Atrial arrhythmia burden shown per patient over the first two years following thoracoscopic ablation. Each row represents an individual patient.

Supplemental Table 1. Details of catheter touch-up interventions following recurrence

Patient	Type of SVT	Interval (months)	Touch-up intervention
1A	AF	6	Reisolation of LPV/Box + CFAE ablation (LA) + CTI lesion
2B	AF	10	MI lesion + CFAE ablation (RAA/IAS)
2B	AFL	18	CTI lesion + CFAE ablation (IAS)
3A	AF	12	CFAE ablation (LA) + LAA isolation + VCS isolation
4A	AF	13	Reisolation of LPV/RPV/Box
5A	AFL	13	MI lesion
6A	AFL	18	CTI lesion
7A	AF	19	Reisolation of LPV/RPV/Box + CTI lesion
7A	AF	29	Reisolation of RPV/Box + CTI lesion
8B	AF	22	Reisolation of LPV/RPV/Box + CTI and MI ablation
9B	AF	23	Reisolation of Box + MI lesion
10B	AF	27	LAA isolation + CTI lesion
11B	AF	28	Ablation LAA ridge + MI lesion + CS ablation
12B	AF	32	Reisolation of Box + LAA base + MI lesion
13B	AF	35	Ablation LAA ridge
14A	AF/AT	36	Isolation of VCS
14A	AF/AT	42	Reisolation of VCS + CFAE ablation (RA)
15B	AF	46	CFAE ablation (LA) + MI lesion
16A	AF/AFL	47	MI and CTI lesions

AF: atrial fibrillation, AFL: atrial flutter, AT: atrial tachycardia, CFAE: complex fractionated atrial electrograms, CS: coronary sinus, CTI: cavotricuspid isthmus, IAS: interatrial septum, LAA: left atrial appendage, LA: left atrium, LPV: left pulmonary veins, MI: mitral isthmus, RPV: right pulmonary veins, RAA: right atrial appendage, RA: right atrium, SVT: supraventricular tachycardia, VCS: vena cava superior

Procedure performed in: A = Center A, B = Center B

Supplemental Table 2. Cox regression analysis for predictors of atrial arrhythmia recurrence.

Variable	HR (95% CI)	*P*-value
Univariate		
Age	1.00 (0.96-1.05)	0.86
Female gender	1.32 (0.62-2.85)	0.47
Years since first AF episode	1.12 (1.00-1.26)	0.05
Left atrial volume index	1.05 (1.02-1.08)	0.001
Body mass index	0.98 (0.91-1.07)	0.72
Prior catheter ablation	1.99 (0.81-4.88)	0.13
Sinus rhythm at end of procedure	0.65 (0.28-1.52)	0.33
LAA exclusion	0.71 (0.35-1.44)	0.34
Multivariable		
Years since first AF episode	1.08 (0.96-1.22)	0.18
Left atrial volume index	1.05 (1.02-1.09)	0.001
Prior catheter ablation	1.06 (0.41-2.76)	0.91

CI: confidence interval, HR: hazard ratio, LAA: left atrial appendage

Supplemental Table 3. Cox regression analysis of categorized LAVI as predictor of atrial arrhythmia recurrence to demonstrate linearity.

LAVI	HR (95% CI)	*P*-value
< 35 ml/m2	Reference group	
35-45 ml/m2	8.6 (1.1-66.5)	0.04
45-55 ml/m2	10.3 (1.3-82.6)	0.03
55-65 ml/m2	23.5 (2.8-195.3)	0.003
> 65 ml/m2	23.9 (2.8-205.6)	0.004

CI: confidence interval, HR: hazard ratio, LAVI: left atrial volume index

Supplemental Table 4. Patient baseline, procedural and follow-up characteristics of the intermittent monitoring group and continuous rhythm monitoring group.

Characteristic	All (*n* = 77)	Intermittent (*n* = 42)	Continuous (*n* = 35)	*P*-value
Baseline characteristics				
Age (years)	58.9 ± 7.7	58.9 ± 7.2	58.9 ± 8.4	0.99
Female	17 (22%)	28 (80%)	32 (76%)	0.69
Time since first AF diagnose (y)	3.8 [1.9-6.3]	3.0 [1.5-5.2]	4.7 [2.9-6.8]	0.02
Left atrial volume index (ml/m^2)	46 ± 13	43 ± 12	50 ± 13	0.02
CHA2DS2-VASc score	1 [0-2]	1 [0-2]	1 [0-2]	0.11
Body Mass Index (kg/m^2)	27.5 ± 3.7	26.7 ± 3.4	28.5 ± 3.9	0.03
Prior catheter ablation	12 (16%)	5 (12%)	7 (20%)	0.33
Procedure				
LAA exclusion	51 (66%)	21 (50%)	30 (86%)	< 0.01
Sinus rhythm end of procedure	68 (88%)	35 (83%)	33 (94%)	0.17
Follow-up				
Follow-up duration	3.0 [1.3-5.2]	2.6 [1.0-5.0]	3.0 [3.0-5.6]	0.78
Catheter touch-up procedures	16 (21%)	6 (14%)	10 (29%)	0.15
Number of touch-up procedures*	1 [1-1]	1 [1-2]	1 [1-1]	0.26
AAD use at latest follow-up	5 (14%)	3 (16%)	2 (13%)	0.90

Data are presented as *n* (%), mean ± SD or median [IQR]. *Within individuals requiring a touch-up procedure.
AAD: antiarrhythmic drug, AF: atrial fibrillation, IQR: interquartile range, TIA: transient ischemic attack, SD: standard deviation

Part Two

Development of clinically relevant human *in vitro* models of atrial fibrillation



Chapter 4



Excised human atrial tissue-based models for investigating atrial electrophysiology

Thesis-only

Niels Harlaar, Robert J. M. Klautz, Thomas J. van Brakel, Antoine A. F. de Vries, Daniël A. Pijnappels

Abstract

Atrial fibrillation (AF) is the most common cardiac arrhythmia for which limited, mostly symptomatic therapeutic options exist. Acquiring better mechanistic insight into AF for developing novel therapeutics is hampered by the lack of representative models of AF. This study aims to better characterize the electrophysiological properties of excised human atrial tissue and to assess whether this tissue can be used to create culturable cardiac tissue slices suitable for ex vivo electrophysiological studies. In this pilot study, 57 atrial appendages were collected during open heart surgery and were subjected to various analyses and procedures, including immunohistochemistry, optical voltage mapping and vibratome tissue slicing. During optical voltage mapping, 28 of 31 collected (unsliced) atrial appendages were excitable upon electrical point stimulation. The area of excitation was variable, with only 32% of the mapped appendages showing excitation in more than half of the tissue. In the excitable appendages, the mean conduction velocity was 40 ± 14 cm/s and the average action potential duration measured 320 ± 106 ms at 80% of repolarisation. Generation of atrial tissue slices proceeded without complications in three-quarters of cases and resulted in 200-350 µm tissue slices with limited structural damage visible under microscopy. However, optical voltage mapping subsequently revealed that only 12% of attempts yielded clearly excitable atrial tissue slices. Efforts to culture the generated atrial tissue slices were made using the liquid-air interface method. Unfortunately, following 24-hour culture, optical voltage mapping revealed these slices to be non-excitable. To conclude, we found a high rate of variability in the excitability of harvested atrial appendages and atrial tissue slices in this study. Further research is necessary to improve on the reliability of this promising preclinical research tool.

Introduction

Atrial fibrillation (AF) is the most common cardiac arrhythmia with an estimated prevalence of 2-4% in the adult population (1), making it an important contributor to morbidity, mortality and healthcare costs (2, 3). The current treatment strategy is aimed at altering the diseased atrial substrate to disfavour AF induction/maintenance (e.g. ablation, anti-arrhythmic drugs) and/or reducing the negative consequences associated with AF (e.g. anti-coagulation, ventricular rate control) (4). Although generally effective, these therapies are associated with a high degree of invasiveness or are associated with significant side effects due to the need for life-long use. Studies aimed at acquiring better mechanistic insight into the initiation, maintenance and termination of AF, with the goal of developing novel therapies, are hampered by the lack of representative models of AF.

Historically, animal(-derived) models have played a prominent role in preclinical studies due to their accessibility, reproducibility and gross similarity to the human heart. The more subtle differences in (patho)physiology and anatomy as compared to actual patients, however, frequently results in failure to translate findings to the clinic (5). Human atrial tissue, routinely available as waste material during cardiac surgery, provides an option that is more representative of human (patho)physiology. The application of this material has predominantly been limited to acute (electrophysiological) measurements due to poor survival and rapid dedifferentiation upon loss of perfusion following resection (6).

One strategy to prolong the *ex vivo* survival of cardiomyocytes is to conserve the extracellular matrix, while maintaining diffusion of nutrients and oxygen. To achieve this, thin tissue slices measuring generally between 300-400 µm have previously been produced of animal heart tissue and explanted human hearts rejected for transplantation (7). These cardiac tissue slices could even be cultured for several days (sometimes up to weeks), while maintaining (a degree of) contractility and excitability. Expanding this technology to readily available surgically excised atrial tissue could create a new source of culturable human atrial cardiomyocytes, that could aid pre-clinical AF research and could even open up the possibility of patient-specific *ex vivo* studies.

The aims of this study are to better characterize the electrophysiological properties of excised atrial tissue and to assess how excised atrial tissue can be

used to create (culturable) cardiac tissue slices suitable for *ex vivo* electrophysiological studies.

Materials and methods

Cardiac tissue collection

This study was conducted with approval of the institutional review board of the Leiden University Medical Center (P13.043) and in compliance with the International Code of Medical Ethics of the World Medical Association. Right atrial appendages were collected following cardiopulmonary bypass, whereas the left atrial appendages were removed in AF patients to reduce their thromboembolic risk. All collected tissue constituted surgical waste material, which otherwise would be discarded. The tissue described in this study was collected between 2015 and 2018.

Atrial appendages resected during cardiac surgery were rapidly transported in cold (4°C) oxygenated modified Tyrode's solution (MTS) containing: NaCl 143 mM, KCl 5.4 mM, $CaCl_2$ 1.8 mM, $MgCl_2$ 0.5 mM, NaH_2PO_4 0.33 mM, Glucose 10 mM, 2,3-Butanedione 2-Monoxime (BDM, Sigma-Aldrich) 10 mM and HEPES-NaOH 10 mM (pH 7.4). Tissue that would be subsequently used for tissue slicing was retrieved in MTS containing 0.9 mM $CaCl_2$ (from now on: ½-MTS). Time between excision and start of processing for optical voltage mapping or tissue slicing was generally shorter than 15 minutes.

Tissue slicing

Tissue samples taken from the atrial appendages (largest dimension generally < 10 mm) were selected for suitable fibre orientation, *i.e.* oriented parallel to the longitudinal axis. Tissue samples were embedded in 4% low melting point agarose (type VII-A, Sigma-Aldrich) prepared using ½-MTS at 37°C. Following solidification of the agarose on ice, samples were fixed to the sample holder of the vibratome (VT1200S, Leica Microsystems) using Histoacryl (Braun) and subsequently covered in cold (4°C) oxygenated ½-MTS. Next, tissue slices 200-350 µm thick were generated using ceramic injector blades (Cadence Inc.) on the vibratome (baseline settings: advancement speed 0.03 mm/s, amplitude 2 mm, z-axis deviation < 0.5 µm). Following slicing, the tissue slices stored in cold (4°C) oxygenated ½-MTS were slowly warmed to room temperature to recover. After 30 minutes of recovery, and a switch to oxygenated MTS, tissue slices were processed for subsequent experiments.

Organotypic culture

Following recovery, slices were washed in six subsequent baths of sterile phosphate buffered saline (PBS) to remove contaminants. Atrial tissue slices were placed on semi-porous PTFE cell culture insert (0.4 µm pore size, Millipore) in a 6-well plate. Culture medium was added under the membrane, consisting of M199 medium (Thermo Fisher Scientific) supplemented with 100 units/mL of penicillin and 100 µg/mL of streptomycin (Thermo Fisher Scientific), 2% B27 supplement (Thermo Fisher Scientific) and 94 ng/mL of both linoleic and oleic acid (Sigma-Aldrich). Slices were kept at 37°C in humidified 95% air-5% CO_2 environment.

Histology

Atrial tissue was fixed using 4% formaldehyde (24 h) and dehydrated by immersion in 70% ethanol (24 h), 96% ethanol (4 h), 100% ethanol (4 h) and 1-butanol (12 h), before being embedded in paraffin. Next, 5 µm sections of the paraffin embedded tissue were cut, mounted on microscope slides (StarFrost, VWR International) and deparaffinized by xylene immersion (10 min) directly after a 30 min incubation period at 60°C. Sections were rehydrated by subsequent immersion in 100% ethanol, 96% ethanol, 70% ethanol, 50% ethanol and demineralized water (5 min per step).

For immunohistochemical staining, subsequent antigen retrieval was performed using trypsin (15 min incubation in 0.05% trypsin [Sigma-Aldrich], pH 7.8, 37°C). To block non-specific background staining, slides were incubated with 10% normal donkey serum (Sigma-Aldrich) in PBST (0.05% Tween 20 [Sigma-Aldrich] in PBS) for 1 h at room temperature. Slides were subsequently exposed to the primary antibody in PBS containing 2% normal donkey serum overnight at 4°C. Secondary antibody incubation was performed in PBS containing 2% normal donkey serum for 2 h at room temperature. Nuclei were stained for 10 min with Hoechst 33342 solution (Thermo Fisher) diluted 1:1,000 in PBS. In between steps, slides were washed with PBST. Details on the antigen retrieval method and antibody usage for each antigen are denoted in **Table 1**.

For haematoxylin and eosin (H&E) staining, sections were first immersed in haematoxylin (J.T. Baker) for 5 min, followed by a 10 min suspension in flowing water. Following dehydration by subsequent immersion in 25%, 50%, 70%, 80% and 96% ethanol (1 min per step), sections were stained with 1% eosin (VWR) in 96% ethanol for 2 min. Following two 1 min suspensions in 96% ethanol,

sections were suspended two times in xylene (VWR) for 1 min, before being mounted in Depex Mounting Media (VWR).

Images were acquired using the Eclipse 80i Upright Microscope (Nikon), which was equipped with filter blocks (all from Nikon): C-FL EPI-FL DAPI (MBE41300, Excitation: 340-380 nm, Emission: 435-485 nm), C-FL EPI-FL TRITC (MBE45600, Excitation: 540/25 nm, Emission: 605/55 nm), C-FL EPI-FL FITC (MBE44720, Excitation: 465-495 nm, Emission: 515-555), and lenses: CFI Plan Fluor 20X (N20XW-PF, Nikon) and CFI Plan Fluor 40X (N40XW-PF, Nikon). Exposure times varied between 50-200ms, depending on the staining.

Table 1. Antibodies.

Antigen	Host	Dilution	Supplier	Catalogue number	Secondary antibody
ACTN2	Mouse	1:200	Sigma-Aldrich	A7811	A10037
COL1A	Rabbit	1:100	Abcam	ab34710	A21206
GJA1	Rabbit	1:500	Sigma-Aldrich	C6219	A10042
GJA5	Goat	1:50	Santa Cruz Biotechnology	sc-20466	A11055
Antigen	**Host**	**Dilution**	**Supplier**	**Catalogue number**	**Conjugate**
Mouse IgG (H+L)	Donkey	1:200	Thermo Fisher Scientific	A10037	Alexa Fluor 568
Rabbit IgG (H+L)	Donkey	1:200	Thermo Fisher Scientific	A10042	Alexa Fluor 568
Goat IgG (H+L)	Donkey	1:200	Thermo Fisher Scientific	A11055	Alexa Fluor 488
Rabbit IgG (H+L)	Donkey	1:200	Thermo Fisher Scientific	A21206	Alexa Fluor 488

Optical voltage mapping.

Excised atrial tissue was rinsed in PBS to remove blood remnants and incubated with 12 µM di-4-ANEPPS (Thermo Fisher Scientific) in MTS for 25 min under continuous agitation and oxygenation at 37°C. Following incubation, atrial tissue was washed in MTS and fixated using specimen pins unto a silicone mat. During optical voltage mapping, the specimen was kept at 37°C and MTS

was routinely sprayed over the epicardium to prevent drying out. Atrial tissue slices were incubated with 12 μM di-4-ANEPPS in MTS for 25 min under continuous agitation and oxygenation at 37°C. Slices were subsequently placed in a perfusion chamber (RC-27L, Warner Instruments) and kept in place using a mesh anchor (SH-26GH/15, Warner Instruments), where a continuous flow of oxygenated MTS (37°C) was provided in-between recordings.

Excitation light (525 ± 25 nm) was delivered by a halogen arc-lamp through epi-illumination after which emission light passed through a dichroic mirror and a long-pass emission filter (> 590 nm). Signals were acquired using a 100×100 pixels complementary metal oxide semiconductor camera (MiCAM Ultima-L, SciMedia) at a spatial resolution of 160 or 250 μm/pixel (depending on the size of the appendage) or 31/79 μm/pixel (depending on the size of the tissue slices) and temporal resolution of 6 ms per frame, with an acquisition time of 6 s.

Electrical stimulation (8 V, 10 ms square pulses) was performed using two parallel stainless-steel electrodes (whole appendages) or epoxy-coated bipolar parallel platinum electrode (tissue slices). The electrodes were connected to an STG 2004 stimulus generator (Multi Channel Systems) driven by MC Stimulus II software (v3.5.0, Multi Channel Systems). The location of pacing was chosen at random, where the best of three locations was used for analysis.

Data was analysed using BrainVision Analyzer (v16.04.20, BrainVision). Signals were averaged with those of the 8 nearest neighbouring pixels to minimise noise artefacts. Conduction velocity (CV) and action potential duration at 80% of repolarization (APD80) were determined at a minimum of three (for CV) and five (for APD) different vectors/locations equally distributed throughout the tissue.

Statistical analysis.

Statistical analyses were performed using GraphPad Prism v9.3.1. Data are presented as Mean ± SD. Restitution was analysed using a mixed-effects analysis, with a Geisser-Greenhouse correction to account for missing values.

Results

Excised human atrial appendages

In total, 57 atrial appendages were collected for the different analyses described in this exploratory study. The left atrial appendage (LAA) was almost exclusively obtained from AF patients, whereas the right atrial appendage

(RAA) was also obtained from patients without a history of AF. Comparing left and right specimens, epicardial fat depositions were generally more prominent on the LAA, sometimes also showing fatty infiltrations into the tissue (**Figure 1a, b**). Another notable difference is the thick endocardial fibroelastosis seen in the LAA, that was generally absent in the RAA. These two changes to (particularly) the left atrium, have been previously associated with the presence of AF (8).

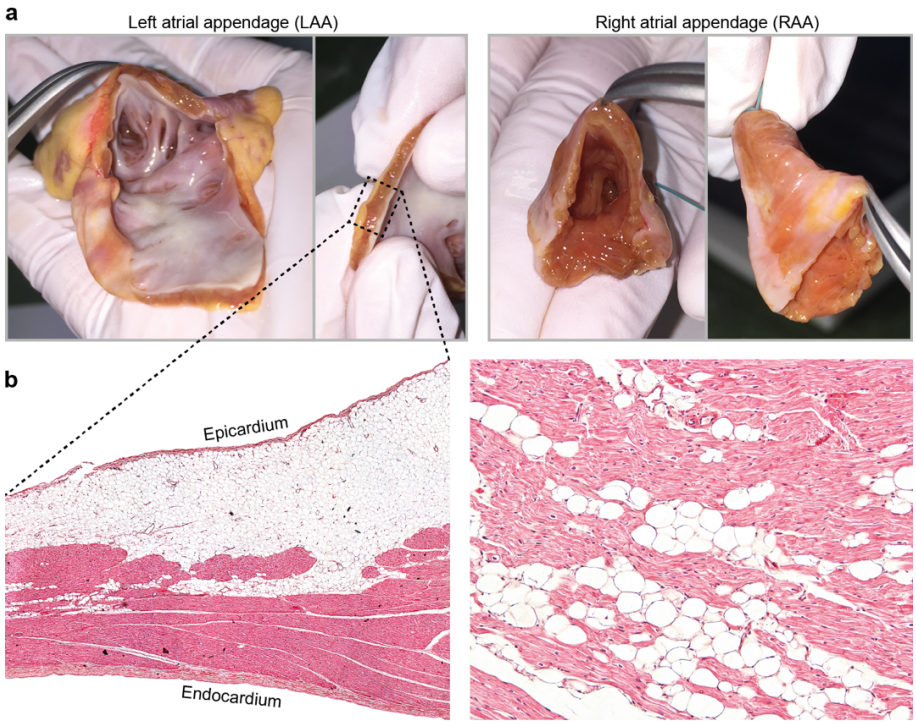


Figure 1. (a) Photographs of the excised atrial appendages of a patient with AF, highlighting the differences in epicardial fat deposition and endocardial fibroelastosis between the LAA and RAA. **(b)** H&E staining showing (left) a transmural section of the LAA and (right) presence of fatty infiltrations into the myocardium.

To assess the general quality of the resected atrial tissue, immunohistochemistry was performed. Strong connexin 40 (GJA5) and connexin 43 (GJA1) signal was located at the intercalated disks, combined with a striated pattern of α-actinin 2 (ACTN2) in the cardiomyocytes and an interstitial signal of type I collagen (COL1A). (**Figure 1c**). Further comparison of type I collagen staining between AF and non-AF patients showed visually thicker interstitial fibrosis in the patients with an history of (persistent) AF (**Figure 1d**). Given the already available literature on the structural between

patients in sinus rhythm and atrial fibrillation (9), no quantitative studies were performed regarding this subject.

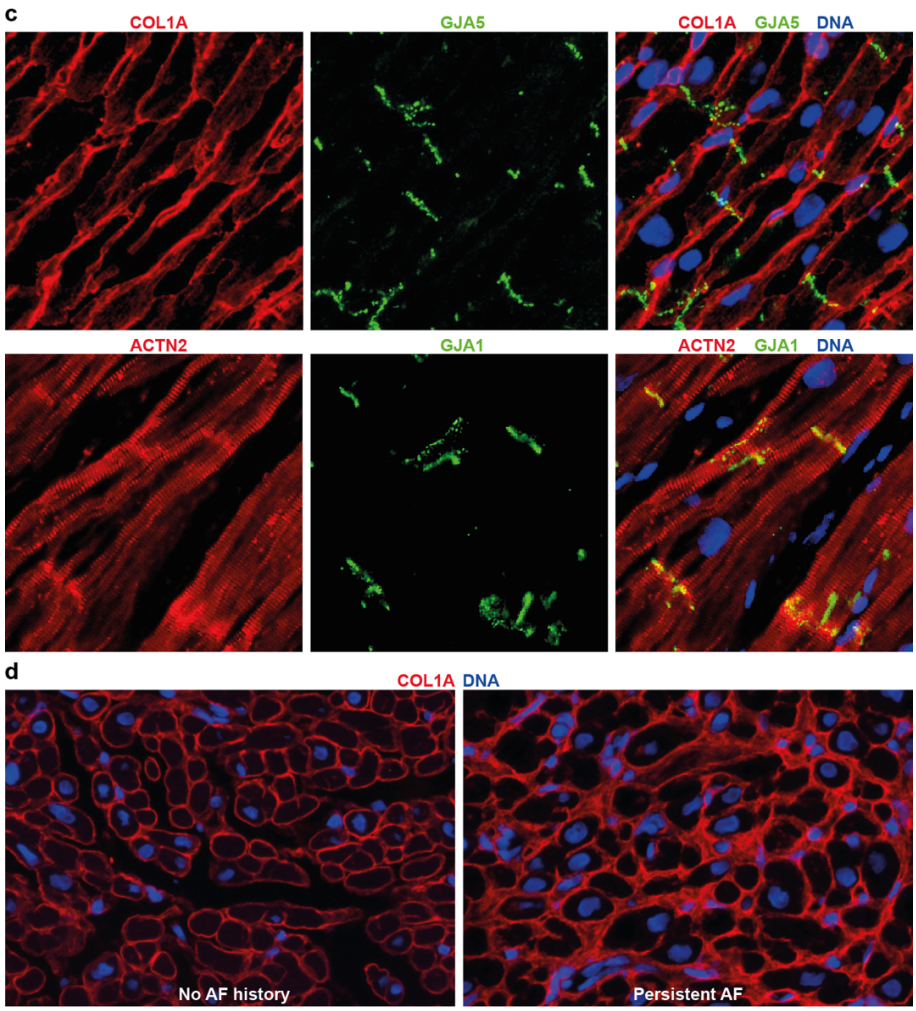


Figure 1 (continued). (c) Immunostaining of excised atrial tissue for type I collagen (COL1A), connexin 40 (GJA5), α-actinin 2 (ACTN2) and connexin 43 (GJA1). **(d)** Staining of type I collagen in RAA tissue of a patient without and with AF to compare the degree of fibrosis.

Optical voltage mapping of atrial appendages

To assess their electrophysiological properties, the atrial appendages were subjected to optical voltage mapping shortly after resection. Here, the far majority of tissue samples were excitable upon local electrical stimulation (28 of 31 samples), although the degree of tissue activation differed strongly as

shown in **Figure 2a, b**. Here, it should be noted that epicardial fat frequently obstructed the myocardium, for which was not corrected in this classification. The optical action potentials were predominantly triangular shaped and measured 320 ± 106 ms at 80% of repolarisation on average, with a mean conduction velocity of 40 ± 14 cm/s (**Figure 2c, d**). The action potential duration (P = 0.03) and conduction velocity (P = 0.16) shortened upon pacing at a decreasing cycle length as shown in **Figure 2e, f**. No spontaneous re-entrant activation or automaticity was observed in any of the samples.

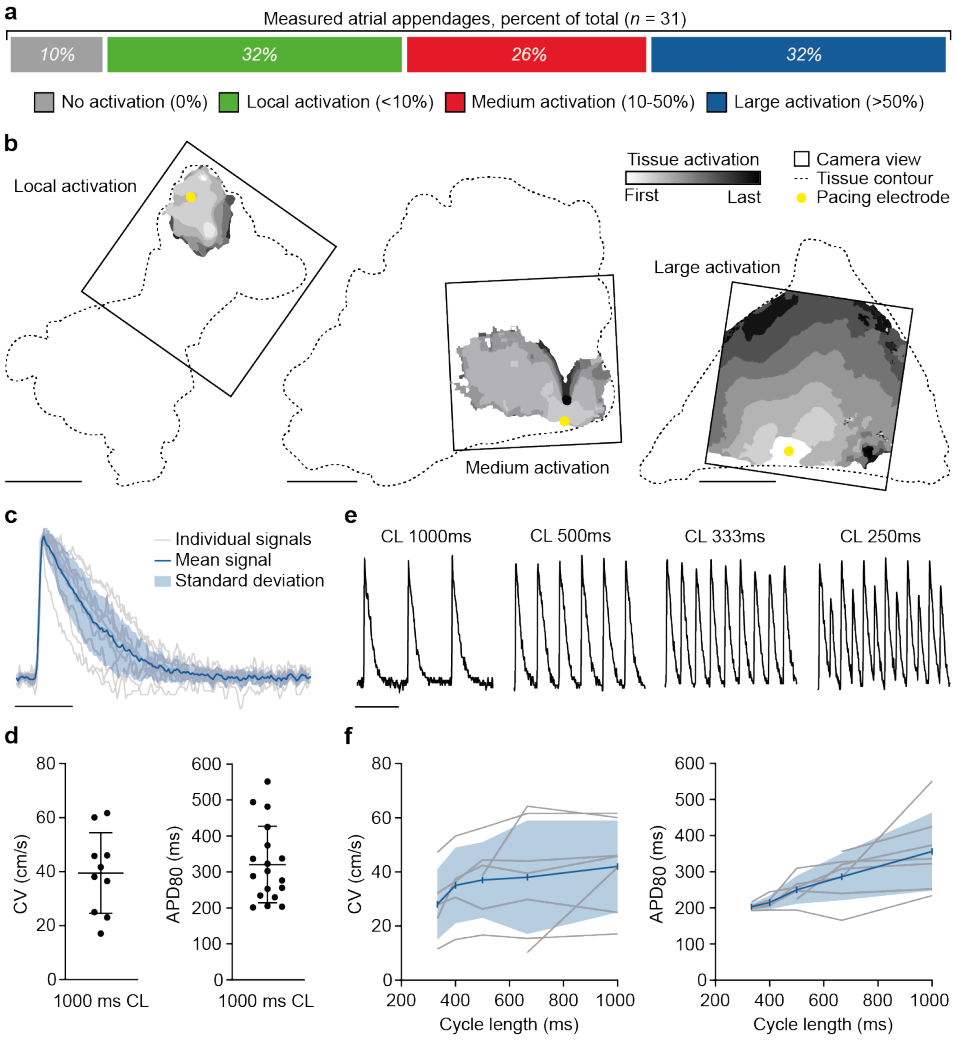


Figure 2 (legend on next page).

Figure 2 (previous page). Electrophysiological properties of excised atrial tissue. **(a)** Area (%) of excised atrial tissue excited upon electrical stimulation, divided into four categories of activation degree ($n = 31$). **(b)** Representative activation maps of the local, medium and large activation categories. Dotted line represents the excised atrial tissue outline. Scale bar, 1 cm. **(c)** Mean optical voltage trace at 1000 ms cycle length ($n = 10$). Scale bar, 200 ms. **(d)** Conduction velocity (CV, $n = 10$) and action potential duration at 80% of repolarization (APD_{80}, $n = 18$) of excised atrial tissue. Mean, SD. **(e)** Representative optical voltage traces of excised atrial tissue at various cycle lengths (CL) of electrical stimulation. Scale bar, 1000 ms. **(f)** APD and CV restitution curves of excised atrial tissue ($n = 7$). Mean shown with individual tissues shown in grey and the highlighted area showing SD.

Cardiac tissue slicing

Next, small samples of the atrial tissue were selected for slicing. In short, these samples were embedded in agarose and sliced into thin tissue slices using a vibratome. These could then be used to perform acute electrophysiological measurements or could potentially be put into culture. This process, as shown in **Figure 3a-d**, has been described in detail the **Methods** section. For this study, a total of 26 appendages were sliced. Of note, between these 26 procedures, minor changes in blade advancement speeds, blade amplitudes, slice thickness and recovery protocol were made to attempt to optimize the procedure.

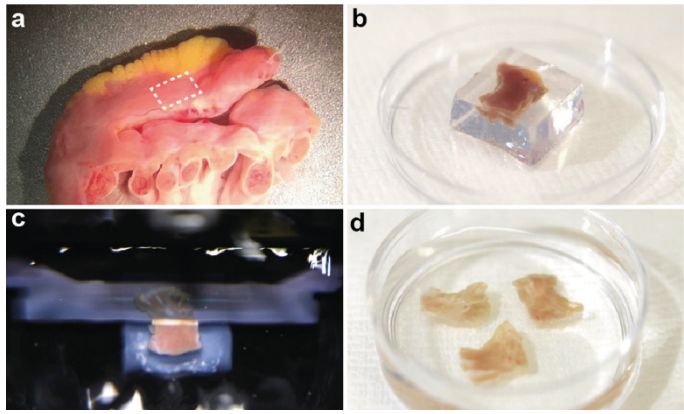


Figure 3. Human atrial tissue slice preparation. **(a)** Sampling of atrial tissue from left atrial appendage. **(b)** Embedding of tissue sample in low-melting agarose. **(c)** Slicing of embedded sample, resulting in **(d)** 350 µm atrial tissue slices.

Optical voltage mapping of atrial tissue slices

Roughly a quarter of attempts were complicated by technical issues, such as tough fibrosis causing the tissue sample to be pulled from the agarose support as shown in **Figure 4a**. Still, in the majority of cases, atrial tissue slices were successfully produced. Upon microscopic inspection, these slices showed minimal damage and relatively clean cutting surfaces (**Figure 4b**). Subsequent optical voltage mapping revealed that only a small subset of slices showed good electrical activation upon pacing (3 out of 26 attempts), as can be seen in **Figure 4c**. These could be stimulated at variable frequencies between 1-4 Hz. The remaining attempts produced slices that showed no electrical activation (11 out of 26 attempts) or poor electrical activation/pacing artifacts (5 out of 26 attempts) as shown in **Figure 4d**. No spontaneous re-entrant activation or automaticity was observed in any of the slices.

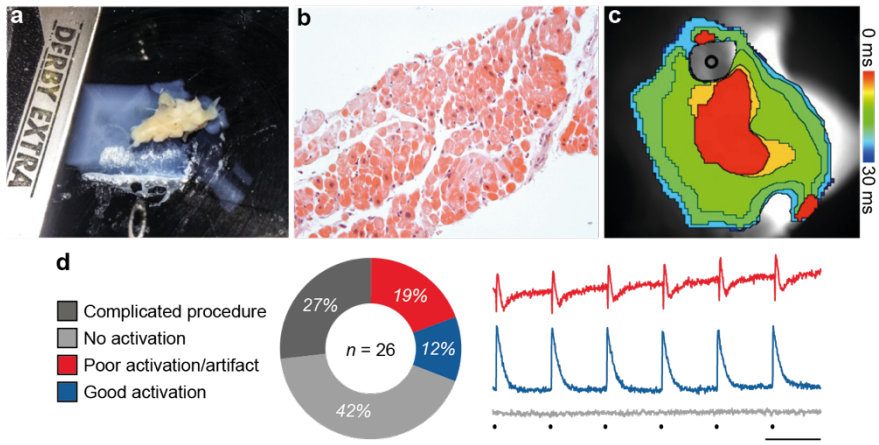


Figure 4. (a) Example of a complicated slicing procedure, where thick fibrosis results in pulling the tissue from the agarose support. **(b)** H&E staining showing a transverse view of an atrial tissue slice. **(c)** Representative activation map of an atrial tissue slice with good capture following electrical pacing and subsequent conduction to the rest of the slice. The black circle shows the position of the pacing electrode. **(d)** Percentage of atrial appendages from which the resulting atrial tissue slices were excitable during optical voltage mapping. On the right, representative optical voltage tracings of the different groups presented on the left during 1Hz electrical pacing. The *n*-number represent the number of atrial appendages, where generally multiple slices were produced per appendage. Here, the best outcome was included. Black dots show electrical stimuli. Scale bar, 1000 ms.

Culturing of atrial tissue slices

Despite the limited success rate described before, a few attempts to culture these slices were made using the liquid-air interface method. Three slices from samples that previously showed some degree of excitability during optical voltage mapping were cultured for 24 hours. Following this culture period, these slices no longer showed signs of excitability. Alternatively, culturing slices that were previously not excitable was also attempted, as it could be hypothesized that recovery following the damaging slicing procedure could improve the phenotype. However, following the 24-hour culture period, these slices remained non-excitable during optical voltage mapping.

Discussion

Atrial appendages are an attractive basis for an experimental model, given their availability and representativeness to the target patient population. In this exploratory study we performed acute electrophysiological measurements of resected atrial appendages using optical voltage mapping, before attempting to create culturable tissue slices that could be analysed using that same technique.

The majority of reported *ex vivo* optical voltage mapping data of human atria is derived from explanted human hearts (10,11). Optical voltage mapping of routinely available excised atrial tissue is less frequently described in literature, to our knowledge only by Krul et al. (12), which studied left atrial appendages removed during thoracoscopic ablation procedures. In our current study, while utilizing a comparable experimental setup, we studied both left- and right atrial tissue samples removed during various types of open-heart surgical procedures. Comparing data, the mean conduction velocity we describe in our study of 40 cm/s is lower than the 55 cm/s described in the study of Krul et al. and lower than measurements in intact human atria (90 cm/s (13)). No data on the action potential duration is reported in the Krul et al. study, but the average action potential duration in human atria is typically between 200-400 ms (14) compared to the 320 ms at 80% of repolarization reported in this study. In the present study, we also provide an overview of the percentage of atrial appendages collected that are excitable and their degree of excitability. These data show that, in the majority of cases, the atrial appendages remain viable and excitable following excision, although variation exists to the degree of excitation. It is unclear if the previously mentioned study has excluded any non-excitable tissues.

Despite the relative high degree of excitability, subsequent slices prepared from the resected atrial tissues were mostly not excitable during optical voltage mapping in our study. During the experiments no obvious bottlenecks could be identified, with it being possible that the cause of the suboptimal outcomes is multifactorial. The slicing protocol used in this study has been adapted from widely used protocols (15) and has been successfully applied in-house for producing excitable animal-derived heart tissue slices (16). When the experiments described in this study were performed (between 2015 and 2018), no studies were published that utilized atrial appendages for generating tissue slices. The bulk of literature described the generation of human ventricular slices from explanted hearts of rejected transplant hearts (7), with only a single study describing the generation of atrial tissue slices from these explant and transplant hearts (17). Here, samples were taken from the crista terminalis, which provide a smooth sample well suited for slicing, as compared to the fine pectinate muscles present in the left and right atrial appendages. Additionally, we found that these atrial appendages frequently contained fatty infiltrations, further hampering sample selection and blocking electrical conduction during optical voltage mapping.

Since the experiments in this study were performed, the field of culturable cardiac tissue slices has advanced significantly since the addition of mechanical load during culture was introduced by two groups in 2019 (18,19). This has allowed culture of cardiac tissue slices for an extended period of time, while preserving most of the contractile and excitable properties. However, the focus has still predominantly been on ventricular tissue slices. Recently, the first study applying this method to atrial tissue slices was published (20), using both atrial appendages and transplant/explant hearts as their tissue source. Here, in addition to the presence of mechanical load, electrical field stimulation and beta-adrenergic stimulation was applied. Using this method, atrial tissue slices maintained a degree of contractility up to 14 days in culture. The authors included an atrial tachyarrhythmia model, where slices were stimulated at 3 Hz as compared to 1Hz, resulting in a decreased contraction force with increased beat-to-beat variation. No electrophysiological readout was included in the study.

While the techniques to culture cardiac tissue slices have significantly improved over the years, it does not provide an explanation for our low success rate in generating excitable atrial tissue slices at baseline. However, based on the points mentioned before, we believe the following factors might contribute. First, the collected tissue samples were not completely uniform, comprising

left and right atrial appendages, which were harvested from both cardioplegically-arrested as well as beating hearts. Unfortunately, the current study protocol does not allow analysis of underlying patient characteristics or variations in operative procedures that might influence success. Second, atrial appendages itself might be a suboptimal tissue source compared to explant/transplant hearts, given the significant local (epicardial) fat depositions, finely trabeculated wall and overall different embryonic origin to the rest of the atria (8,21). Third, optical voltage mapping of the collected atrial appendages has demonstrated varying degrees of excitability. Given the difficulty to check excitability before slicing sample selection, it is possible that non-excitable parts of the appendage are selected for slicing. Fourth, the readout chosen (analysis of action potential generation and conduction following point stimulation during optical voltage mapping) is perhaps not feasible in atrial tissue slices, and is maybe too demanding as opposed to the electrical field stimulation or contraction analysis performed in the previously described studies (17,20). Fifth, following the damaging slicing procedure, atrial slices might require a recovery interval during which they are optimally mechanically, electrically and biochemically supported/stimulated, something which was not (optimally) applied in our current study.

To conclude, in this exploratory study we have assessed the *ex vivo* electrophysiological properties of resected atrial appendages. Where nearly all appendages were excitable upon electrical stimulation, the area of tissue that subsequently conducted the electrical activation differed strongly between the samples. The subsequent generation of atrial tissue slices from this material was successful, however it only yielded a very low percent of excitable tissue slices, likely due to several factors of influence that were difficult to address using the current study setup.

References

1. Benjamin EJ, Muntner P, Alonso A, Bittencourt MS, Callaway CW, Carson AP, et al. Heart Disease and Stroke Statistics-2019 Update A Report From the American Heart Association. Circulation. 2019;139(10):E56-E528.

2. Benjamin EJ, Wolf PA, D'Agostino RB, Silbershatz H, Kannel WB, Levy D. Impact of atrial fibrillation on the risk of death. Circulation. 1998;98(10):946-52.

3. Ringborg A, Nieuwlaat R, Lindgren P, Jonsson B, Fidan D, Maggioni AP, et al. Costs of atrial fibrillation in five European countries: results from the Euro Heart Survey on atrial fibrillation. Europace. 2008;10(4):403-11.

4. Hindricks G, Potpara T, Dagres N, Arbelo E, Bax JJ, Blomstrom-Lundqvist C, et al. 2020 ESC Guidelines for the diagnosis and management of atrial fibrillation developed in collaboration with the European Association for Cardio-Thoracic Surgery (EACTS): The Task Force for the diagnosis and management of atrial fibrillation of the European Society of Cardiology (ESC) Developed with the special contribution of the European Heart Rhythm Association (EHRA) of the ESC (vol 42, pg 373, 2021). Eur Heart J. 2021;42(40):4194-.

5. Robinson NB, Krieger K, Khan FM, Huffman W, Chang M, Naik A, et al. The current state of animal models in research: A review. Int J Surg. 2019;72:9-13.

6. Voigt N, Pearman CM, Dobrev D, Dibb KM. Methods for isolating atrial cells from large mammals and humans. J Mol Cell Cardiol. 2015;86:187-98.

7. Amesz JH, Zhang L, Everts BR, De Groot NMS, Taverne YJHJ. Living myocardial slices: Advancing arrhythmia research. Front Physiol. 2023;14.

8. Ho SY, Cabrera JA, Sanchez-Quintana D. Left Atrial Anatomy Revisited. Circ-Arrhythmia Elec. 2012;5(1):220-U364.

9. Corradi D, Callegari S, Maestri R, Benussi S, Alfieri O. Structural remodeling in atrial fibrillation. Nat Clin Pract Card. 2008;5(12):782-96.

10. Zhao JC, Hansen BJ, Csepe TA, Lim P, Wang YF, Williams M, et al. Integration of High-Resolution Optical Mapping and 3-Dimensional Micro-Computed Tomographic Imaging to Resolve the Structural Basis of Atrial Conduction in the Human Heart. Circ-Arrhythmia Elec. 2015;8(6):1514-7.

11. Efimov IR, Nikolski VP, Salama G. Optical imaging of the heart. Circ Res. 2004;95(1):21-33.

12. Krul SPJ, Berger WR, Smit NW, van Amersfoorth SCM, Driessen AHG, van Boven WJ, et al. Atrial Fibrosis and Conduction Slowing in the Left Atrial Appendage of Patients Undergoing Thoracoscopic Surgical Pulmonary Vein Isolation for Atrial Fibrillation. Circ-Arrhythmia Elec. 2015;8(2):288-95.

13. Heida A, van Schie MS, van der Does WFB, Taverne YJHJ, Bogers AJJC, de Groot NMS. Reduction of Conduction Velocity in Patients with Atrial Fibrillation. J Clin Med. 2021;10(12).

14. Jalife J, Stevenson WG. Zipes and Jalife's Cardiac Electrophysiology: From Cell to Bedside, E-Book: Elsevier Health Sciences; 2021.

15. Watson SA, Scigliano M, Bardi I, Ascione R, Terracciano CM, Perbellini F. Preparation of viable adult ventricular myocardial slices from large and small mammals. Nat Protoc. 2017;12(12):2623-39.

16. Watanabe M, Feola I, Majumder R, Jangsangthong W, Teplenin AS, Ypey DL, et al. Optogenetic manipulation of anatomical re-entry by light-guided generation of a reversible local conduction block. Cardiovasc Res. 2017;113(3):354-66.

17. Kang C, Qiao Y, Li G, Baechle K, Camelliti P, Rentschler S, et al. Human Organotypic Cultured Cardiac Slices: New Platform For High Throughput Preclinical Human Trials. Sci Rep-Uk. 2016;6.

18. Fischer C, Milting H, Fein E, Reiser E, Lu K, Seidel T, et al. Long-term functional and structural preservation of precision-cut human myocardium under continuous electromechanical stimulation in vitro. Nature Communications. 2019;10.

19. Watson SA, Duff J, Bardi I, Zabielska M, Atanur SS, Jabbour RJ, et al. Biomimetic electromechanical stimulation to maintain adult myocardial slices in vitro. Nature Communications. 2019;10.

20. Amesz JH, de Groot NMS, Langmuur SJJ, el Azzouzi HE, Tiggeloven VPC, van Rooij MMMM, et al. Biomimetic cultivation of atrial tissue slices as novel platform for in-vitro atrial arrhythmia studies. Sci Rep-Uk. 2023;13(1).

21. Beigel R, Wunderlich NC, Ho SY, Arsanjani R, Siegel RJ. The left atrial appendage: anatomy, function, and noninvasive evaluation. JACC Cardiovasc Imaging. 2014;7(12):1251-65.

Chapter 5



Conditional immortalization of human atrial cardiomyocytes for generating *in vitro* models of atrial fibrillation

Nat Biomed Eng. 2022;6:389-402.

Niels Harlaar, Sven O. Dekker, Juan Zhang, Rebecca R. Snabel, Marieke W. Veldkamp, Arie O. Verkerk, Carla Cofiño Fabres, Verena Schwach, Lente J.S. Lerink, Mathilde R. Rivaud, Aat A. Mulder, Willem E. Corver, Marie José T.H. Goumans, Dobromir Dobrev, Robert J.M. Klautz, Martin J. Schalij, Gert Jan C. Veenstra, Robert Passier, Thomas J. van Brakel, Daniël A. Pijnappels[#], Antoine A.F. de Vries[#]
# Equal contribution

Abstract

Clinically relevant *in vitro* models of human disease require large numbers of human parenchymal cells like cardiomyocytes. The current lack of a scalable and robust source of well-differentiated human atrial myocytes limits the development of in vitro models of atrial fibrillation (AF). Here, we report that a lentiviral vector-based conditional cell immortalization procedure allows the production (through a quadrillion-fold cell multiplication) of large numbers of fully functional atrial myocytes. The doxycycline-controlled expression of a recombinant simian virus 40 large T gene in human foetal atrial myocytes resulted in the generation of 15 monoclonal cell lines with molecular, cellular and electrophysiological properties resembling those of primary atrial myocytes following doxycycline withdrawal. The immortalized atrial myocytes were used to create multicellular AF models. These models displayed fibrillatory activity with frequencies of 6-8 Hz, consistent with clinical AF manifestation, which could be terminated by administration of clinically approved antiarrhythmic drugs. The conditional cell immortalization method described herein may be used to generate functional lines of other human parenchymal cell types for the development of human disease models.

Introduction

Preclinical biomedical research across academia and industry strongly relies on *in vitro* models to advance pathophysiological insight and develop novel therapeutics. Human disease models based on (cultured) animal cells are becoming less popular due to 1) the growing awareness of the existence of principal differences in (patho)physiology between humans and animals and 2) the increasing public opposition to animal testing (1). This has created a large demand for difficult to obtain human parenchymal cells, including cardiomyocytes, hepatocytes and neurons. Acquisition of such terminally differentiated cell types is complicated by the fluctuating availability and inconsistent quality of source material including post-mortem samples, surgical waste, non-transplanted donor tissue and biopsies. Additionally, these cell types cannot be multiplied *in vitro* and rapidly dedifferentiate in culture, severely restricting the window of use after isolation. Also, permanent human cell lines of tumour origin or created through genetic engineering generally have not been able to recapitulate the functional properties of the primary cells from which they were derived, because in most cell types continuing proliferation inhibits differentiation (2).

Many of these drawbacks have been overcome by the establishment of human embryonic stem cell (hESC) lines (3) and, more recently, of human induced pluripotent stem cell (hiPSC) lines (4,5), in conjunction with the development of new methods to derive various differentiated cell types from them. As a result, human (pluripotent) stem cell-based 2- and 3-dimensional multicellular *in vitro* models including organoids (6) are rapidly gaining popularity for human disease modelling, target identification, drug development and therapeutic testing. A particularly attractive feature of hiPSCs is the ease with which they can be generated from individual patients allowing the development of patient-specific disease models, thereby creating unique opportunities for personalized medicine. Despite the many advantages of human (pluripotent) stem cell-based *in vitro* models, there are still several factors that limit their application: 1) Derivation of specialized cells from human (pluripotent) stem cells is often a complex and laborious process with a variable outcome; 2) Producing large numbers of specialized cells with a high degree of phenotypic uniformity from human (pluripotent) stem cells is difficult; 3) The differentiated progeny of human (pluripotent) stem cells typically has an immature phenotype and thus functionally differs from adult human cells.

In an attempt to address these limitations, we recently developed a monopartite lentiviral vector (LV)-based system for the conditional immortalization of primary mammalian cells (7,8). At the heart of this system is a recombinant simian virus 40 (SV40) large T (LT) gene, whose expression is driven by a cell type-specific promoter and can be repeatedly switched on and off by means of the tetracycline/doxycycline (dox)-controlled transcription silencer TetR-KRAB (9,10). In the present study, we employ this conditional immortalization to generate lines of human atrial myocytes (AMs) with preserved cardiomyogenic differentiation capacity. The reasons for choosing human AMs as target cells are two-fold: 1) Their highly specialized nature and specific functional properties (*i.e.* excitability and contractility), provide a stringent test for the effectiveness of our conditional cell immortalization system. 2) The rapid worldwide increase in the prevalence of atrial fibrillation (AF) (11), its high socioeconomic burden (12), the incomplete mechanistic understanding (13) along with substantial translational challenges (14) and the suboptimal treatment options (15), have created an urgent need for a robust source of human AMs to overcome the current lack of clinically relevant (*in vitro*) models of AF (16).

Transduction of human foetal AMs (hfAMs) with the TetR-KRAB-regulated LT-encoding LV resulted in the generation of 15 monoclonal cell lines designated hiAMs that rapidly proliferated in the presence of dox and differentiated into excitable and contractile cells with molecular, cellular and electrophysiological properties of AMs after dox withdrawal. These cell lines were used to establish multicellular *in vitro* AF models featuring fibrillatory activity with clinically relevant dynamics and activation frequencies, which could be terminated with traditional antiarrhythmic drugs. The development of the hiAM lines provides proof-of-concept of a versatile method to produce, in a simple and rapid manner, massive numbers of authentic human cells for comprehensive disease modelling.

Results

Generation and selection of hiAMs

To conditionally immortalize human atrial cardiomyocytes, human foetal atrial tissue (gestational age 18 weeks) was dissociated. The resulting cell suspension was transduced with LV particles containing a dox-inducible SV40 LT expression unit driven by the strong hybrid striated muscle-specific MHCK7 promoter (17), targeting the cardiomyocyte population in the atrial cell mixture

(**Figure 1a, Supplemental Figure 1**). Two to three weeks after induction of SV40 LT synthesis through addition of dox and reseeding cells at ultralow density, proliferating colonies comprising 100-200 cells appeared (**Figure 1b**). To assess whether the conditional immortalization was successful, 95 proliferating colonies were isolated, expanded and graded using predefined criteria to assess both the proliferative activity of the cells in the presence of dox and their ability to reacquire the differentiated properties of AMs following dox removal (**Figure 1c, Supplemental Figure 1**). To meet these criteria, the monoclones should display the following properties: 1) proliferate well in the presence of dox (> 15 population doublings [PDs] with a doubling time < 120 h), 2) cease proliferation following dox removal and acquire a cardiomyocyte-like phase-contrast appearance after 12 days of culture in differentiation medium, 3) stain negative for proliferation marker Ki-67 and positive for cardiac troponin T (TNNT2) at 12 days after dox withdrawal and 4) generate and conduct (typical atrial) electrical impulses following cardiomyogenic differentiation in confluent monolayers (action potential [AP] duration [APD] at 80% repolarization [APD_{80}] < 300 ms and conduction velocity [CV] > 10 cm/s) (**Figure 1d,e, Supplemental Figure 1**). Fifteen of the 95 (15.8%) monoclones, designated human immortalized AMs (hiAMs), adhered to all 4 predefined criteria indicating successful generation, through conditional immortalization, of human cardiomyocyte lines with preserved cardiomyogenic differentiation capacity.

Characterization of hiAMs during proliferation and after differentiation

Three of the 15 hiAM clones (*i.e.* hiAM clones 2.38, 2.52 and 2.90) were randomly selected for in-depth characterization (**Figure 1f**). The number of lentiviral integrations in these clones ranged from 4 to 6 (**Supplemental Table 1**). Analysis of their DNA content revealed all 3 clones to comprise predominantly cells with DNA indices between 1.7 and 1.8 (**Supplemental Figure 2, Supplemental Table 2**). The doubling time of the 3 selected hiAM clones in the presence of dox was 55 ± 5 h (**Figure 1g**). Proliferating hiAMs contained a much higher percentage of Ki-67-positive nuclei than freshly isolated hfAMs (**Figure 1h**). The low Ki-67 expression in hfAMs is consistent with the limited mitotic activity of human cardiomyocytes in the second semester of gestation (18). hiAMs could be expanded for at least 50 PDs without a noticeable reduction in proliferation rate, resulting in ≥ quadrillion-fold cell multiplication. Dox omission in the culture medium resulted in a strong (*i.e.* > 2000-fold) reduction

of the SV40 LT level in hiAMs over the course of 12 days, as determined by western blotting (**Figure 1i**). At the same time, hiAMs no longer displayed any Ki-67-positive nuclei.

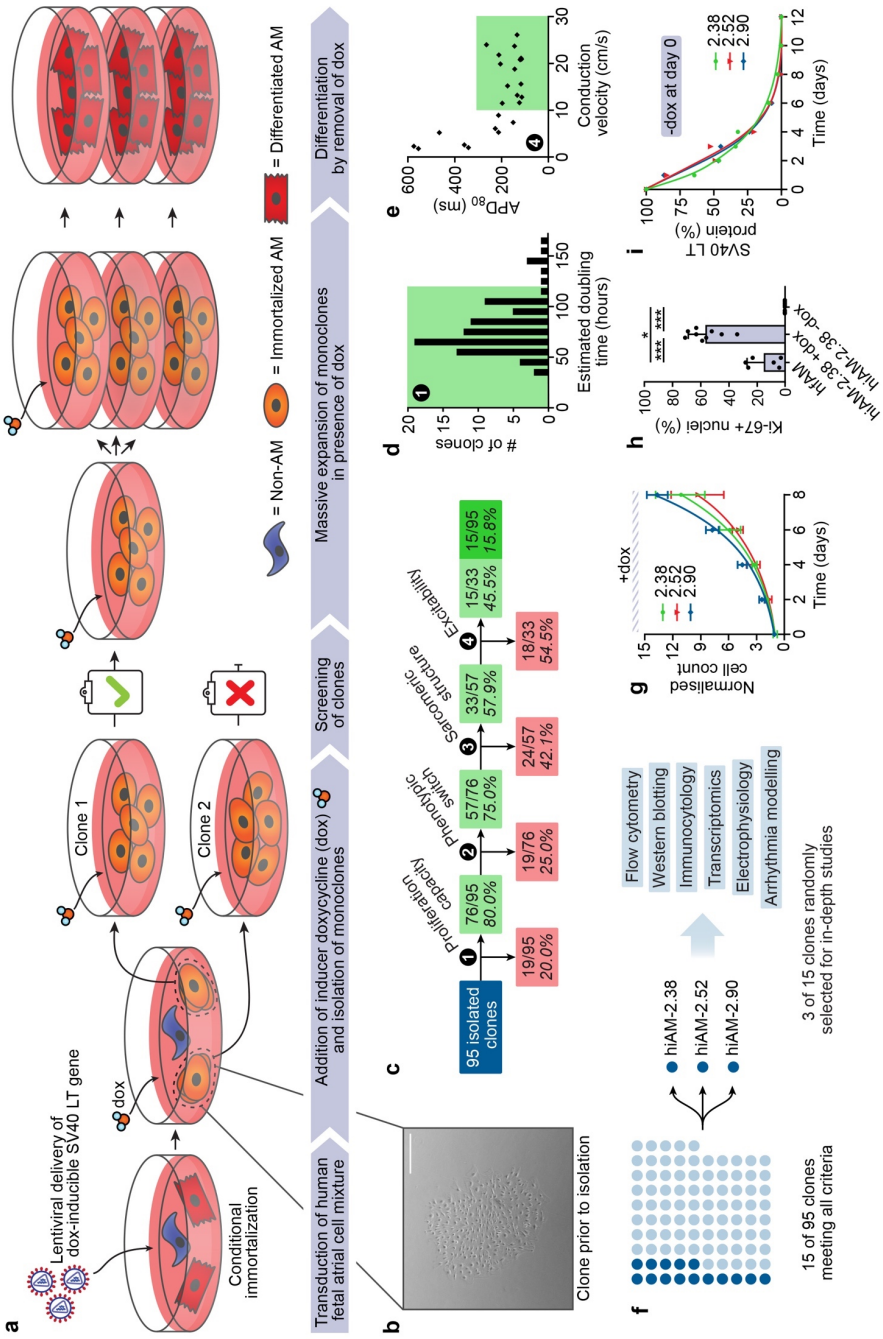


Figure 1 (legend on next page).

Figure 1 (previous page). Generation and selection of hiAM monoclones. **(a)** Schematic overview of the conditional immortalization of hfAMs, generation and selection of hiAM monoclones, massive hiAM expansion in the presence of dox and cardiomyogenic differentiation of hiAMs following dox removal. **(b)** Representative phase-contrast image of a hiAM monoclone prior to isolation. Scale bar, 500 µm. **(c)** Flowchart of hiAM monoclone selection based on 4 main criteria with corresponding drop-off rates (see **Supplemental Figure 1** for additional data). **(d)** Estimated doubling time of isolated hiAM monoclones based on passaging intervals. The highlighted area (doubling time ≤ 120 h) represents a pass on the first selection criterium. **(e)** Selection based on excitability of hiAM monoclones using optical voltage mapping as part of the fourth selection criterium. The highlighted area represents selected monoclones with a CV ≥ 10 cm/s and APD_{80} ≤ 300 ms. **(f)** Summary of monoclone selection. hiAM clones 2.38, 2.52 and 2.90 were selected for further characterization. **(g)** Quantification of hiAM proliferation in the presence of dox (n = 3 independent experiments per monoclone; mean shown, error bars indicate SD). **(h)** Ki-67-positive nuclei determined by immunocytochemistry in hfAM (n = 2), proliferating (+dox, n = 3) hiAM and differentiated (-dox, n = 3) hiAM cultures. Three random areas per culture were selected for quantification. n signifies independent samples/differentiations. *P < 0.05, ***P < 0.001, one-way analysis of variance with Tukey *post-hoc* analysis. Mean shown, with error bars indicating SD. **(i)** SV40 LT levels in proliferating hiAM-2.38, -2.52 and -2.90 measured by western blotting over 12 days of differentiation following removal of dox at day 0 (n = 1 per monoclone).

The 12-day transition from a proliferating to a differentiated hiAM, which is simply initiated by the removal of dox and a change from proliferation to differentiation medium, was accompanied by the reappearance of spontaneous synchronous contractions similar to those observed in freshly isolated hfAMs (**Supplemental Video 1**). Immunostaining for the sarcomeric proteins α-actinin 2 (ACTN2), TNNT2 and the atrial isoform of myosin regulatory light chain 2 (MLC2a), showed that the highly organized sarcomeres observed in hfAMs were lost following conditional immortalization and induction of proliferation, but reappeared when hiAMs were growth-arrested by dox withdrawal and allowed to redifferentiate for 12 days (**Figure 2a, Supplemental Figure 3**). Flow cytometric analysis showed that hiAM differentiation yielded highly pure cell populations, comprising on average 99.1% ACTN2-positive and 97.2% TNNT2-positive cells (**Supplemental Figure 4**). Gap junctional protein connexin 43, which was concentrated at cell-cell interfaces in hfAMs, also disappeared when proliferation was induced and again formed neatly organized cell-cell connections following hiAM differentiation (**Figure 2a**). Additionally, hiAM differentiation caused an increase in the levels of the atrium-specific gap junctional protein connexin 40 (**Supplemental Figure 3**). Detailed imaging by transmission electron

microscopy revealed the presence of well-organized sarcomeres, perinuclear and intermyofibrillar mitochondria and intercalated discs in differentiated hiAMs (**Supplemental Figure 5**). Sarcomere lengths appeared to be slightly shorter in differentiated hiAMs (1.79-1.83 µm) compared to hfAMs (1.96 µm, **Supplemental Figure 3**). At all stages, hfAMs and hiAMs stained negative for the ventricular isoform of myosin regulatory light chain 2 (MLC2v), corroborating their atrial origin and specificity.

We next performed RNA-sequencing to study the transcriptome of proliferating and cardiomyogenically differentiated hiAMs (**Figure 2b**). Principal component analysis and heatmap of global gene expression data illustrated a clear separation between the transcriptomes of the proliferating (D0) and differentiated (D12) hiAM clones (**Figure 2c**). Grouped comparison revealed 6078 differentially expressed genes (DEGs), of which 2652 were downregulated and 3426 were upregulated when transitioning from proliferation to differentiation (log2-fold change > 1 and false discovery rate [FDR]-corrected P < 0.001, **Supplemental Data File 1**). Differential gene expression of individual clones showed a large overlap (**Figure 2d**). Downregulated genes standing out (including MKI67, AURKB, CDK1, CCNA2 and POLE) appeared to be closely involved with cell proliferation, whereas upregulated genes (such as ACTN2, MYH6, KCNJ2, CACNA1C and GJA5) were associated with a differentiated AM phenotype (**Figure 2e**). These observations were confirmed by gene ontology (GO) analysis of the up- and down-regulated genes (**Figure 2f, Supplemental Figure 6**). GO terms enriched during hiAM proliferation were mainly related to DNA replication and cell division, whereas the most enriched GO terms post-differentiation were involved in myofibrillogenesis, energy metabolism and cardiac muscle contraction. The differential expression levels of atrial and ventricular marker genes, such as MYL7/MYL2 (19669.6 vs. 0.2 transcripts per million [TPM]) and MYH6/MYH7 (1126.4 vs. 15.6 TPM), as well as the high abundance of NPPA transcripts (8494.6 TPM), further confirmed the atrial phenotype of differentiated hiAMs (**Supplemental Figure 7**). Collectively, these results demonstrate that the conditional immortalization by TetR-KRAB-regulated SV40 LT gene expression allows hfAMs to effectively switch between proliferative and differentiated states, which could not be achieved with permanent immortalization (**Supplemental Figure 8**).

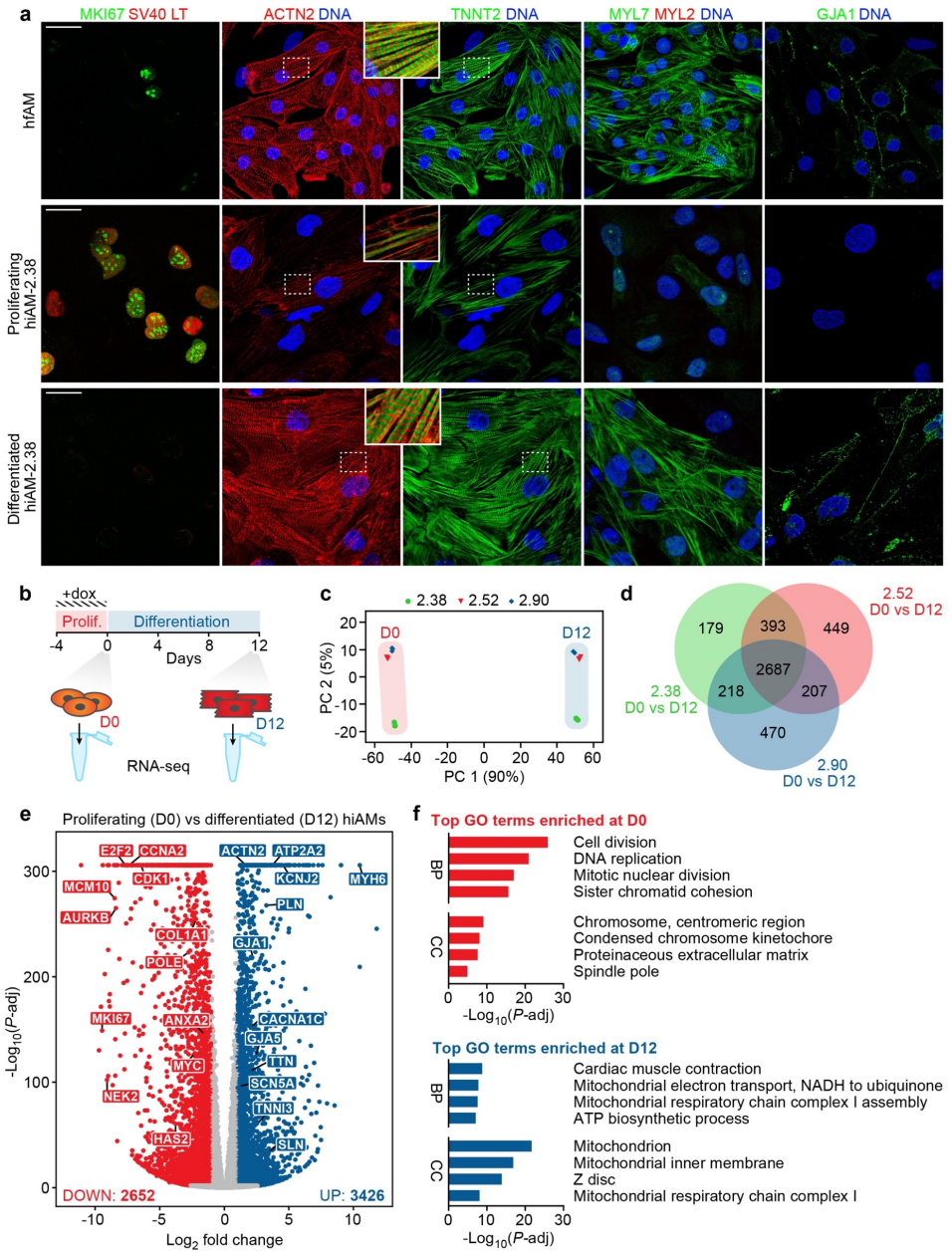


Figure 2. Characterization of the hiAM phenotype during proliferation and after 12 days of differentiation. **(a)** Immunostaining of hfAMs and of proliferating and differentiated hiAM-2.38 for Ki-67 (MKI67), SV40 LT, α-actinin 2 (ACTN2), cardiac muscle troponin T (TNNT2), the atrial and ventricular isoform of myosin regulatory light chain 2 (MYL7 and MYL2, respectively) and connexin-43 (GJA1). Scale bar, 25 µm. **(b)** Schematic representation of sample collection timeline for RNA-sequencing. **(c)** Principal

component (PC) analysis of global gene expression data (n = 3 biological replicates per time point and hiAM clone). **(d)** Venn diagram of differentially expressed genes (DEGs) between proliferating (D0) and differentiated (D12) hiAM-2.38, -2.52 and -2.90. Genes with > 1 TPM at D0 or D12, an absolute $\log_2$-fold change > 1 and an FDR-corrected P < 0.001 are shown. **(e)** Volcano plot of gene expression in proliferating *vs.* differentiated hiAMs (grouped analysis of hiAM clones 2.38, 2.52 and 2.90). Selected genes of interest are labelled. Please note that due to filtering applied in the comparison of the individual clones, the number of DEGs is lower than in the grouped analysis. **(f)** Top 4 biological process (BP) and cellular component (CC) GO terms enriched in proliferating (D0) and differentiated (D12) hiAMs (see **Supplemental Figure 6** for all enriched GO terms).

Maturity of the differentiated hiAM transcriptome

Benchmarking of hiAM maturity was first performed by comparison of the global hiAM transcriptome against compendia of gene expression data from human foetal cardiac tissues (19) and human adult tissues (20). For reference purposes, also the transcriptomic maturity of hESC-derived atrial cardiomyocytes (hESC-AMs) was determined. The transcription profiles of hESC-AMs and differentiated hiAMs best correlated with those of atrial myocardium. However, the transcriptome of hESC-AMs correlated modestly better with that of foetal atrial myocardium, whereas the gene expression profile of hiAMs was somewhat closer to that of adult atrial myocardium (**Figure 3a**).

Differential gene expression analysis between hESC-AMs and hiAMs revealed 2276 DEGs upregulated in hESC-AMs and 1869 DEGs upregulated in hiAMs (**Figure 3b**). Neither of the gene sets was exclusively expressed in the heart, but overall the DEGs upregulated in hiAMs were more abundantly expressed (**Figure 3c**). Clustering analysis revealed that a subset of the upregulated DEGs had striated muscle-specific expression, which included SCN5A, CASQ2 and SLN for hiAMs, and MYL2, TTN and RYR2 for hESC-AMs (**Supplemental Figure 9, Supplemental Data File 2**). Finally, rank-based comparison of selected maturity-related gene sets in hiAMs, hESC-AMs, foetal atrial myocardium and adult atrial myocardium revealed differences in structural, electrophysiological, contractile and metabolic properties (full overview in **Supplemental Figure 10**). Overall, these data indicate that the gene expression profile of differentiated hiAMs possesses many features of the adult atrial myocardial transcriptome.

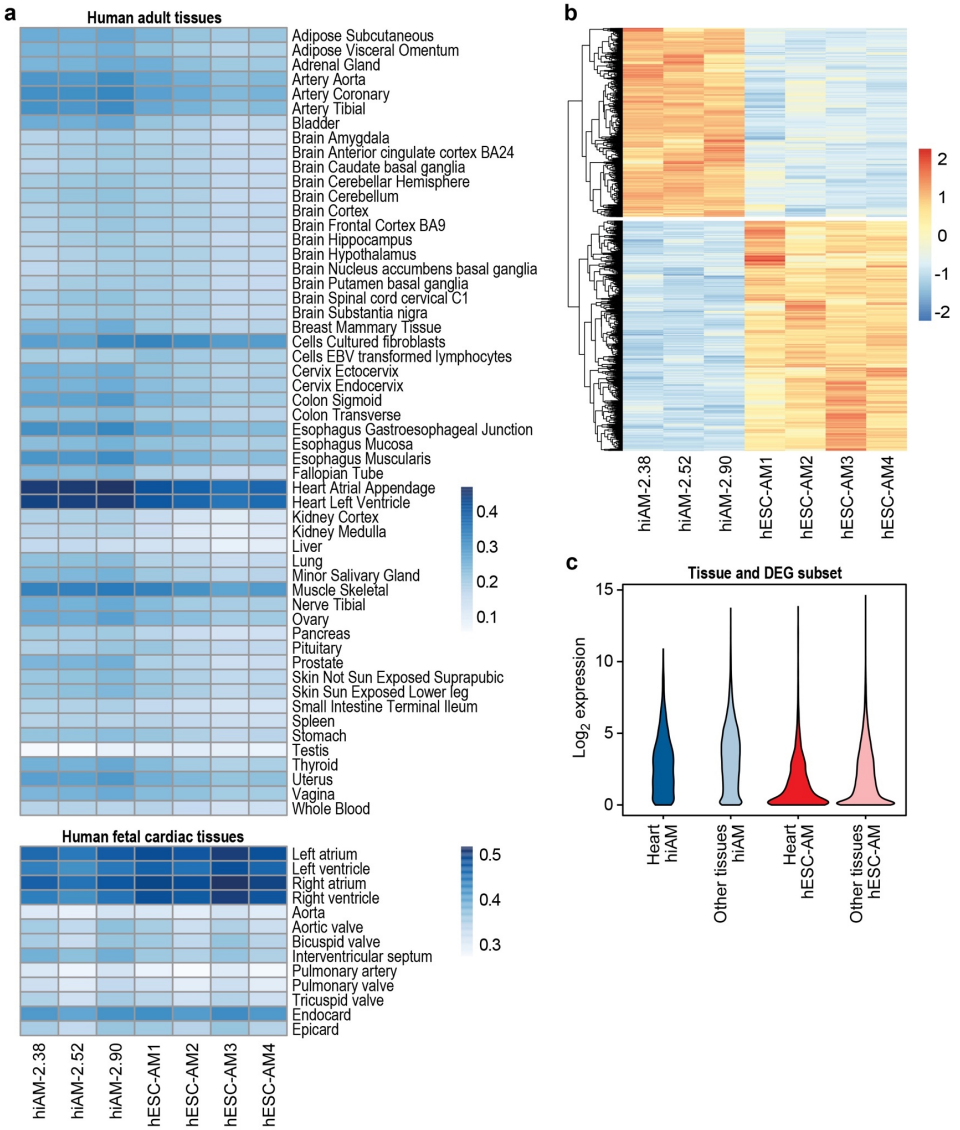


Figure 3. Characterization of differentiated hiAM and hESC-AM transcriptomes. **(a)** Global transcriptome comparison of 3 hiAM clones (hiAM-2.38, -2.52 and -2.90) and of 4 hESC-AM replicates against a compendium of human adult tissues and human foetal cardiac tissues. Scale bar indicates Spearman correlation. **(b)** Differential gene expression between hiAMs and hESC-AMs. Scale bar indicates row-scaled and centred expression values. **(c)** Expression levels of differentially expressed genes (DEGs) separated based on hiAM or hESC-AM specificity and cardiac or non-cardiac specificity.

Electrophysiological properties of differentiated hiAMs

The electrophysiological properties of cardiomyogenically differentiated hiAMs were first studied by single-cell patch-clamp analysis. Differentiated hiAM-2.38 had a resting membrane potential (RMP) similar to that of human adult AMs (haAMs) and significantly more negative than the RMP of hfAMs (**Figure 4a,b**). Additionally, the maximal AP amplitude in hiAM-2.38 was larger than in hfAMs but smaller than in haAMs, whereas the AP plateau amplitude was higher in hiAM-2.38 compared to both hfAMs and haAMs. The maximum AP upstroke velocity of hiAM-2.38 was between that of hfAMs and haAMs. APD at 20, 50 and 90% of repolarisation did not significantly differ between hfAMs, hiAM-2.38 and haAMs. AP characteristics similar to hiAM-2.38 were also observed in differentiated hiAM-2.52 and hiAM-2.90 (**Supplemental Figure 11, Supplemental Table 3**). Subsequent voltage-clamp recordings in hiAM-2.38 showed the presence of a strong Na^+ current (I_{Na}) and robust steady-state K^+ currents (**Supplemental Figure 12**), which were consistent with the fast upstroke velocity and haAM-like RMP of hiAM-2.38, respectively. Finally, a strong atrial-selective 4-AP (50 μM)-sensitive ultrarapid delayed rectifier K^+ current (I_{Kur}) was present in hiAMs, validating their atrial electrophysiological phenotype (**Supplemental Figure 12, Supplemental Table 4**). Overall, the electrophysiological properties of differentiated hiAMs strongly resemble those of primary human AMs.

Next, we assessed the conduction of APs in multicellular preparations by optical voltage mapping. Upon 1-Hz electrical point stimulation, cell layers (2-cm^2) of hiAM-2.38 displayed homogeneous conduction of APs (**Figure 4c,d**) with a CV of 24.4 ± 2.3 cm/s and APD_{80} of 136 ± 12 ms (**Figure 4e**), with APD restitution occurring at high activation frequencies (**Figure 4f**). Optical voltage mapping of hiAM-2.52 and hiAM-2.90 also showed homogeneous conduction of APs at speeds of 19.4 ± 2.0 cm/s and 11.9 ± 2.0 cm/s and with an APD_{80} of 129 ± 15 ms and 103 ± 9 ms, respectively (**Supplemental Figure 11**). Since confluent monocultures of hfAMs or haAMs could not be established because of shortage of source material, difficulties in removing the large percentage of non-cardiomyocytes from the starting material, minimal cardiomyocyte proliferation and/or poor cardiomyocyte survival, we used hESC-AMs for comparison. Due to limited production capacity of phenotypically homogenous hESC-AM populations, this comparison was performed in confluent 1-cm^2 cell layers. While hESC-AM layers had a high spontaneous beating rate consistent with their immature phenotype, spontaneous activity was rarely observed in hiAM-2.38 layers, but could be induced by chronotropic

stimulation (**Supplemental Figure 13**). Following 1-Hz electrical point stimulation, conduction in hESC-AM layers appeared more heterogeneous and was > 10-fold slower compared with hiAM-2.38 layers of the same size (**Figure 4g-i, Supplemental Video 2**). In terms of optical AP characteristics, the optical upstroke time was longer in hESC-AMs compared with hiAM-2.38 (28 ± 6 vs. 12 ± 1 ms, $P < 0.001$, $n = 6$ and 7, respectively) while APD_{80} did not statistically differ between hESC-AMs and hiAMs. Similar differences in kinetics were found when comparing optically recorded Ca^{2+} transients between hESC-AM and hiAM-2.38 layers (**Supplemental Results, Supplemental Figure 14**).

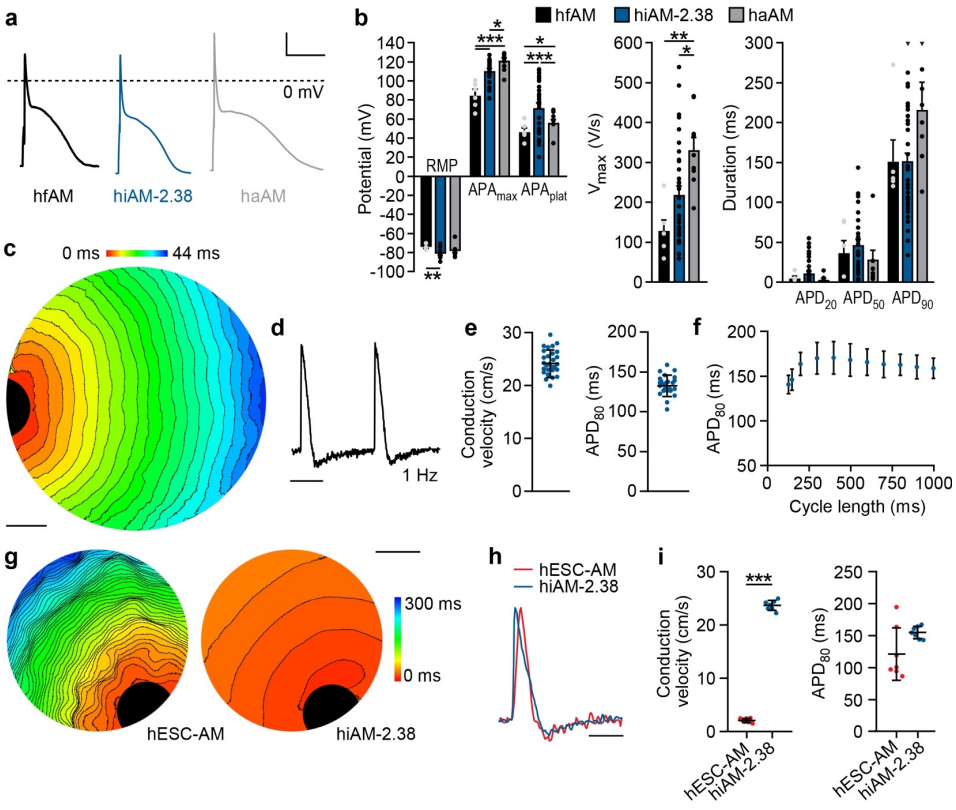


Figure 4. Electrophysiological characteristics of differentiated hiAMs. **(a)** Representative AP traces and **(b)** mean AP parameters of single hfAMs ($n = 6$ cells from 2 independent preparations), single differentiated hiAM-2.38 ($n = 39$ cells from 11 independent differentiations) and single haAMs ($n = 9$ cells) during 1-Hz electrical stimulation. APA_{max}, maximal AP amplitude. APA_{plat}, AP plateau amplitude. V_{max}, maximum AP upstroke velocity. $APD_{20/50/90}$, action potential duration at 20, 50 and 90% of repolarization. Scale bars in **(a)** x = 100 ms, y = 20 mV. The dotted line in **(a)** indicates the zero mV level. Data shown as mean with error bars indicating SEM. $^{**}P < 0.01$, $^{***}P <$

0.001, one-way analysis of variance with Tukey *post-hoc* analysis. **(c-f)** Optical voltage mapping of confluent layers of differentiated hiAMs in a 24-well format following 1-Hz electrical point stimulation. **(c)** Representative activation map of hiAM layer. Isochrones, 2 ms. Scale bar, 2 mm. **(d)** Representative optical voltage trace of hiAMs from **(c)**. Scale bar, 500 ms. **(e)** Mean CV and APD_{80} in confluent hiAM layers (n = 28 layers from 8 independent differentiations). Mean shown, with error bars indicating SD. **(f)** APD restitution curve of hiAM-2.38 (n = 10 layers from 2 independent differentiations). Mean shown, with error bars indicating SD. **(g-h)** Optical voltage mapping of confluent hESC-AM and differentiated hiAM-2.38 layers in a 48-well format. **(g)** Representative activation maps of hESC-AM and hiAM-2.38 layers. Isochrones, 6 ms. Scale bar, 2 mm. **(h)** Representative optical voltage traces from hESC-AMs and hiAMs of **(g)**. Scale bar, 250 ms. **(i)** Mean CV and APD_{80} during 1-Hz electrical stimulation in hESC-AM (n = 7 layers from 3 independent differentiations) and differentiated hiAM (n = 7 layers from 2 independent differentiations) layers. Mean shown, with error bars indicating SD. ***P < 0.001, unpaired t-test.

Robustness of hiAM differentiation

From the perspective of standardization, we assessed the robustness of hiAM differentiation. Massive expansion of hiAMs did not jeopardize their cardiomyogenic differentiation potential. Comparison of optical voltage mapping data of hiAM-2.38 that had undergone different PDs (between 28 and 46) before cardiomyogenic differentiation, revealed no significant change in average CV or APD_{80} (**Figure 5a, Supplemental Figure 15**). Also, no variation in structural characteristics as assessed by immunostaining for ACTN2 and TNNT2 was observed over this broad range of PDs (**Supplemental Figure 15**). Furthermore, repeatedly switching hiAMs back and forth between proliferation and differentiation did not noticeably alter their respective phenotypes. Specifically, the number of Ki-67-positive nuclei during proliferation, as well as the CV, APD_{80} and TNNT2 immunostaining pattern after differentiation were not affected by the repeated phenotypic transitions (**Figure 5b, Supplemental Figure 16**).

Next, we tested whether hard-to-control variations in the culture medium, such as the variable composition of foetal bovine serum (FBS) (21), would affect cardiomyogenic differentiation. The CV of hiAM cultures differentiated with 4 different sources of FBS did not significantly differ (**Figure 5b**). Similarly, no effect on APD_{80} was found, except that the premium FBS from USA origin had a minimal shortening effect on APD_{80} as compared to the FBS from South America, New Zealand and Brazil (**Figure 5b**). Finally, we investigated whether cryopreservation of differentiated hiAMs (in addition to cryopreservation of proliferating hiAMs) would be feasible. Thawing of hiAMs that had been

cryopreserved at day 8 of differentiation, *i.e.* just before they exhibit contractions, resulted in 91.9 ± 1.6% of viable cells and an attachment efficiency of 70.4 ± 5.2% (**Figure 5c**). Following 6 additional days of culture in supplemented differentiation medium to complete cardiomyogenesis, the hiAM layers did not show significant differences in electrophysiological characteristics when compared to control layers established with hiAMs that had not been cryopreserved in a partially differentiated state (**Figure 5d**). Together, these data demonstrate robust hiAM differentiation irrespective of passage history, culture conditions or intermediate cryopreservation.

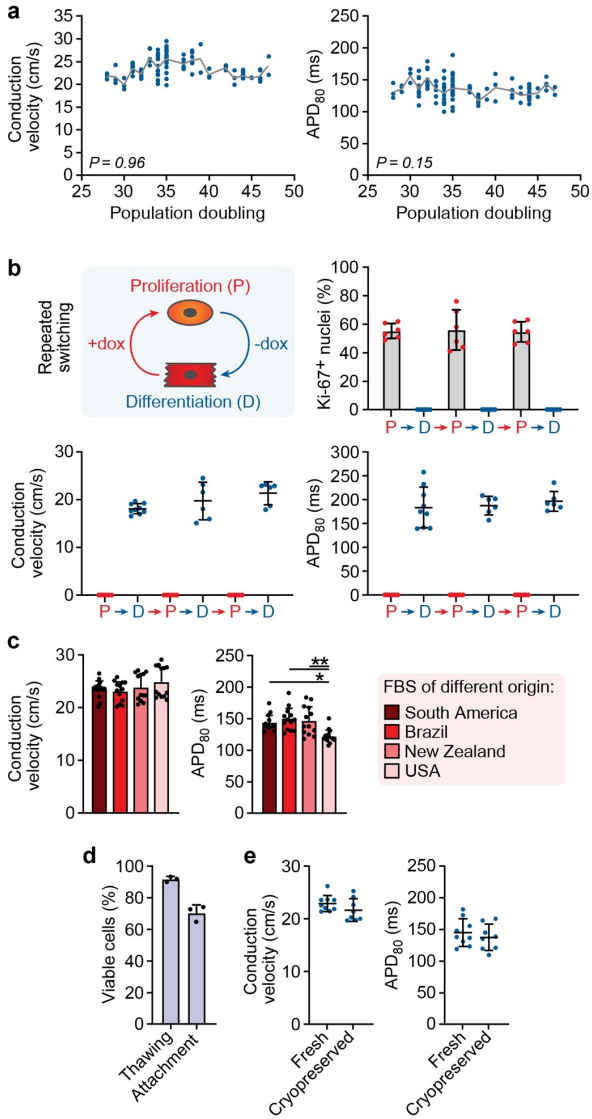


Figure 5 (legend on next page).

Figure 5 (previous page). Robustness and effect of cryopreservation on hiAM differentiation capacity. **(a)** CV and APD_{80} of hiAM-2.38 layers measured using optical voltage mapping over a broad range of PDs (n = 111). Stability of mean CV and APD_{80} at various PDs was tested using the Pearson correlation coefficient. **(b)** Percentage of hiAM-2.38 with Ki-67-positive nuclei determined by immunocytochemistry and CV and APD_{80} of hiAM-2.38 measured by optical voltage mapping during repeated switching between proliferation (P) and differentiation (D). n = 6-9 layers per time point from 3 independent experiments. **(c)** Electrophysiological characteristics of hiAM-2.38 layers following differentiation using FBS of various origins and suppliers: South America (standard serum, S1860, Biowest), Brazil (10270098, Thermo Fisher Scientific), New Zealand (A3160901, Thermo Fisher Scientific) and USA (Premium FBS, 16000036, Thermo Fisher Scientific; n = 13 layers per group from 3 independent differentiations). *P < 0.05, **P < 0.01, one-way analysis of variance with Tukey *post-hoc* analysis. **(d)** Viability (determined by the Trypan Blue dye exclusion test) and attachment efficiency after thawing of hiAMs that had been cryopreserved at day 8 of differentiation (n = 3 batches each comprising 3 vials with 10^6 hiAMs per vial). **(e)** Electrophysiological characteristics using optical voltage mapping of freshly differentiated hiAM-2.38 (n = 9 layers from 3 independent differentiations) *vs.* cryopreserved differentiated hiAM-2.38 layers (n = 8 layers from 3 independent differentiations). **(b-e)** Mean shown, with error bars indicating SD.

hiAMs as atrial arrhythmia model

We next investigated the suitability of hiAMs for AF modelling. As induction of reentry in hiAM layers was not feasible in the 2-cm^2 format and the average area of reentrant circuits in human AF is ~3 cm^2 (22,23), we used 10-cm^2 confluent hiAM layers to provide space for multiple reentrant circuits. hESC-AM layers of 1 cm^2 were included for comparison, because of the aforementioned difficulty to establish larger confluent monolayers of these cells. Upon high-frequency electrical point stimulation, arrhythmic activity with varying degrees of complexity could be induced in both 1-cm^2 hESC-AM and 10-cm^2 hiAM layers (**Figure 6a,b, Supplemental Video 3**). Reentrant activity induced in hESC-AM layers had an average activation frequency of 3.0 ± 0.8 Hz, which was consistent with previous reports of arrhythmic hESC-AM layers (24). In hiAM-2.38 layers, however, the average activation frequency was significantly higher (7.5 ± 1.0 Hz, **Figure 6c**). Also in hiAM-2.52 and hiAM-2.90 layers, reentrant activity with high activation frequencies could be induced (7.2 ± 0.8 and 7.9 ± 0.6 Hz, respectively, **Supplemental Figure 17**). Interestingly, these activation frequencies very closely resemble those previously measured in the clinic in AF patients (25-27). As expected from the faster CV in hiAM layers, reentrant circuit wavelength was greater in hiAM-2.38 layers than in hESC-AM layers (**Figure 6d**). As a result, the arrhythmia complexity (expressed as number of

reentrant circuits per cm^2) was higher in hESC-AM layers compared to hiAM-2.38 layers (**Figure 6e, Supplemental Video 4**). Similar data were obtained in arrhythmic hiAM-2.52 and hiAM-2.90 layers (**Supplemental Figure 17**). Moreover, in hESC-AM layers, the cycle length of reentrant circuits was much longer than the baseline APD_{80}, whereas in hiAMs these two parameters were very similar (**Figure 6f**). Thus, reentrant circuits in hESC-AMs displayed a large temporal excitable gap compared to nearly no gap in hiAMs (**Supplemental Figure 17**), which suggests that the slow CV in hESC-AM layers might be responsible for the low activation frequencies. Overall, hiAM monolayers better recapitulate the dynamics of human AF than hESC-AM monolayers.

Effects of traditional antiarrhythmic drugs in hiAM-based AF model

The applicability of the hiAM-based AF model to study pharmacological interventions was tested using sotalol and flecainide, two antiarrhythmic drugs commonly used for rhythm control in AF patients (28-30). Dimethylsulfoxide (DMSO), which served as solvent/vehicle for flecainide, did not affect the CV or APD in hiAM-2.38 layers subjected to 1-Hz electrical point stimulation. Increasing concentrations of sotalol had also no effect on CV, but did dose-dependently increase the APD_{80} (**Figure 7a, Supplemental Figure 18**), as would be expected by its strong inhibitory effect on the rapid delayed rectifier K^+ current (I_{Kr}) (31). Flecainide, which mainly inhibits I_{Na} and I_{Kr} (32), decreased the CV and prolonged the APD_{80} in a dose-dependent matter. For each compound, 3 incremental doses were selected (DMSO: 0.01, 0.03 and 0.1%; Sotalol: 3, 10 and 30 μM; Flecainide 1, 3 and 10 μM), including clinically relevant concentrations (**Figure 7b**).

Following the induction of stable reentry in hiAM-2.38 cultures, slow infusion of DMSO rarely resulted in termination of reentrant activity (**Figure 7c,d**). DMSO also did not significantly alter the activation frequency, with the exception of the 0.01% dose which slightly reduced the frequency (**Figure 7e**). Sotalol infusion resulted in sporadic termination of reentrant activity, although for none of the doses termination rates significantly differed from those caused by DMSO treatment. The activation frequency, however, was significantly reduced for all sotalol concentrations in a dose-dependent manner. Finally, infusion of flecainide did result in frequent arrhythmia termination at the two highest doses and also significantly reduced the activation frequency in a dose-dependent manner. These observations were also confirmed in hiAM-2.52 and hiAM-2.90 cultures (**Supplemental Figure 19**). For these clones, 0.1% DMSO did

not terminate any reentrant activity, whereas 10 µM flecainide resulted in frequent reentry termination. Thus, using the hiAM-based AF model, we were able to recapitulate the effects exerted by common antiarrhythmic drugs in AF patients at clinically relevant activation frequencies (**Supplemental Video 5**).

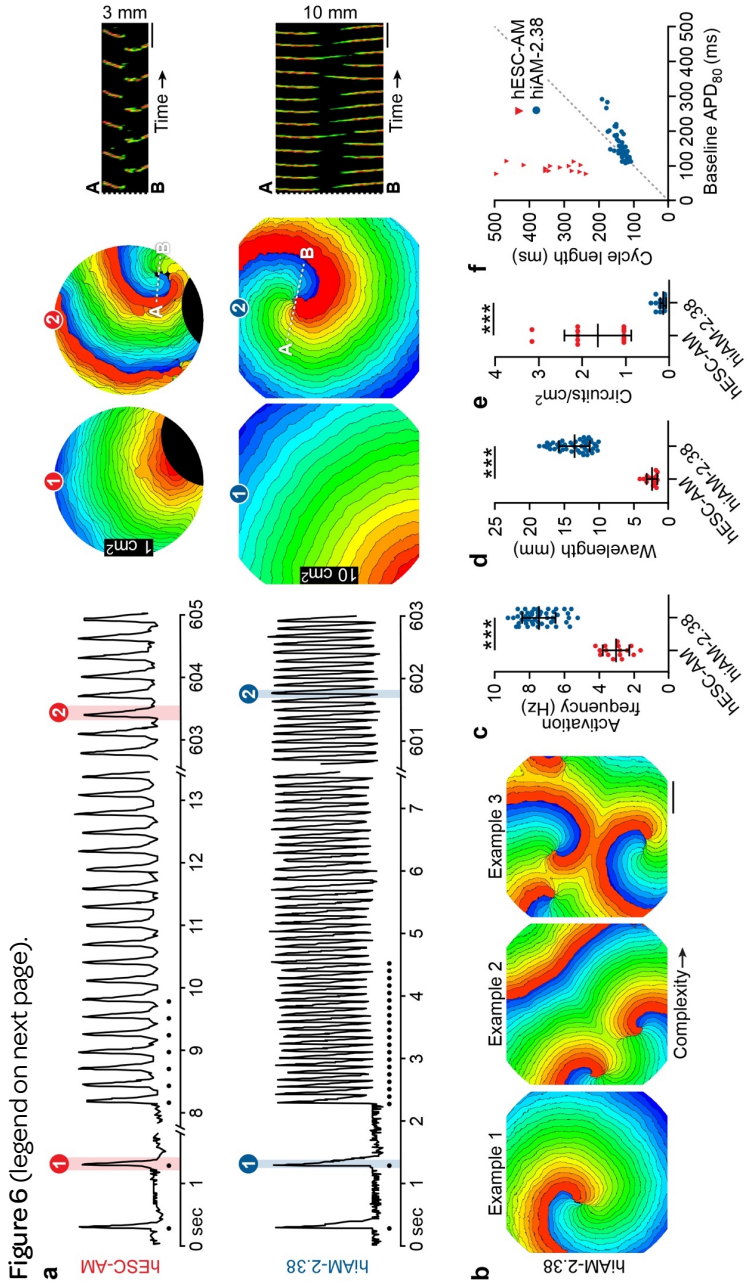


Figure 6 (legend on next page).

Figure 6 (previous page). hESC-AM- and hiAM-based atrial arrhythmia models. **(a)** Optical voltage traces of reentrant circuit induction by high frequency electrical pacing in 1-cm^2 hESC-AM and 10-cm^2 differentiated hiAM cultures (left). Corresponding activation maps before and after arrhythmia induction (middle). Line scan analysis between points A and B assessing reentrant circuit stability (right). Dots above the axes represent time points of electrical stimulation. Isochrones, 12 ms (hESC-AMs), 6 ms (hiAMs). Scale bar, 250 ms. **(b)** Example of three 10-cm^2 hiAM-2.38 cultures following induction of reentrant activity of increasing complexity, *i.e.* with an increasing number of reentrant circuits. Isochrones, 6 ms. Scale bar, 5 mm. **(c)** Mean activation frequency of hESC-AM and hiAM cultures following induction of reentrant circuits. **(d)** Mean wavelength of reentrant circuits. **(e)** Arrhythmia complexity following stabilization expressed as number of reentrant circuits per cm^2. **(f)** Correlation between baseline APD_{80} and cycle length of induced reentrant circuits in hESC-AM and hiAM cultures. **(c-e)** Mean shown, with error bars indicating SD. ***P < 0.001, unpaired t-test. **(c-f)** hESC-AM: n = 16 arrhythmia episodes from 7 independent cultures, hiAM-2.38: n = 56 independent cultures.

Figure 7 (next page). Effects of antiarrhythmic drugs in the hiAM-based atrial arrhythmia model. **(a)** Effects of various concentrations of DMSO (solvent/vehicle control), sotalol or flecainide on CV (red, left axis) and APD_{80} (blue, right axis) in differentiated 2-cm^2 hiAM-2.38 cultures (n = 5 cultures for each compound). Repeated measured analysis of variance with Tukey *post-hoc* analysis. **(b)** Representative optical voltage traces of differentiated hiAM-2.38 in the presence of various concentrations of DMSO, sotalol or flecainide. Scale bar, 100 ms. **(c)** Representative optical voltage traces of arrhythmic hiAM-2.38 cultures before and after infusion of DMSO (0.1%), sotalol (30 μM) or flecainide (10 μM). Dots above the lower axis represent time points of electrical stimulation. **(d)** Rate of reentrant circuit termination in arrhythmic hiAM-2.38 cultures at 10 min after infusion of DMSO, sotalol or flecainide. The termination rates at the different sotalol and flecainide concentrations were compared with the termination rate of the combined DMSO concentrations using the Chi-square test. **(e)** Change (Δ) in activation frequency in arrhythmic hiAM-2.38 cultures following DMSO, sotalol or flecainide infusion (baseline compared to 10 min after infusion or prior to termination). Paired t-test. **(f)** Continuous monitoring of mean activation frequency in arrhythmic hiAM-2.38 cultures prior to and after infusion of compounds at the indicated concentrations. **(c-f)** Additional details on arrhythmia dynamics and termination mechanisms following drug infusion are provided in **Supplemental Figure 20. (d-f)** n = 8-10 experiments for each dose, from 57 independent cultures. **(a, e)** Mean shown, with error bars indicating SD. **(a, d, e)** *P < 0.05, **P < 0.01, ***P < 0.001.

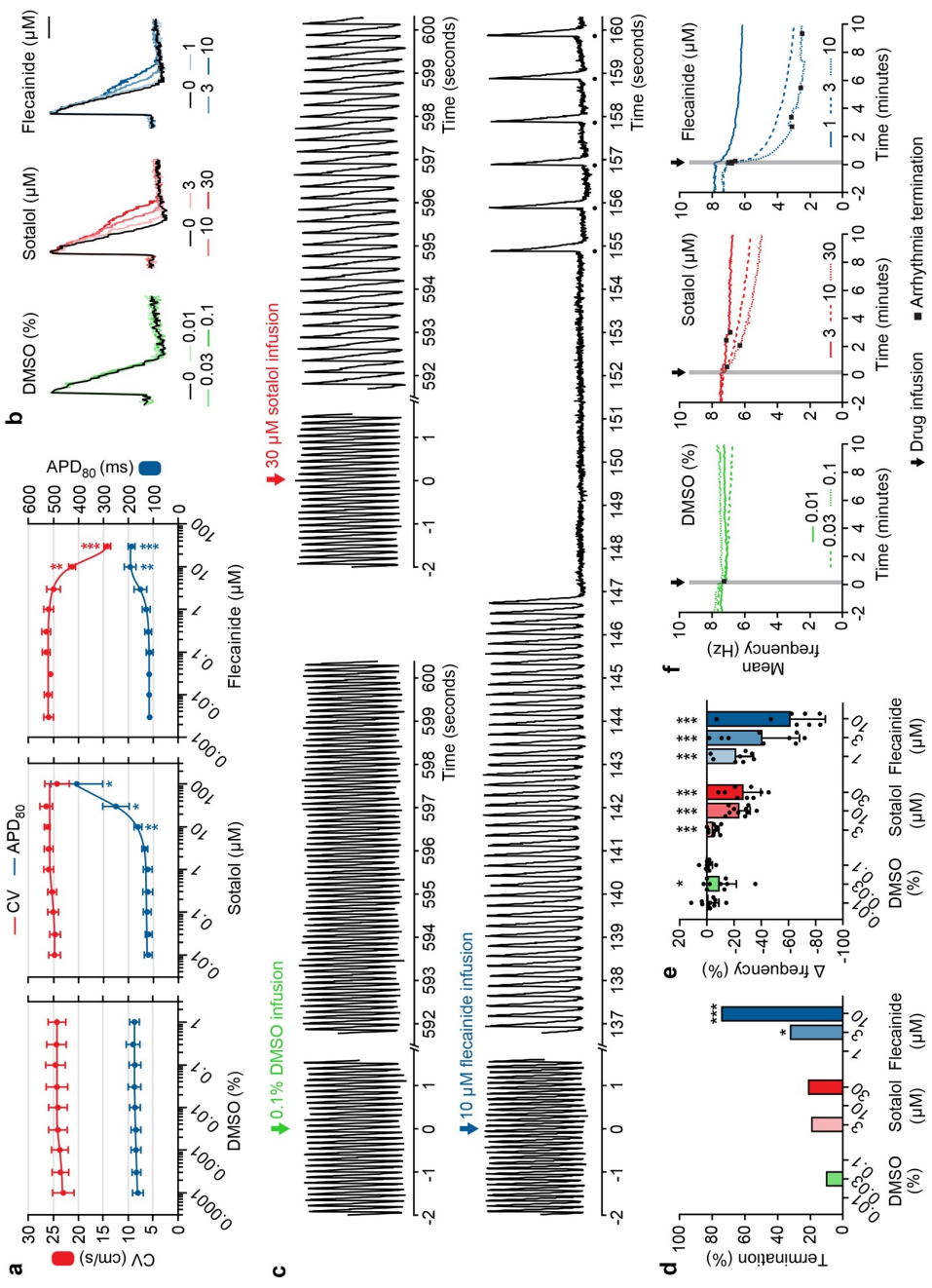


Figure 7 (legend on previous page).

Discussion

Preclinical biomedical research across academia and industry has created a large demand for difficult to obtain human parenchymal cells to increase pathophysiological insight and develop novel therapeutics. Although recent progress in human pluripotent stem cell (hPSC) technology has greatly advanced the development of human disease models, several challenges remain regarding their scalability, representativeness and reproducibility. To address these issues, we developed an LV-based method for the conditional immortalization of primary mammalian cells. In this study, we describe the generation of standardized lines of human AMs with preserved cardiomyogenic differentiation capacity as a demonstration of the efficacy of this method. These so-called hiAM lines display strict control over proliferation and differentiation, allowing massive (*i.e.* quadrillion-fold) cell expansion followed by differentiation towards fully functional (*i.e.* excitable and contractile) human AMs. The generation of these differentiation-competent human cardiomyocyte lines enabled the creation of human AF models that featured fibrillatory activity at clinically relevant frequencies, which could be terminated using antiarrhythmic drugs used in clinical practice.

The development of human cardiac muscle cell lines with preserved cardiomyogenic differentiation capacity has been the scope of several studies over the last decades (33,34). Thus far, human cardiomyocyte lines failed to recapitulate the structural and functional characteristics of the primary cells from which they were derived. Here, we show that this shortcoming can be overcome by imposing stringent control over SV40 LT expression in the target cells. The resulting hiAM lines allow straightforward production of contractile and excitable AMs in quantities not conceivable heretofore (*e.g.* one hiAM line can generate the number of cardiomyocytes present in 100,000 human adult hearts). Due to the monoclonal nature of hiAM lines and the high efficiency with which the cells undergo cardiomyogenic differentiation, pure populations of human AMs can be produced with great ease. This provides a clear advantage over derivation of AMs from hPSCs, which is a rather laborious and time-consuming multiphase process that generally includes a purification step (35,36) to select against the non-AMs remaining with current differentiation protocols (24,37,38). Moreover, differentiation completely abolishes proliferation of hiAMs while hPSC-derived cardiomyocytes still display some residual mitotic activity (39,40). Additionally, our comparative transcriptome analyses show that differentiated hiAMs closer match the gene expression

profile of haAMs than hESC-AMs. Also, hPSC-AMs from different studies have a non-physiological average RMP of approximately -56 mV, reflecting their immature electrophysiological phenotype (24,37,38,41). Differentiated hiAMs, on the other hand, display an average RMP of -79 mV, which is well within the -70 to -85 mV range reported for haAMs (42-44). The depolarized membranes of hPSC-AMs likely contribute to the slow AP propagation observed in confluent 2/3D cultures of these cells (24,45,46). Above -70 mV, a considerable fraction of Na^+ channels becomes inactivated, resulting in a decrease of AP upstroke velocity and a consequential reduction of CV. Although the CV in hiAM layers is significantly faster than in layers of hPSC-AMs (up to 30 cm/s vs. up to 2.5 cm/s), it is still slower than the 60-75 cm/s reached in human adult atrial tissue (47). This can, at least in part, be explained by the absence of anisotropic organization and neurohumoral regulation in the monolayers of differentiated hiAMs (48), providing a rationale for the future application of *in vitro* patterning technology to create cables/sheets of uniaxially aligned hiAMs and thereby increase the (longitudinal) CV in these structures along with neurohormonal stimulation.

The basic electrophysiological properties of hiAMs and hPSC-AMs also directly influence their applicability for AF modelling. The first report (24) of reentrant circuit induction in (non-purified) hESC-AM layers showed activation at a mean frequency of 3.2 Hz, which is very similar to the 3.0 Hz we found in our (purified) hESC-AM layers, but much lower than the 7.5 Hz in hiAM layers. For reference, activation frequencies measured in AF patients range between 6 to 8 Hz, depending on the type of AF (25-27). When studying the influence of antiarrhythmic drugs on reentry dynamics, activation frequencies resembling clinical AF are critical because of (reverse) rate-dependent effects. For instance, the I_{Na}-blocking activity of flecainide is increased at higher activation frequencies (49), which could explain why termination of reentry using 10 μM flecainide was possible in the majority of hiAM layers, while this was previously not successful in hESC-AM layers (24). As our hiAM-based AF model displays the main electrophysiological phenomena driving AF and provides new possibilities over existing models for studies into arrhythmia dynamics and antiarrhythmic drug discovery, a future extension would be to move towards more advanced 3D *in vitro* models of AF. Atrium-like 3D tissues have recently been generated using hPSC-AMs (46,50,51), but due to their small size (largest dimension ≤ 5 mm) they cannot accommodate reentrant circuits with characteristics similar to human AF. Advances in bioprinting technology have already demonstrated the feasibility of creating large and complex (cardiac)

scaffolds required for tissue engineering of whole human hearts (52). The main limiting factor for the creation of such large tissue constructs to date, has been the difficulty associated with generating the hundreds of millions/billions of well-differentiated cells necessary to populate these constructs. Although a recent report has shown that this problem may at least be partially overcome by a new method allowing the expansion of hiPSC-derived ventricular myocytes (40), it remains to be seen whether it can also induce multiplication of hPSC-AMs. Accordingly, the extensive scalability, cost-effectiveness and robustness of hiAM differentiation might provide a new impulse to create larger human atrial constructs for disease modelling, mechanistic studies and drug screening.

The ability to generate large numbers of differentiated hiAMs in an effective and robust manner may furthermore open the possibility to use them for biopharmaceutical production of, for instance, cardiomyocyte-derived exosomes and cardiokines (53). The latter property together with the monoclonal origin of hiAMs and the high controllability of their phenotype and gene expression profile, makes these cells particularly suitable for (very) high-resolution "omics" studies by obviating the need for cell selection and by providing plentiful input material. This offers new possibilities 1) to identify yet unknown factors involved in cardiomyocyte proliferation and differentiation, and 2) to find novel therapeutic targets, especially when combined with (opto)genetic, pharmaceutical, chemical or physical interventions to mimic disease states.

Although hiAM lines have many advantages over current AM sources, their suitability for regenerative purposes is limited due to the use of an integrating LV encoding an oncoprotein (*i.e.* SV40 LT) for (conditional) immortalization, which harbours the risk of tumour formation. hiAMs may, however, still be applied in animal models to optimize cardiac cell therapy, and may help to find new leads for endogenous induction of myocardial regeneration through stimulation of cardiomyocyte proliferation *in situ*. Although the high controllability and synchronicity of the transition from proliferation to differentiation could make hiAMs an excellent model for studying the molecular mechanisms underlying this transition, they will not fully represent the natural course of events due to the very nature (*i.e.* viral oncoprotein-dependent conditional immortalized state) of the cells. Moreover, the aneuploid status of hiAMs, which is associated with expression of SV40 LT (54), might limit certain applications with high sensitivity to potential gene imbalances. Nevertheless, this status did not result in apparent deviations from the AM phenotype based

on our comprehensive comparative analyses. In addition, the initial investment associated with the development of these cell lines, as well as the need for access to primary cardiac material, makes the conditional immortalization technique less suited than hiPSC technology for widescale patient-specific disease modelling. Still, using gene delivery or genome editing technologies, hiAM sublines with genetic modifications could easily be created, allowing studying the effects of these alterations in a highly standardized cell system. For instance, as described in the **Supplemental Results**, we could show that differentiated hiAMs with lentiviral short hairpin RNA-mediated knockdown of TBX5 expression display very similar disturbances of Ca^{2+} dynamics as observed in Holt-Oram syndrome (**see Supplemental Figure 21**). The ease with which hiAMs can be genetically modified makes it possible to perform comprehensive mechanistic studies mimicking the different types of atrial disease (55), allowing dissection of the precise molecular signatures of the diverse atrial cardiomyopathies, fostering thereby the development of novel preventive anti-AF therapies.

In summary, the conditional immortalization of hfAMs has enabled the creation of 1) the fully differentiation-competent lines of human cardiomyocytes and 2) human *in vitro* models of AF displaying clinically relevant features, which can be readily genetically modified to also mimic specific inherited atrial cardiomyopathies. This provides proof-of-concept of a versatile new method to produce, in a simple and rapid manner, massive numbers of authentic human cells for the development of representative human *in vitro* models for animal-free disease investigation, target identification along with drug discovery and therapeutic testing.

Methods

LV production

To generate vesicular stomatitis virus G protein-pseudotyped LV.iMHCK7.LT-WT particles, near confluent monolayers of 293T cells (56) were transfected with LV shuttle construct pLV.iMHCK7.LT-WT (**Supplemental Figure 1**) and the packaging plasmids psPAX2 (Addgene, plasmid number: 12260) and pLP/VSVG (Thermo Fisher Scientific, K497500) at a molar ratio of 2:1:1. pLV.iMHCK7.LT-WT is identical to pLV.iMHCK7.LT-tsA587 except for the replacement of the coding sequence of the temperature-sensitive SV40 LT mutant tsA58 by that of wild-type LT. The 293T cells were cultured in high-glucose Dulbecco's modified Eagle's medium (DMEM, Thermo Fisher Scientific, 41966) with 10% FBS (Thermo Fisher Scientific, 10270-106). The transfection mixture, consisting of 35 µg of plasmid DNA and 105 µg of linear 25-kDa polyethyleneimine (Polysciences, 23966) in 2 mL of 150 mM NaCl per 175-cm^2 cell culture flask (Greiner Bio-One, 660160), was directly added to the culture medium. Approximately 16 h later, the transfection medium was replaced by 15 mL of fresh high-glucose DMEM supplemented with 5% FBS and 25 mM HEPES-NaOH (pH 7.4). At ~48 h after the start of the transfection procedure, the culture supernatants were collected, cleared from cellular debris by centrifugation at room temperature (RT) for 10 min at 3,750×*g* and subsequent filtration through 0.45-µm pore-sized, 33-mm diameter polyethersulfone Millex-HP syringe filters (Merck Millipore, SLHP033RB). The LV particles were further purified and concentrated by underlaying 30 mL of vector suspension in a 38.5-ml polypropylene ultracentrifuge tube (Beckman Coulter, 326823) with 5 mL of 20% (wt/vol) sucrose in phosphate-buffered saline (PBS) and subsequent centrifugation for 2 h at 4°C with slow acceleration and without braking at 15,000 revolutions per min in an SW32 rotor (Beckman Coulter, 369650). Next, the supernatants were discarded and each pellet was suspended in 500 µl of PBS-1% bovine serum albumin (Sigma-Aldrich, A2153) by overnight incubation with gentle shaking at 4°C. The concentrated vector suspension was divided on ice in 100 µl aliquots for storage at -80°C.

Ethics Statement

Human foetal cardiac samples were obtained after elective abortions and with written informed consent. Donors were not incentivised/compensated. The samples were delivered to the researcher without any information except for the age of the foetus to guarantee full anonymity of the donors. This study was

conducted with approval of the institutional review board of the Leiden University Medical Centre (P08.087) and in compliance with the International Code of Medical Ethics of the World Medical Association.

Isolation and culture of hfAMs

The atria were separated from the ventricles of the foetal heart, minced into pieces of ~1 mm^2 and dissociated by 2 successive 30-min treatments with collagenase type I (225 U/ml, Worthington Biochemical, LS004196) and DNase I (20 U/ml, Sigma-Aldrich, DN25) under gentle agitation at 37°C. Cells were pelleted by centrifugation for 10 min at 160×*g* and RT. The supernatant was removed and cells were resuspended in Ham's F10 medium (Thermo Fisher Scientific, 11550) supplemented with 100 units/mL of penicillin and 100 µg/mL of streptomycin (Thermo Fisher Scientific, 15070-063), 10% heat-inactivated FBS (Thermo Fisher Scientific, 10500) and 10% heat-inactivated horse serum (Thermo Fisher Scientific, 26050). The cell suspension was transferred to uncoated Primaria culture dishes (Corning, 353803) and incubated for 75 min at 37°C in a humidified atmosphere of 95% air-5% CO_2 to allow preferential attachment of non-cardiomyocytes. Unattached cells were filtered through a nylon cell strainer (Corning, 431751) containing evenly spaced 70-µm mesh pores and seeded for experiments. For conditional immortalization, 10^4 cells/cm^2 were seeded in a 6-well culture plate (Corning, 3506) coated with fibronectin from bovine plasma (100 µg/mL, Sigma-Aldrich, F1141). For immunocytochemistry and patch-clamping, respectively 5×10^4 and 2.5×10^4 cells/cm^2 were seeded on fibronectin-coated glass coverslips in 24-well plates (Corning, 3524).

Conditional immortalization and selection of hiAM monoclones

The human foetal atrial cell mixture was transduced with 2.5 µl of concentrated LV.iMHCK7.SV40-LT-WT stock (*i.e.* the vector yield of 1.65×10^5 producer cells), following 2 days of recovery. Three days following transduction, the culture medium was changed to hiAM proliferation medium, consisting of Advanced DMEM/F-12 (Thermo Fisher Scientific, 12634), 2 mM GlutaMAX (Thermo Fisher Scientific, 35050061), 2% FBS (Biowest, S1810), 100 units/mL of penicillin and 100 µg/mL of streptomycin supplemented with 100 ng/ml doxycycline hyclate (Sigma-Aldrich, D9891) to induce SV40 LT expression. After the observation of cell proliferation, cells were detached using Accutase (BD Biosciences, 561527) and plated at a density of 10 cells/cm^2 in 145-mm diameter culture dishes (Greiner Bio-One, P7737) in the presence of hiAM proliferation medium. These

dishes were maintained for 2-3 weeks at 37°C in a humidified atmosphere of 95% air-5% CO_2 until colonies of 100-200 cells were observed. Individual colonies were then isolated with the aid of glass cloning cylinders (⌀ 6 mm, Corning, 3166-6) and treated with Accutase, after which the collection of cells inside each cylinder was transferred to single wells of a 48-well plate (Corning, 3548) in hiAM proliferation medium. Isolated colonies were given a unique number, expanded up to 106 cells and graded based on their proliferative and differentiation qualities. The conditional immortalization was considered successful for hiAM monoclones that 1) when given dox-containing hiAM proliferation medium proliferated beyond 15 PDs with a PD time shorter than 120 h and 2) in the presence of dox-free hiAM differentiation medium (see below) a) stopped proliferating and gradually acquired a cardiomyocyte-like phase-contrast appearance, b) lost proliferation marker Ki-67 expression and eventually consisted of > 50% of TNNT2-positive cells as assessed by immunocytochemistry and c) were electrically excitable with a minimal CV of 10 cm/s and maximal APD80 of 300 ms following optical voltage mapping of 1-cm^2 monolayers ≥ 12 days after dox removal. All selection criteria, including corresponding drop-off rates per criterium, can be found in **Supplemental Figure 1**.

Proliferation and differentiation of hiAMs

Proliferating hiAMs were cultured in uncoated TC-treated CELLSTAR flasks (Greiner Bio-One, 6901755, 658175, 660175) in the aforementioned hiAM proliferation medium. Culture medium was refreshed every 2-3 days. When confluency approached 90%, proliferating hiAMs were subjected to a 10-min treatment with Accutase at 37°C and carefully triturated into a (nearly) single-cell suspension. Next, the cells were pelleted by centrifugation for 5 min at 160×*g* and RT and transferred in a 1:2 to 1:4 ratio to new culture flasks for further multiplication, or seeded in appropriate culture plates for cardiomyogenic differentiation. Differentiation of hiAMs was performed in fibronectin-coated culture plates and initiated by changing the hiAM proliferation medium to hiAM differentiation medium, consisting of Advanced DMEM/F-12 (Thermo Fisher Scientific, 12634), 2 mM GlutaMAX and 2% Biowest FBS. Starting at day 4 of differentiation (the initiation of differentiation being day 0), hiAM differentiation medium was supplemented with 20 ng/ml triiodo-L-thyronine (T3) hormone (Sigma-Aldrich, T6397), 400 ng/ml dexamethasone (Centrafarm, 55091), 8 μM LF3 (Selleck Chemicals, S8474) or 10 μM ICRT14 (Sigma-Aldrich, SML0203) and 10 μM phenylephrine (Sigma-Aldrich, P6126).

Culture medium was refreshed every 2 days during differentiation. At day 12 of differentiation, the hiAMs were considered fully differentiated as at that time point CV and APD reached their plateau values. All experiments in this study were performed between day 12 to 15 after initiation of differentiation.

Proliferation assay

To assess the proliferation rates of individual hiAM clones in the presence of dox, 2×10^3 cells/cm^2 were seeded in multiple 100-mm diameter culture dishes (Corning, 430167). At 48-h intervals following culture initiation, cells were detached using Accutase, collected in hiAM proliferation medium and mixed in a 1:1 ratio with 0.4% Trypan Blue (Sigma-Aldrich, T8154). Following brief incubation, cells were counted using a CytoSMART Cell Counter (Corning). PD times were calculated by fitting data with an exponential growth equation (GraphPad Prism, v8.0.1, GraphPad Software).

Immunocytochemistry and image quantification

hfAMs and hiAMs were seeded at a density of 8×10^4 cells/cm^2 on fibronectin-coated coverslips prior to fixation with 4% buffered formaldehyde (Added Pharma, 14144751) for 30 min at 4°C. Cells were permeabilized by incubation with PBS/0.1% Triton X-100 (Sigma-Aldrich, X100) for 10 min, incubated with PBS/10% normal donkey serum (NDS, Sigma-Aldrich, D9663) for 30 min to block non-specific background staining and subsequently exposed to the primary antibody in PBS containing 0.5% NDS for 2 h, all at RT. After each treatment, cells were washed 3 times with PBS. Secondary antibody incubation was performed in PBS containing 0.5% NDS for 45 min and nuclei were stained for 10 min with Hoechst 33342 solution (Thermo Fisher Scientific, H-3570) diluted 1:1000 in PBS. For an overview of the antibodies and the dilutions at which they were applied, see **Supplemental Table 5**. Coverslips were mounted on StarFrost slides (VWR International, KNITVS112731FEA.01) using VECTASHIELD (Vector Laboratories, H-1000-10) and imaged with an Eclipse 80i Upright Microscope (during clone screening, Nikon Instruments) or TCS SP8 White Light Laser Confocal Microscope (during characterization, Leica Microsystems). Details on the use of the fluorescence microscopes are provided in the **Supplemental Methods**.

Counting of Ki-67-positive nuclei on the basis of mean grey values was performed using ImageJ (v1.52a, http://imagej.nih.gov/). For hiAMs, all Hoechst 33342-positive nuclei were analysed. In the case of the primary hfAMs, only the Nkx-2.5-positive nuclei were considered to avoid analysis of the non-

cardiomyocytes present in the samples. The mean grey value of each nucleus was compared to a threshold to distinguish between positive and negative nuclei. Sarcomere length was calculated by measuring the z-line distance of multiple adjacent sarcomeres in cell layers stained for ACTN2 (LAS X, v3.6.0, Leica Microsystems).

Western blotting

Adherent hiAMs were lysed on ice in RIPA buffer (50 mM Tris-HCl [pH 8.0], 150 mM NaCl, 1% NP-40, 0.5% sodium deoxycholate, 0.1% sodium dodecyl sulfate) supplemented with Roche cOmplete Mini Protease Inhibitor Cocktail (Sigma-Aldrich, 4693124001). The lysate was passed 3 times through a 30-gauge needle (BD Biosciences, 324826), centrifuged for 20 min at 4ºC and 16.000×*g*, after which the supernatant was collected and stored at -80ºC. Protein concentrations in the cleared lysates were determined using the Pierce BCA Protein Assay Kit (Thermo Fisher Scientific, 23225). Proteins were size-fractionated in Invitrogen Bolt 10% Bis-Tris Plus gels (Thermo Fisher Scientific, NW00102BOX) and transferred to Amersham Hybond P 0.45-µm polyvinylidene difluoride membranes (GE Healthcare, GEHE10600023) by wet electroblotting using a Bolt Mini Blot Module (Thermo Fisher Scientific). Membranes were incubated for 1 h in 2% ECL Prime blocking reagent (GE Healthcare, RPN418) dissolved in Tris-based saline/0.1% Tween 20 (TBST). Membranes were then incubated for 1 h with the primary antibody in TBST/2% ECL Prime blocking reagent, washed 5 times with TBST and incubated for 1 h with corresponding horseradish peroxidase-conjugated secondary antibodies. Information about the antibodies used can be found in **Supplemental Table 5**. Following 5 washes with TBST, membranes were covered with SuperSignal West Femto Maximum Sensitivity Substrate (Thermo Fisher Scientific, 34095) and chemiluminescence was measured using the ChemiDoc Touch Imaging System (Bio-Rad Laboratories) or iBright FL1500 Imaging System (Thermo Fisher Scientific). In some cases the blot was stripped following imaging using Restore PLUS Western Blot Stripping Buffer (Thermo Fisher Scientific, 46430) for an additional round of immunostaining. Protein levels were quantified with the aid of Image Lab (v6.0.1, Bio-Rad Laboratories) or the on-instrument software of the iBright FL1500 Imaging System, using levels of the housekeeping proteins and loading controls glyceraldehyde 3-phosphate dehydrogenase (GAPDH) or lamin A/C (LMNA) for normalization purposes.

RNA-sequencing hiAM proliferation vs. differentiation

Total RNA was extracted from proliferating and differentiated hiAMs seeded at a density of 10^5 cells/cm^2 (10^6 cells per sample) using the RNeasy Plus Mini Kit (Qiagen, 74104) according to manufacturer's instructions. RNA-sequencing was performed by GenomeScan (Leiden, the Netherlands). Quality and integrity of the RNA were confirmed using a 2100 Bioanalyzer Instrument (Agilent Technologies), with a measured RNA quality number of 10.0 for all samples. Library preparation was performed using the NEBNext Ultra II Directional RNA Library Prep Kit for Illumina in combination with the NEBNext Poly(A) mRNA Magnetic Isolation Module (New England Biolabs, E7765). Sample quality and yield after cDNA synthesis and polymerase chain reaction enrichment were measured with the bioanalyzer (range average size 445-524 base pairs [bp]). Clustering and DNA sequencing (50-82 million 150-bp paired-end reads) using the NovaSeq6000 DNA sequencer (Illumina) was performed according to manufacturer's protocols. Image analysis, base calling and quality check were performed with the Illumina data analysis pipeline RTA3.4.4 and Bcl2fastq (v2.20). Prior to alignment, the reads were trimmed for adapter sequences using Trimmomatic (v0.30). Reads were aligned to the Homo sapiens reference genome (GRCh37.75) using Tophat (v2.0.14) and read counts were determined using HTSeq (v0.6.1p1). Additionally, TPM values were calculated to compare gene expression levels between groups. Differential gene expression (Wald test) was assessed by analysing read counts with the DESeq2 package (v1.14.1) in the R platform (v3.3.0). Genes with an absolute log2-fold change > 1.0 (*i.e.* a > twofold absolute change) and false discovery rate (FDR)-corrected $P < 0.001$ were considered differentially expressed. Comparison of differentially expressed genes (DEGs) between clones was limited to genes with > 1 TPM in the proliferative state or at day 12 of cardiomyogenic differentiation to exclude DEGs with very low overall expression. Gene set enrichment analysis was performed in DAVID (v6.8).

RNA-sequencing hESC-AMs and hiAMs

Total RNA was extracted from hESC-AMs (10^6 cells per sample) using the NucleoSpin RNA kit (Macherey-Nagel, 740955) according to manufacturer's instructions. Total RNA extraction from hiAMs has been described above. Libraries were generated from 200 ng RNA using the KAPA-RNA HyperPrep kit with RiboErase (Roche, 8098131702) to remove ribosomal RNA, according to manufacturer's instructions. Library amplification was performed with 11 cycles, after which the size distribution was determined with a 2100 Bioanalyzer Instrument. Paired-end library sequencing was performed with the

NextSeq500 sequencing system (Illumina). Trimming of the reads and alignment was performed with seq2science (v0.4.0, available on Zenodo, https://doi.org/10.5281/zenodo.4451349). In short, Fastp (57) (v0.20.1) trimmed the low quality 3' ends and Salmon (58) (v1.3.0) quant aligned the reads to the GRCh38.p13 genome from Ensembl, after which tximeta (59) (v1.4.3) generated the gene expression matrix. The counts per million (CPM) were log1p-transformed. The published foetal dataset by Cui et al. (19) was retrieved as count matrix and the mean of expression was calculated per tissue type. The 2000 most variable genes within this dataset were determined with the variance-stabilized transformation method in Seurat (60) (v3). The selection of most variable genes in the GTEx portal dataset (20) was performed by taking the genes with a coefficient of variation > 2. Differential gene expression analysis (Wald test) between hESC-AMs and hiAMs was performed with the R package DESeq2 (61) (v1.22.2). The differential gene list was filtered for a log2-fold change > 1 and *P*-adjusted value < 0.01 (4145 significant differential genes in total), and visualized with pheatmap (v1.0.12). To establish if there were significant differences in specific gene list ranks between the samples, the Wilcoxon signed-rank test (two-sided) was used in pairwise comparisons.

Generation of hESC-AMs

NKX2.5eGFP/+-COUP-TFIImCherry/+ hESCs, as described before (35), were maintained as undifferentiated colonies in Essential 8 medium (Thermo Fisher Scientific, A1517001) on vitronectin (Thermo Fisher Scientific, A14700)-coated culture plastics. Differentiation of these cells to AMs was performed using the previously described spin embryoid body protocol with retinoic acid treatment (35,41). To generate pure populations of hESC-AMs, eGFP- and mCherry-double positive cells were purified around day 17 of differentiation using a Sony Biotechnology SH800 flow cytometer after exclusion of dead cells and debris according to side and forward scatter. After sorting, cells were suspended in TID medium (61) and transferred to vitronectin-coated 48-well culture plates to establish confluent monolayers. Optical voltage mapping of hESC-AMs was performed 5-11 days after replating.

Cellular electrophysiology

Differentiated hiAMs were dissociated by incubation with a 5 U/mL papain (Worthington Biochemical, LS003127) and 1 mM L-cysteine (Sigma-Aldrich, C6852) solution in PBS for 10 min at 37°C. Next, an equal volume of stop

solution was added, consisting of 1 mg/mL soybean trypsin inhibitor (Sigma-Aldrich, T9253) and 40 µg/mL DNase I in PBS. Cells were pelleted by centrifugation for 5 min at 160×*g* at RT and plated at densities of 3-6×10^4 cells/cm^2 on fibronectin-coated 12-mm diameter glass coverslips (VWR International, 631-1577), and measured over the 3 following days.

Single-cell APs and membrane currents were recorded using Axopatch 200B and MultiClamp 700B amplifiers (Molecular Devices). Signals were low-pass filtered at 5-kHz cut-off frequency and digitized at 40 and 20 kHz for APs and membrane currents, respectively. Data acquisition and analysis were accomplished with pClamp (v10.7, Molecular Devices) and custom-made software. Series resistance was compensated by ≥ 80%. Patch pipettes were pulled from borosilicate glass (Harvard apparatus) and had resistances of 2.0-3.0 MΩ after filling with the solutions as indicated. Potentials were corrected for the calculated liquid junction potential (63). Cell membrane capacitance (C_m) was estimated by dividing the time constant of the decay of the capacitive transient in response to 5 mV hyperpolarizing voltage clamp steps from −40 mV by the series resistance.

APs were recorded using the amphotericin-perforated patch-clamp technique at 36 ± 0.2°C. The bath solution was a modified Tyrode's solution containing (in mM): 140 NaCl, 5.4 KCl, 1.8 $CaCl_2$, 1.0 $MgCl_2$, 5.5 glucose and 5.0 HEPES-NaOH (pH 7.4). The pipette solution contained (in mM): 125 K-gluconate, 20 KCl, 5.0 NaCl, 0.44 amphotericin B (Sigma-Aldrich, A2411) and 10 HEPES-KOH (pH 7.2). APs were elicited at 1-Hz by 3-ms, ~1.2× threshold current pulses through the patch pipette. Parameters from ten consecutive APs were averaged. APs from haAMs were measured in non-depolarized single, rod-shaped cardiomyocytes (64), which were isolated for a previous study (65). In short, cells were enzymatically isolated with the chunk method from left atrial appendages as described previously (65). These appendages were obtained from patients in sinus rhythm undergoing cardiac surgery (coronary bypass grafting or valve surgery), and included in the multicentre PREDICT AF study (66). The patient characteristics are as reported previously (65). Details on the Na^+ and K^+ current recordings in hiAMs are provided in the **Supplemental Methods**.

Optical voltage mapping

To assess AP properties and propagation in monolayers, hiAMs were seeded in fibronectin-coated 48-well, 24-well or 6-well culture plates at a density of 4×10^5 cells/cm^2 and differentiated as described. Alternatively, hESC-AMs were seeded at a density of 5.8×10^5 cells/cm^2 in vitronectin-coated 48-well culture

plates. Cell layers of hiAMs or hESC-AMs were incubated with 8 μM di-4-ANEPPS (Thermo Fisher Scientific, D1119) in DMEM/F-12 (Thermo Fisher Scientific, 11039) for 10 min in a humidified 95% air-5% CO2 incubator at 37°C. Following incubation, medium was changed to fresh DMEM/F-12 and cells were placed on a 37°C warming plate for the duration of the experiment. During optical voltage mapping, excitation light (525 ± 25 nm) was delivered by a halogen arc-lamp through epi-illumination. Emission light passed through a dichroic mirror and a long-pass emission filter (> 590 nm). Signals were acquired using a 100×100 pixels complementary metal oxide semiconductor camera (MiCAM05-Ultima, SciMedia) at a spatial resolution of 165 (48/24-well) or 250 (6-well) μm/pixel, and a temporal resolution between 2 and 6 ms per frame depending on the type and duration of experiment. Acquisition times varied between 4 and 12 s for characterization studies, and up to 2 min for arrhythmia studies. Data was analysed using BrainVision Analyzer (v16.04.20, BrainVision). Signals were averaged with those of the 8 nearest neighbouring pixels to minimize noise artefacts. CV, APD and activation frequency were determined at a minimum of 5 different vectors/locations equally distributed throughout the culture. Arrhythmia wavelength was calculated by multiplying average CV and APD_{90}. Temporal excitation gap was calculated by subtracting APD_{90} during arrhythmic activation from the cycle length. Activation frequency over time was determined by analysing peak to peak intervals through a custom MATLAB (vR2016a, MathWorks) script on high-pass filtered data at selected locations in the culture.

Electrical stimulation and arrhythmia induction

Electrical point stimulation during optical voltage mapping was performed using an epoxy-coated bipolar platinum electrode, delivering 8-V, 10-ms square pulses. The electrode was connected to a STG 2004 stimulus generator (Multi Channel Systems) driven by MC Stimulus II software (v3.5.0, Multi Channel Systems). Baseline AP properties and propagation were calculated during 1-Hz electrical pacing (i.e. 1000-ms cycle length). Restitution was calculated by pacing at a cycle length of 1000 ms (S1) followed by an additional stimulus (S2) at a variable cycle length. Arrhythmia induction was performed by delivering 20 to 40 stimuli at the shortest cycle length at which 1:1 capture was maintained (range 90-180 ms), generally starting with a cycle length equal to the APD_{80}.

Arrhythmia studies and drug interventions

To determine relevant compound dosage, flecainide acetate salt (Sigma-Aldrich, F6777) dissolved in DMSO (CryoMACS, Miltenyi Biotec, 170-076-303), sotalol hydrochloride (Sigma-Aldrich, S0278) dissolved in demineralized water and DMSO (solvent/vehicle control), were tested on 2-cm^2 hiAM layers at increasing doses during optical voltage mapping, until loss of excitability. For each compound, 3 escalating doses were chosen, to include various effect sizes in a clinically relevant range. Induced reentrant circuits were monitored for 5 min to confirm stability before compounds were infused to study their effect on reentrant circuit characteristics. Flecainide, sotalol or DMSO as control, all at 3 concentrations, were slowly infused in a 1:1 volume ratio into cultures with reentrant circuits during optical voltage mapping using an infusion pump (Acromed Medical Systems) controlling infusion rate and volume (3 mL at 0.16 mL/s). Cultures were continuously monitored from 2 min prior to drug infusion until 10 min after the start of the drug treatment.

Cryopreservation

hiAMs at day 8 of cardiomyogenic differentiation were dissociated by papain treatment, pelleted by centrifugation and resuspended in cold (4°C) culture medium. Next, an equal volume of ice-cold 80% FBS/20% DMSO was added dropwise to the suspension, after which cryovials containing 10^6 cells/mL were frozen to −80°C at a rate of −1°C/min. Twenty-four h later, the cells were placed in nitrogen vapor for long-term storage. Cells were thawed by swirling vials in a 37°C bath, immediately followed by dropwise addition of cold (4°C) culture medium until a tenfold dilution was reached. Cells were pelleted by centrifugation, resuspended in supplemented hiAM differentiation medium and cultured for 6 days in this medium to complete differentiation. Cell viability after dissociation and after thawing as well as replating efficiency of the cells was determined by 0.4% Trypan Blue staining (1:1 ratio) and manual counting using a haemocytometer.

Statistics and Reproducibility

Statistical analyses were performed using GraphPad Prism (v8.0.1, GraphPad Software). Data are presented as mean ± standard deviation (SD) or mean ± standard error of the mean (SEM), unless otherwise indicated. Normally distributed data between independent groups was tested for statistical significance using the unpaired t-test (2 groups) or using the one-way analysis of variance with Tukey or Dunnett post-hoc analysis (3 or more groups). Dependent groups were tested using a paired t-test (2 groups) or using a

repeated measure one-way analysis of variance with Tukey or Dunnett post-hoc analysis (3 or more groups). Non-normally distributed independent data were compared using the Mann-Whitney test. Dependent non-normally distributed data of multiple groups were compared using the Friedman test with Dunn post-hoc analysis. The stability of mean CV and APD at various PDs was tested by calculating the Pearson correlation coefficient. Rates of reentrant activity termination were compared between groups using the Chi-square test. All testing was performed two-sided. Statistical significance was expressed as following for clarity: *P < 0.05, **P < 0.01, ***P < 0.001. Precise P-values can be found in **Supplemental Data File 3**. Representative micrographs were chosen from a number of images (generally $n \geq 3$), based on multiple independent differentiations.

Data and materials availability

LV.iMHCK7.SV40-LT-WT particles can be obtained by academic research groups under a material transfer agreement (contact hiAM@lumc.nl for inquiries). The main data supporting the results in this study are available within the paper and its **Supplemental Information**. Certain raw and analysed datasets generated during the study are too large to be publicly shared, yet they are available for research purposes from the corresponding authors on reasonable request. The RNA-sequencing data described in this study is available at the NCBI's Gene Expression Omnibus (GEO) under GEO accession numbers GSE156824 and GSE178473. The Whole Genome Sequencing data is available under BioProject accession number PRJNA760786.

Acknowledgments

The authors thank Jia Liu (LUMC, Leiden, the Netherlands) for constructing plasmid pLV.iMHCK7.SV40-LT-WT and producing LV.iMHCK7.SV40-LT-WT particles, Tessa van Herwaarden (LUMC, Leiden, the Netherlands) for collecting human foetal atrial tissue, Bini Klein (LUMC, Leiden, the Netherlands) for donating the SV40 LT-encoding plasmid pAT153.SV40ori, Stephen Hauschka (University of Washington, Seattle, WA) for providing construct +aMHCKChCAT encoding the MHCK7 promoter, Didier Trono (Swiss Federal Institute of Technology Lausanne, Lausanne, Switzerland) for making available the LV shuttle plasmid pLVET-tTR-KRAB, Carolina Jost (LUMC, Leiden, the Netherlands) for assistance with interpretation and annotation of transmission electron microscopy data and Ursula Ravens (University of Freiburg, Freiburg, Germany) for useful discussions.

References

1. Robinson, N. B. et al. The current state of animal models in research: A review. *Int J Surg*. 2019;72:9-13.

2. Ruijtenberg, S. & van den Heuvel, S. Coordinating cell proliferation and differentiation: Antagonism between cell cycle regulators and cell type-specific gene expression. *Cell Cycle*. 2016;15:196-212.

3. Thomson, J. A. et al. Embryonic stem cell lines derived from human blastocysts. *Science*. 1998;282:1145-7.

4. Takahashi, K. et al. Induction of pluripotent stem cells from adult human fibroblasts by defined factors. *Cell*. 2007;131:861-72.

5. Yu, J. et al. Induced pluripotent stem cell lines derived from human somatic cells. *Science*. 2007;318:1917-20.

6. Kim, J., Koo, B. K. & Knoblich, J. A. Human organoids: model systems for human biology and medicine. *Nat Rev Mol Cell Biol*. 2020.

7. Liu, J. et al. Generation and primary characterization of iAM-1, a versatile new line of conditionally immortalized atrial myocytes with preserved cardiomyogenic differentiation capacity. *Cardiovasc Res*. 2018;114:1848-59.

8. Liu, J. et al. Conditionally immortalized brown preadipocytes can switch between proliferative and differentiated states. *Biochim Biophys Acta Mol Cell Biol Lipids*. 2019;1864:158511.

9. Deuschle, U., Meyer, W. K. & Thiesen, H. J. Tetracycline-reversible silencing of eukaryotic promoters. *Mol Cell Biol*. 1995;15:1907-14.

10. Szulc, J., Wiznerowicz, M., Sauvain, M. O., Trono, D. & Aebischer, P. A versatile tool for conditional gene expression and knockdown. *Nat Methods*. 2006;3:109-16.

11. Chugh, S. S. et al. Worldwide epidemiology of atrial fibrillation: a Global Burden of Disease 2010 Study. *Circulation*. 2014;129:837-47.

12. Kim, M. H., Johnston, S. S., Chu, B. C., Dalal, M. R. & Schulman, K. L. Estimation of total incremental health care costs in patients with atrial fibrillation in the United States. *Circ Cardiovasc Qual Outcomes*. 2011;4:313-20.

13. Nattel, S., Heijman, J., Zhou, L. & Dobrev, D. Molecular Basis of Atrial Fibrillation Pathophysiology and Therapy: A Translational Perspective. *Circ Res*. 2020;127:51-72.

14. Heijman, J., Guichard, J. B., Dobrev, D. & Nattel, S. Translational Challenges in Atrial Fibrillation. *Circ Res.* 2018;122:752-73.

15. Kirchhof, P. The future of atrial fibrillation management: integrated care and stratified therapy. *Lancet*. 2017;390:1873-87.

16. van Gorp, P. R. R., Trines, S. A., Pijnappels, D. A. & de Vries, A. A. F. Multicellular In vitro Models of Cardiac Arrhythmias: Focus on Atrial Fibrillation. *Front Cardiovasc Med*. 2020;7:43.

17. Salva, M. Z. et al. Design of tissue-specific regulatory cassettes for high-level rAAV-mediated expression in skeletal and cardiac muscle. *Mol Ther*. 2007;15:320-9.

18. Huttenbach, Y., Ostrowski, M. L., Thaller, D. & Kim, H. S. Cell proliferation in the growing human heart: MIB-1 immunostaining in preterm and term infants at autopsy. *Cardiovasc Pathol*. 2001;10:119-23.

19. Cui, Y. et al. Single-Cell Transcriptome Analysis Maps the Developmental Track of the Human Heart. *Cell Rep*. 2019;26:1934-50

20. Consortium, G. T. The Genotype-Tissue Expression (GTEx) project. *Nat Genet*. 2013;45:580-5.

21. Baker, M. Reproducibility: Respect your cells! *Nature*. 2016;537:433-5.

22. Narayan, S. M., Shivkumar, K., Krummen, D. E., Miller, J. M. & Rappel, W. J. Panoramic electrophysiological mapping but not electrogram morphology identifies stable sources for human atrial fibrillation: stable atrial fibrillation rotors and focal sources relate poorly to fractionated electrograms. *Circ Arrhythm Electrophysiol*. 2013;6:58-67.

23. Balouch, M. et al. Impact of rotor temperospatial stability on acute and one-year atrial fibrillation ablation outcomes. *Clin Cardiol*. 2017;40:383-9.

24. Laksman, Z. et al. Modeling Atrial Fibrillation using Human Embryonic Stem Cell-Derived Atrial Tissue. *Sci Rep*. 2017;7:5268.

25. Sanders, P. et al. Spectral analysis identifies sites of high-frequency activity maintaining atrial fibrillation in humans. *Circulation*. 2005;112:789-97.

26. Schuessler, R. B. et al. Spatial and temporal stability of the dominant frequency of activation in human atrial fibrillation. *J Electrocardiol*. 2006;39:S7-12.

27. Yoshida, K. et al. Left atrial pressure and dominant frequency of atrial fibrillation in humans. *Heart Rhythm*. 2011;8:181-7.

28. January, C. T. et al. 2014 AHA/ACC/HRS guideline for the management of patients with atrial fibrillation: a report of the American College of Cardiology/American Heart Association Task Force on Practice Guidelines and the Heart Rhythm Society. *J Am Coll Cardiol*. 2014;64:e1-76.

29. Kirchhof, P. et al. 2016 ESC Guidelines for the management of atrial fibrillation developed in collaboration with EACTS. *Eur Heart J*. 2016;37:2893-962.

30. Hindricks, G. et al. 2020 ESC Guidelines for the diagnosis and management of atrial fibrillation developed in collaboration with the European Association of Cardio-Thoracic Surgery (EACTS). *Eur Heart J*. 2020.

31. Sanguinetti, M. C. & Jurkiewicz, N. K. Two components of cardiac delayed rectifier K+ current. Differential sensitivity to block by class III antiarrhythmic agents. *J Gen Physiol*. 1990;96:195-215.

32. Melgari, D., Zhang, Y., El Harchi, A., Dempsey, C. E. & Hancox, J. C. Molecular basis of hERG potassium channel blockade by the class Ic antiarrhythmic flecainide. *J Mol Cell Cardiol*. 2015;86:42-53.

33. Davidson, M. M. et al. Novel cell lines derived from adult human ventricular cardiomyocytes. *J Mol Cell Cardiol*. 2005;39:133-47.

34. Goldman, B. I., Amin, K. M., Kubo, H., Singhal, A. & Wurzel, J. Human myocardial cell lines generated with SV40 temperature-sensitive mutant tsA58. *In Vitro Cell Dev Biol Anim*. 2006;42:324-31.

35. Schwach, V. et al. A COUP-TFII Human Embryonic Stem Cell Reporter Line to Identify and Select Atrial Cardiomyocytes. *Stem Cell Reports*. 2017;9:1765-79.

36. Ban, K., Bae, S. & Yoon, Y. S. Current Strategies and Challenges for Purification of Cardiomyocytes Derived from Human Pluripotent Stem Cells. *Theranostics*. 2017;7:2067-77.

37. Lee, J. H., Protze, S. I., Laksman, Z., Backx, P. H. & Keller, G. M. Human Pluripotent Stem Cell-Derived Atrial and Ventricular Cardiomyocytes Develop from Distinct Mesoderm Populations. *Cell Stem Cell*. 2017;21:179-94.

38. Argenziano, M. et al. Electrophysiologic Characterization of Calcium Handling in Human Induced Pluripotent Stem Cell-Derived Atrial Cardiomyocytes. *Stem Cell Reports*. 2018;10:1867-78.

39. Branco, M. A. et al. Transcriptomic analysis of 3D Cardiac Differentiation of Human Induced Pluripotent Stem Cells Reveals Faster Cardiomyocyte Maturation Compared to 2D Culture. *Sci Rep*. 2019;9:9229.

40. Buikema, J. W. et al. Wnt Activation and Reduced Cell-Cell Contact Synergistically Induce Massive Expansion of Functional Human iPSC-Derived Cardiomyocytes. *Cell Stem Cell*. 2020;27:50-63.

41. Devalla, H. D. et al. Atrial-like cardiomyocytes from human pluripotent stem cells are a robust preclinical model for assessing atrial-selective pharmacology. *EMBO Mol Med*. 2015;7:394-410.

42. Voigt, N. et al. Enhanced sarcoplasmic reticulum Ca2+ leak and increased Na+-Ca2+ exchanger function underlie delayed afterdepolarizations in patients with chronic atrial fibrillation. *Circulation*. 2012;125:2059-70.

43. Voigt, N. et al. Cellular and molecular mechanisms of atrial arrhythmogenesis in patients with paroxysmal atrial fibrillation. *Circulation*. 2014;129:145-56.

44. Heijman, J. et al. Atrial Myocyte NLRP3/CaMKII Nexus Forms a Substrate for Post-Operative Atrial Fibrillation. *Circ Res*. 2020.

45. Nakanishi, H. et al. Geometrical Patterning and Constituent Cell Heterogeneity Facilitate Electrical Conduction Disturbances in a Human Induced Pluripotent Stem Cell-Based Platform: An In vitro Disease Model of Atrial Arrhythmias. *Front Physiol*. 2019;10:818.

46. Goldfracht, I. et al. Generating ring-shaped engineered heart tissues from ventricular and atrial human pluripotent stem cell-derived cardiomyocytes. *Nat Commun*. 2020;11:75.

47. Harrild, D. & Henriquez, C. A computer model of normal conduction in the human atria. *Circ Res*. 2000;87:E25-36.

48. Valderrabano, M. Influence of anisotropic conduction properties in the propagation of the cardiac action potential. *Prog Biophys Mol Biol*. 2007;94:144-68/

49. Salvage, S. C. et al. Multiple targets for flecainide action: implications for cardiac arrhythmogenesis. *Br J Pharmacol*. 2018;175:1260-78.

50. Lemme, M. et al. Atrial-like Engineered Heart Tissue: An In Vitro Model of the Human Atrium. *Stem Cell Reports*. 2018;11:1378-90.

51. Zhao, Y. et al. A Platform for Generation of Chamber-Specific Cardiac Tissues and Disease Modeling. *Cell*. 2019;176:913-27.

52. Lee, A. et al. 3D bioprinting of collagen to rebuild components of the human heart. *Science*. 2019;365:482-7.

53. Yu, H. & Wang, Z. Cardiomyocyte-Derived Exosomes: Biological Functions and Potential Therapeutic Implications. *Front Physiol*. 2019;10:1049.

54. Chang, T. H., Ray, F. A., Thompson, D. A. & Schlegel, R. Disregulation of mitotic checkpoints and regulatory proteins following acute expression of SV40 large T antigen in diploid human cells. *Oncogene*. 1997;14:2383-93

55. Goette, A. et al. EHRA/HRS/APHRS/SOLAECE expert consensus on atrial cardiomyopathies: Definition, characterization, and clinical implication. *Heart Rhythm*. 2017;14:e3-e40.

56. DuBridge, R. B. et al. Analysis of mutation in human cells by using an Epstein-Barr virus shuttle system. *Mol Cell Biol*. 1987;7:379-87.

57. Chen, S., Zhou, Y., Chen, Y. & Gu, J. fastp: an ultra-fast all-in-one FASTQ preprocessor. *Bioinformatics*. 2018;34:i884-i90.

58. Patro, R., Duggal, G., Love, M. I., Irizarry, R. A. & Kingsford, C. Salmon provides fast and bias-aware quantification of transcript expression. *Nat Methods*. 2017;14:417-9.

59. Love, M. I. et al. Tximeta: Reference sequence checksums for provenance identification in RNA-seq. *PLoS Comput Biol*. 2020;16:e1007664.

60. Stuart, T. et al. Comprehensive Integration of Single-Cell Data. *Cell*. 2019;177:1888-902.

61. Love, M. I., Huber, W. & Anders, S. Moderated estimation of fold change and dispersion for RNA-seq data with DESeq2. *Genome Biol*. 2014;15:550.

62. Birket, M. J. et al. Contractile Defect Caused by Mutation in MYBPC3 Revealed under Conditions Optimized for Human PSC-Cardiomyocyte Function. *Cell Rep*. 2015;13:733-45.

63. Barry, P. H. & Lynch, J. W. Liquid junction potentials and small cell effects in patch-clamp analysis. *J Membr Biol*. 1991;121:101-17.

64. Verkerk, A. O. et al. Patch-Clamp Recordings of Action Potentials From Human Atrial Myocytes: Optimization Through Dynamic Clamp. *Front Pharmacol*. 2021;12:649414.

65. Casini, S. et al. Absence of Functional Nav1.8 Channels in Non-diseased Atrial and Ventricular Cardiomyocytes. *Cardiovasc Drugs Ther*. 2019;33:649-60.

66. van den Berg, N. W. E. et al. PREventive left atrial appenDage resection for the predICtion of fuTure atrial fibrillation: design of the PREDICT AF study. *J Cardiovasc Med (Hagerstown)*. 2019;20:752-61.

Supplemental Methods

Flow cytometric assessment of human immortalized atrial myocyte (hiAM) ploidy

For assessment of ploidy, differentiated hiAMs were detached using papain, pelleted by centrifugation (200×*g*, 5 min) and fixed by a 20-min incubation with 90% methanol of -20°C. Prior to fixation, half of the cell suspension was spiked with peripheral blood mononuclear cells (PBMCs) to provide a diploid standard. Following the addition of an equal volume of ice-cold PBS-0.1% TWEEN 20 (PBST; Sigma-Aldrich, P1379), the cells were pelleted, washed with ice-cold PBST, stained with 2.5 µM DAPI (BioLegend, 422801) in PBS/5.0% bovine serum albumin (BSA)/0.5% TWEEN 20 by incubation for 30 min at room temperature (RT) and stored overnight at 4°C in the same solution before measurement. Prior to flow cytometric analysis on the FACSCanto II with FACSDiva 8.0 software (both from BD Biosciences), samples were filtered through a cell strainer with a 35-µm nylon mesh (Falcon Tube with Filter Cap, Thermo Fisher Scientific, 352235). Cytometer Setup and Tracking beads (BD Biosciences, 641319) were used to check cytometer performance and guaranty data quality. Cells were excited using solid state lasers of 20 mW and 488 nm and of 60 mW and 405 nm. Forward scatter (FSC), side scatter (SSC) and DAPI fluorescence (452/45 nm band pass filter) area (A), height (H) and width (W) were recorded and stored as FCS 3.0 list mode data files. During acquisition a live gate was applied selecting single-cell events using DAPI-A vs DAPI-W pulse processing. A minimum of 30,000 single-cell events were collected of each sample using a low flow rate, maintaining optimal hydrodynamic focusing. Data were analysed using WinList 8 linked to ModFit LT 5.0 (both from Verity Software House) using 256 channel resolution for DNA content analysis. The relative median channel number of the PBMCs' G1 population was used as DNA diploid reference to determine hiAM ploidy. A hypodiploid, aneuploid 2, aneuploid 3 statistical model was used for analysis, as this provided the best fit (*i.e.* fair to good) with a reduced Chi-square (RCS) never exceeding 3.2. Additionally, ModFit LT handled aggregates and debris after manual correction for evident aggregates using DAPI-A vs DAPI-W pulse processing.

Flow cytometric assessment of hiAM purity

Differentiated hiAMs were detached using papain, pelleted by centrifugation (200×*g*, 5 min), fixed by incubation with 4% buffered formaldehyde for 15 min at RT and permeabilized by a treatment of ≥ 20 min with 90% methanol of -

20°C. hiAMs were incubated with primary antibodies in PBS-0.5% BSA for 1 h at RT followed by a 30-min incubation at RT with Alexa 488-conjugated secondary antibodies in PBS-0.5% BSA. Between each step, cells were washed twice with PBS-0.5% BSA. For an overview of the antibodies and the dilutions at which they were used, see **Supplemental Table 5**. Analysis was performed with an Accuri C6 flow cytometer (BD Biosciences), equipped with 473- and 552-nm lasers. The hiAM samples were excited with the 473-nm laser and the emitted light was passed through a 586/15 nm band pass filter before being captured by the photodetector. Cells stained only with the fluorochrome-conjugated secondary antibody were included as control. Gating of hiAMs was performed as shown in **Supplemental Figure 4**. Per sample, 5,000-20,000 gated events were analysed using the BD Accuri C6 Software (v1.0.264).

Transmission electron microscopy

Differentiated hiAMs were fixed for 1 h at RT by addition of an equal volume of fixative (3% glutaraldehyde in 0.1 M cacodylate buffer pH 7.4) to the hiAM culture medium. After washing the monolayers 3 times with 0.1 M cacodylate buffer, the cells were post-fixed for 1 h on ice with 1% osmium tetroxide, 1.5% potassium ferricyanide in 0.1 M cacodylate buffer. Next, the sample was dehydrated by a graded series of ethanol in water followed by a graded series of LX 112 resin (Ladd Research, 21210) in ethanol. After the final incubation step with 100% LX 112, BEEM capsules (Tedd Pella, 21600) filled with LX 112 were placed on the fixed cells. After polymerization of the LX 112, the BEEM capsules were snapped off the surface of the culture dishes. Ultrathin sections (90 nm) parallel to the surface were made on a Reichert Ultracut S (Leica Microsystems). Following post-staining of the sections with uranyl acetate and lead citrate, the electron microscopy images were taken with a FEI Technai Twin T12 transmission electron microscope (Thermo Fisher Scientific) operating at 120 kV, using a Gatan OneView camera on binning 2. Overlapping images were collected and stitched together into a big image as described (67).

TBX5 knockdown

Oligodeoxyribonucleotides for generating a lentiviral vector (LV) encoding a short hairpin RNA (shRNA) targeting all transcripts of human TBX5 were designed with the aid of the GPP Web Portal from the Broad Institute. To rule out off-target effects, a target sequence was selected that did not show an overlap of > 13 nucleotides with any other human transcript as determined using BlastN (National Center for Biotechnology Information). The sequences of the

oligodeoxyribonucleotides for generating a control shRNA targeting firefly luciferase (PpLuc) were derived from the MISSION shRNA Library (SHC007, Sigma-Aldrich). The annealing products of both oligodeoxyribonucleotide pairs (see **Supplemental Table 6** for nucleotide sequences) were inserted in between the human RNU6-1 gene promoter and an RNA polymerase III termination sequence of an LV shuttle plasmid that also contained a human UBC gene (HsUBC) promoter-driven expression unit encoding the Aequorea victoria enhanced green fluorescent protein (eGFP). The correctness of the shRNA-encoding constructs was validated by diagnostic restriction enzyme digestions as well as by Sanger sequencing. LV production was performed as described in the main manuscript.

Whole genome sequencing

Genomic DNA of 5×10^5 proliferating hiAMs was isolated using the ISOLATE II Genomic DNA Kit (Meridian Bioscience, BIO-52066) according to manufacturer's instructions. Samples were sent to BGI Genomics for whole genome sequencing. Here, following quality control by agarose gel electrophoresis, genomic DNA was fragmented by sonification (Covaris). Fragments with an average length of 350 base pairs were selected and underwent end-repairing and A-tailing reactions. Adapters were ligated to A-tailed fragments and amplified by ligation-mediated polymerase chain reaction. The amplified DNA fragments were then denatured and circularized by splint-mediated DNA ligation. After removal of remaining non-circularized DNA templates by exonuclease treatment, the single-stranded DNA circles were converted into DNA nanoballs (DNBs) by rolling circle amplification. The DNBs were loaded into patterned nanoarrays and pair-end sequencing was performed on the BGISEQ-500 platform. Sequencing-derived raw image files were processed by BGISEQ-500 base calling software. Raw data was filtered to remove reads containing sequencing adapters, reads whose low-quality base ratio (base quality ≤ 5) was more than 50% and reads whose unknown base ('N' base) ratio was more than 10%. These clean reads were aligned to human reference genome GRCh37 using Burrows-Wheeler Aligner (v0.7.12). Local realignment around insertions/deletions and base quality score recalibration were performed using GATK (v3.3.0), with duplicate reads removed by Picard (v1.118). Lentiviral integration sites were determined by locating reads that aligned to (one of the termini of) the proviral DNA sequence of LV.iMHCK7.LT-WT and to the human reference genome.

Ca^{2+} imaging

To compare Ca^{2+} handling of hiAMs and human embryonic stem cell-derived atrial cardiomyocytes (hESC-AMs), the same protocol was used as described in the main text for optical voltage mapping except that the cellular monolayers (all in 48-well format) were incubated with 2.5 µM RHOD-2 AM (Thermo Fisher Scientific, R1245MP) instead of di-4-ANEPPS in DMEM/F-12 for 30 min. The same imaging system and filter sets were used as for optical voltage mapping and data was recorded at a spatial resolution of 165 µm/pixel and a temporal resolution of 6 ms per frame. Data were analysed using BrainVision Analyzer software (Brain Products) and noise artefacts were minimized by averaging of the signals at a selected pixel and its 8 nearest neighbours. Signal amplitude of the Ca^{2+} transient, time to peak, 50% decay time and conduction velocity (CV) were determined at multiple locations equally distributed throughout the culture. The effect of L-type Ca^{2+} channel activity modulation on Ca^{2+} handling by hiAMs and hESC-AMs was studied using the antagonist verapamil hydrochloride (Sigma-Aldrich, V4629) and agonist Bay K8644 (Sigma-Aldrich, B112). Both drugs were added from 10 mM stock solutions in dimethylsulfoxide (DMSO) to the hiAM and hESC-AM layers.

Cellular electrophysiology extended

The Na^+ current (I_{Na}) was recorded using the ruptured whole cell configuration at RT (21 ± 0.2°C). The bath solution for I_{Na} recordings contained (in mM): NaCl 20, CsCl 120, $CaCl_2$ 1.8, $MgCl_2$ 1.0, glucose 5.5, HEPES 5.0, pH 7.4 (CsOH). Nifedipine (5 µM) was added to block the L-type Ca^{2+} current. Pipette solution contained (in mM): NaCl 3.0, CsCl 133, $MgCl_2$ 2.0, Na_2ATP 2.0, TEACl 2.0, EGTA 10, HEPES 5.0, pH 7.2 (CsOH). The current-voltage (I-V) relationship and voltage dependency of (in)activation were determined by means of custom voltage-clamp protocols as depicted schematically in **Supplemental Figure 12a,c**. In short, I_{Na} density and voltage dependence of activation were determined by 50-ms depolarizing pulses (between -80 and +40 mV) from a holding potential of –120 mV. Voltage-dependent inactivation was obtained by measuring the peak currents during a 50-ms test step to -20 mV, which followed a 500-ms prepulse to membrane potentials between -140 and -20 mV to allow inactivation. The holding potential was –120 mV. All voltage clamp steps were applied with a 5-sec cycle length. Peak I_{Na} was defined as the difference between peak and steady-state current. Current density was calculated by dividing the measured currents by cell capacitance (C_m). To determine the activation characteristics of I_{Na}, I-V curves were corrected for

differences in driving force and normalized to maximum peak current. Steady-state activation and inactivation curves were fitted using the Boltzmann equation I/Imax=A/(1+exp((V1/2-V)/k)) to determine V1/2 (membrane potential for the half-maximal [in]activation) and the slope factor k. K^+ currents were recorded using the amphotericin-perforated patch-clamp technique at 36 ± 0.2°C with similar solutions as used for the action potential (AP) recordings. K^+ currents were determined by means of custom voltage-clamp protocols as depicted schematically in the **Supplemental Figure 12d,f,g**. K^+ currents were activated in response to 500-ms steps from different holding potentials (-40 and -80 mV) to voltages ranging from -120 to +50 mV in 10-mV increments. All voltage clamp steps were applied with a 5-sec cycle length. Steady-state K^+ currents were defined as the current at the end of the 500-ms voltage steps. Transient outward K^+ current was defined as the difference between the peak outward current and the current amplitude at the end of the 500-ms voltage clamp step. The ultrarapid component of the delayed rectifier K^+ current (I_{Kur}) was measured as the steady-state current sensitive to 50 μM 4 aminopyridine (4-AP, Sigma-Aldrich, A78403) (68,69). All currents were normalized for cell size by dividing current amplitude by C_m.

Immunocytochemistry imaging

The Eclipse 80i Upright Microscope (Nikon) was equipped with filter blocks (all from Nikon): C-FL EPI-FL DAPI (MBE41300, Excitation: 340-380 nm, Emission: 435-485 nm), C-FL EPI-FL TRITC (MBE45600, Excitation: 540/25 nm, Emission: 605/55 nm), C-FL EPI-FL FITC (MBE44720, Excitation: 465-495 nm, Emission: 515-555), and lenses: CFI Plan Fluor 20X (N20XW-PF, Nikon) and CFI Plan Fluor 40X (N40XW-PF, Nikon). Exposure times varied between 100-300ms, depending on the staining. Confocal images were acquired in 3 channels using the TCS SP8 White Light Laser Confocal Microscope (Leica Microsystems) with the following settings: Channel 1, Laser (405 nm) intensity 0.5-1%, HyD (410-499 nm) gain 30. Channel 2, Laser (499 nm) intensity 1-2%, HyD (505-607 nm) gain 30. Channel 3, Laser (577 nm) intensity 2-5%, HyD (607-757 nm) gain 30. Intensity depended on the staining. The images were acquired using the HC PL APO CS2 63x/1.40 OIL lens (11506350, Leica Microsystems). Averaging of 3 frames was applied. The scan speed was 600 Hz, pinhole 95.5 μm and Z-stacking up to 10 frames was applied (thickness 0.4-1 μm).

Supplemental Results

Ploidy of hiAMs

Assessment of hiAM ploidy was performed using differentiated hiAM-2.38, -2.52 and -2.90 at population doublings (PDs) 35-37. These PDs are in the middle of those used to generate the other data in this study for which cells from PD 28-46 were employed. The DNA content of the 3 clones was very similar showing small populations of cells with average DNA indexes (DIs) of 0.9 and 3.5, and a large population of cells with an average DI of 1.7. (**Supplemental Figure 2**). These 3 cell populations, comprised on average 6.9, 9.1 and 84.1% of all cells, respectively. Due to the technical difficulty to exclude all cell doublets from the analysis, some of the cells with an apparent DI of 3.5 may actually consists of cell pairs with a DI of 1.7. Data per clone can be found in **Supplemental Table 2**.

Ca2+ dynamics of hESC-AMs and hiAMs

Baseline comparison of optical Ca^{2+} transients revealed significantly longer time to peak durations, shorter 50% decay times and lower CVs in 1-cm^2 hESC-AM layers when compared to equally sized layers of differentiated hiAMs (**Supplemental Figure 14a-c**). Additionally, hESC-AMs and hiAMs responded differently to the L-type Ca^{2+} channel modulators verapamil and Bay K8644 (**Supplemental Figure 14d,e**). Most notably, the amplitude of Ca^{2+} transients in hESC-AMs was strongly reduced by 100 nM verapamil, while the same concentration of verapamil had only a minimal inhibitory effect on hiAMs. Furthermore, hESC-AMs did no longer exhibit any Ca^{2+} transients in the presence of 1 µM verapamil, whereas these were still observed in hiAMs. For reference, the therapeutic serum concentration of verapamil was reported to be 0.2-0.9 µM (70). Extreme sensitivity to L-type Ca^{2+} current blockade and subsequent loss of Ca^{2+} transients has been previously described in human pluripotent stem cell-derived cardiomyocytes (71), suggesting deficient Ca^{2+}-induced Ca^{2+} release as the most likely mechanism. Another interesting observation is the respective decrease and increase of CV in the presence of verapamil and Bay K8644 only seen in hESC-AM layers. Taken together with the significantly lower expression of SCN5A (Nav1.5) in hESC-AMs compared to hiAMs (**Supplemental Data File 2**), these data might suggest a larger dependence on an increase of cytosolic Ca^{2+} in the generation and propagation of APs in hESC-AM layers.

Effect of TBX5 knockdown on Ca^{2+} dynamics in hiAMs

Holt-Oram syndrome, which is characterized by developmental heart defects, diastolic dysfunction and arrhythmias, is caused by mutations in the TBX5 gene (72,73). Previous studies have indicated disrupted Ca^{2+} handling as important mechanism for the diastolic dysfunction reported in Holt-Oram patients (74). To test the suitability of hiAMs for disease modelling beyond atrial arrhythmias, we studied the effect of decreased TBX5 expression on Ca^{2+} dynamics. For this purpose, hiAM-2.52 layers were transduced shortly after initiation of differentiation with different doses of LVs encoding a TBX5-specific shRNA or a negative control PpLuc-specific shRNA. Following 12 days of differentiation, this resulted in a 2- to 8-fold decrease in TBX5 protein levels for the lowest and highest dose of the TBX5-specific shRNA-encoding vector when compared to unmodified hiAMs (**Supplemental Figure 21a,b**). Subsequent optical Ca^{2+} imaging revealed dose-dependent changes in Ca^{2+} transients after TBX5 knockdown compared to control hiAMs (**Supplemental Figure 21c,d**). Specifically, TBX5 knockdown resulted in significantly lower Ca^{2+} signal amplitudes, longer time to peak durations and slower CVs. As expected, no changes in Ca^{2+} transients were observed following PpLuc knockdown. These findings confirm the results of previous studies in which a reduction in TBX5 expression in cardiomyocytes caused disturbances of normal Ca^{2+} handling in these cells (75-77). Overall, these data demonstrate that genetic modification of hiAMs is straightforward and illustrate their suitability for human disease studies beyond atrial arrhythmia modelling.

Supplemental Discussion

Conditional immortalization of human cardiomyocytes using simian virus 40 (SV40) large T (LT)

In the past, SV40 LT has been successfully used to generate lines of various types of foetal, neonatal and adult parenchymal human cells with phenotypic properties resembling those of the primary cells from which they were derived (78-80). Several of these cell lines have found widespread use 1) for fundamental research, 2) as models of human disease and for 3) pharmacological and toxicological screening. Davidson and colleagues (81) showed that SV40 LT is also able to immortalize ventricular cardiomyocytes of human adults (haVMs) but the resulting AC16 cells were not excitable and not contractile. The most likely explanation for the loss of cardiomyocyte functionality in the AC16 cells is the specific technique used to generate these cells, which involved the fusion of SV40 LT-transformed human skin fibroblasts with haVMs. The permanent expression of LT in these cells together with the (initial) presence of two nuclei executing distinct gene expression programs may have resulted in loss of their cardiomyocyte identity. This idea is supported by our observation that continuous expression of LT blocks the differentiation of hiAMs into functional cardiomyocytes (**Supplemental Figure 8**). An advantage of the approach used by Davidson et al. is that the cardiomyocytes are exposed to high levels of LT immediately after cell fusion allowing their rapid conversion into proliferative cells. In contrast, after transduction with LV.iMHCK7.LT-WT particles, it takes several days before cardiomyocytes produce substantial amount of LT. Thus, the main challenge for the successful application of our condition cell immortalization system to adult human cardiomyocytes seems to be to keep the cells in a proper condition long enough to enter into a proliferative state.

Supplemental References

67. Faas, F. G. et al. Virtual nanoscopy: generation of ultra-large high resolution electron microscopy maps. J Cell Biol. 2012;198:457-469.

68. Wang, Z., Fermini, B. & Nattel, S. Sustained depolarization-induced outward current in human atrial myocytes. Evidence for a novel delayed rectifier K+ current similar to Kv1.5 cloned channel currents. Circ Res. 1993;73:1061-1076.

69. Caballero, R. et al. In humans, chronic atrial fibrillation decreases the transient outward current and ultrarapid component of the delayed rectifier current differentially on each atria and increases the slow component of the delayed rectifier current in both. J Am Coll Cardiol. 2010;55:2346-2354.

70. Opie, L. H. Pharmacological differences between calcium antagonists. Eur Heart J. 1997;18 Suppl A:A71-79.

71. Itzhaki, I. et al. Calcium handling in human induced pluripotent stem cell derived cardiomyocytes. PLoS One. 2011;6:e18037.

72. Basson, C. T. et al. Mutations in human TBX5 [corrected] cause limb and cardiac malformation in Holt-Oram syndrome. Nat Genet. 1997;15:30-35.

73. Li, Q. Y. et al. Holt-Oram syndrome is caused by mutations in TBX5, a member of the Brachyury (T) gene family. Nat Genet. 1997;15:21-29.

74. Zhu, Y. et al. Tbx5-dependent pathway regulating diastolic function in congenital heart disease. Proc Natl Acad Sci U S A. 2008;105:5519-5524.

75. Nadadur, R. D. et al. Pitx2 modulates a Tbx5-dependent gene regulatory network to maintain atrial rhythm. Sci Transl Med. 2016;8:354ra115.

76. Churko, J. M. et al. Defining human cardiac transcription factor hierarchies using integrated single-cell heterogeneity analysis. Nat Commun. 2018;9:4906.

77. Kathiriya, I. S. et al. Modeling Human TBX5 Haploinsufficiency Predicts Regulatory Networks for Congenital Heart Disease. Dev Cell. 2021;56:292-309.

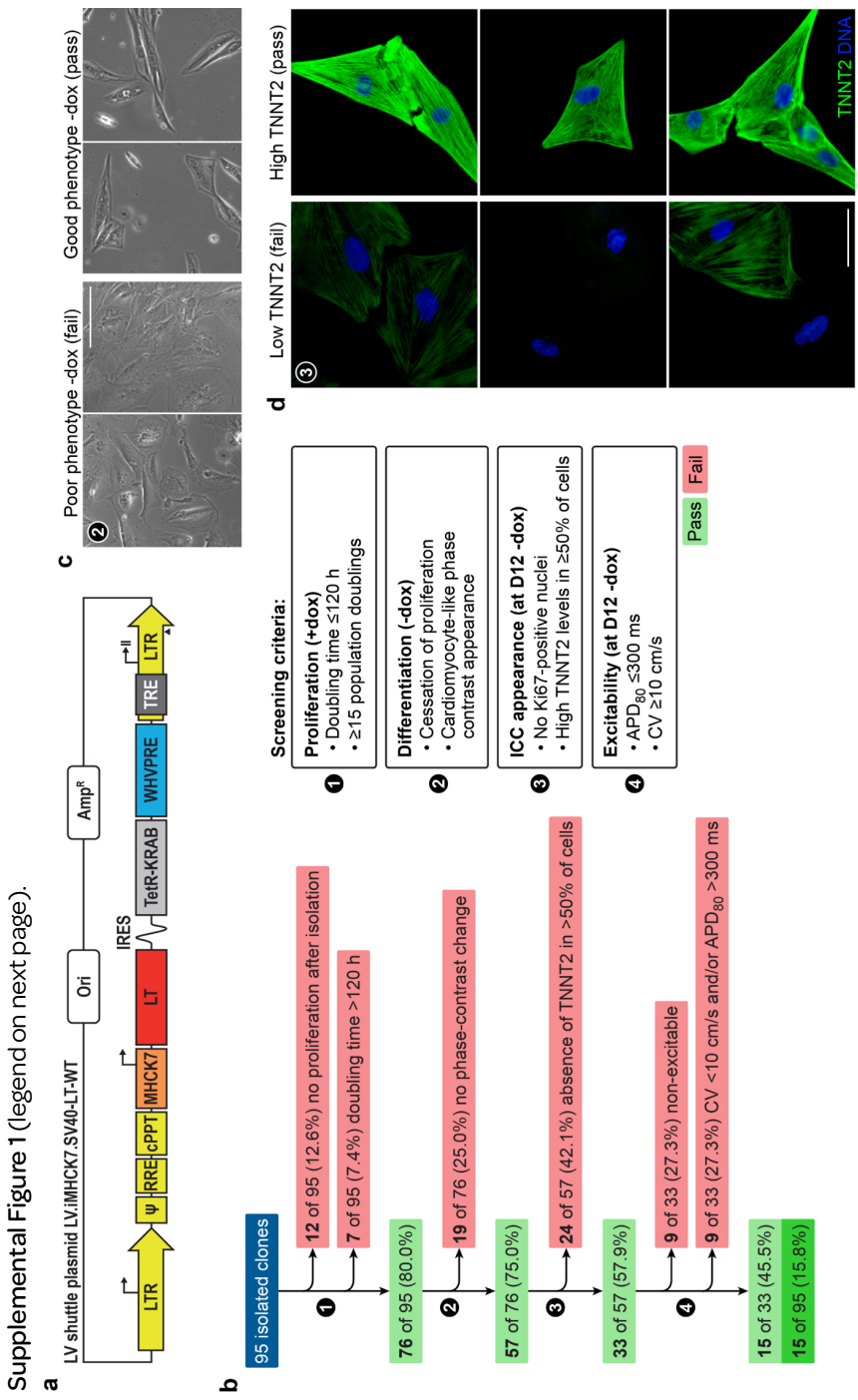
78. Ramboer, E. et al. Strategies for immortalization of primary hepatocytes. J Hepatol. 2014;61:925-943.

79. Scharfmann, R., Staels, W. & Albagli, O. The supply chain of human pancreatic beta cell lines. J Clin Invest. 2019;129:3511-3520.

80. Sato, M., Shay, J. W. & Minna, J. D. Immortalized normal human lung epithelial cell models for studying lung cancer biology. Respir Investig. 2020;58:344-354.

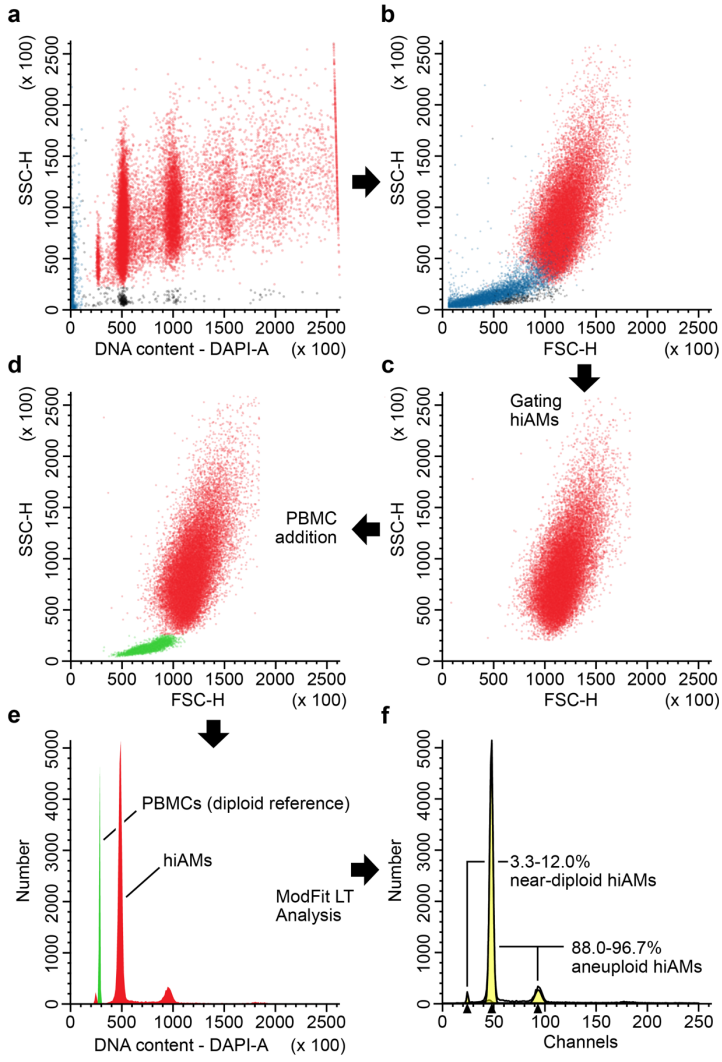
81. Davidson, M. M. et al. Novel cell lines derived from adult human ventricular cardiomyocytes. J Mol Cell Cardiol. 2005;39:133-147.

Supplemental Data

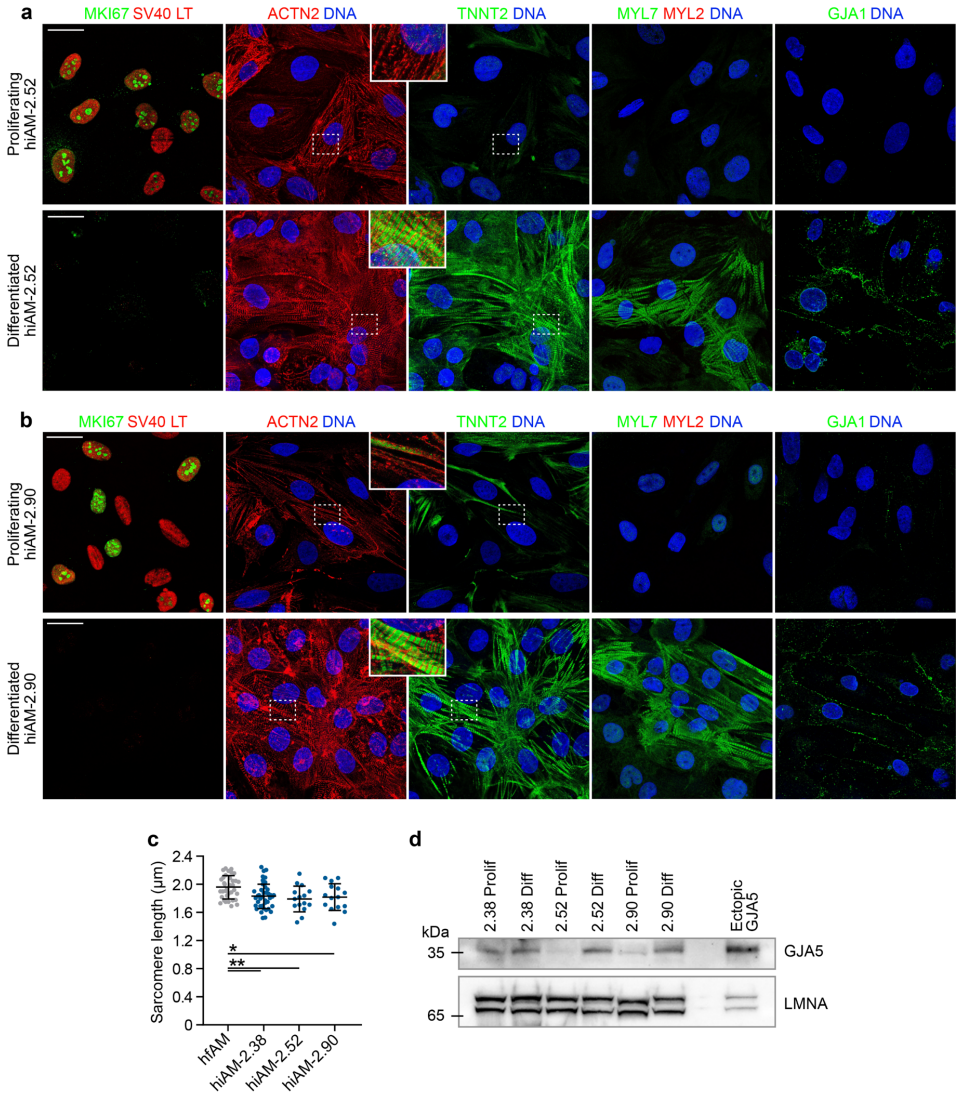


Supplemental Figure 1 (legend on next page).

Supplemental Figure 1 (previous page). Extended data on the generation and selection of hiAM monoclones. **(a)** LV shuttle plasmid LV.iMHCK7.SV40-LT-WT. Ori, bacterial origin of replication. Amp^R, *Escherichia coli* ß-lactamase gene. LTR, human immunodeficiency virus type 1 (HIV1) long terminal repeat. ψ, HIV1 packaging signal. RRE, HIV1 Rev-responsive element. cPPT, HIV1 central polypurine tract and termination site. MHCK7, chimeric striated muscle-specific promoter. LT, coding sequence of wildtype oncogenic SV40 LT antigen. IRES, encephalomyocarditis virus internal ribosome entry site. TetR-KRAB, coding sequence of hybrid tetracycline-controlled transcriptional repressor. WHVPRE, woodchuck hepatitis virus posttranscriptional regulatory element. TRE, tetracycline-responsive promoter element consisting of 7 repeats of a 19-nucleotide tetracycline operator (tetO) sequence. **(b)** Extended flowchart of hiAM clone selection based on 4 main criteria with corresponding drop-off rates. ICC, Immunocytochemistry. TNNT2, cardiac troponin T. **(c)** Example of 2 hiAM monoclones displaying no cardiomyocyte-like change in phase contrast and of 2 monoclones showing a cardiomyocyte-like alteration in phase contrast after 12 days of culture in the absence of doxycycline (dox; criterion 2, differentiation). Scale bar, 100 µm. **(d)** Example of 3 hiAM monoclones that do and of 3 hiAM clones that do not pass the third criterion (*i.e.* immunocytochemical appearance) due to high and low TNNT2 expression, respectively, as assessed by ICC. Scale bar, 50 µm.

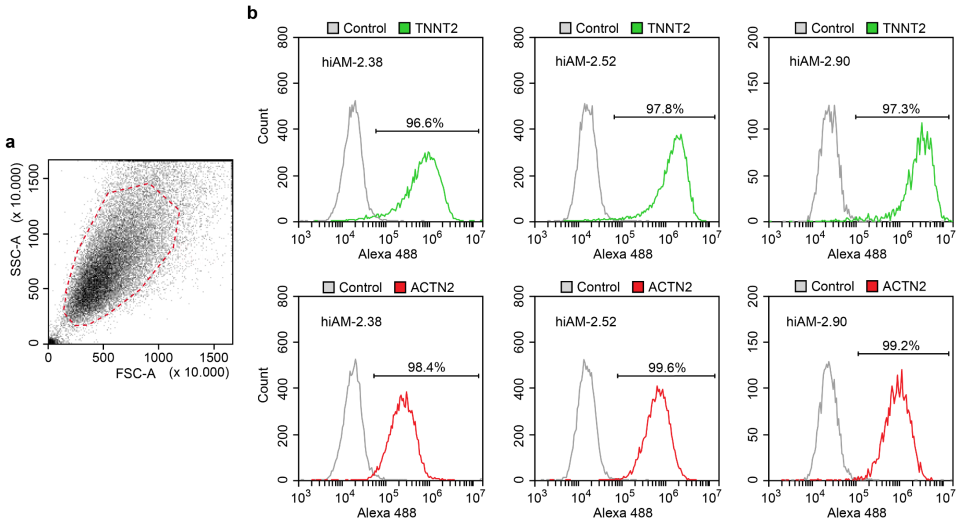


Supplemental Figure 2. Flow cytometric assessment of hiAM ploidy. Diagram showing the process of determining the ploidy of differentiated hiAMs with female peripheral blood mononuclear cells (PBMCs) serving as diploid reference. Scatter plots of **(a)** side scatter height (SSC-H) *vs.* DAPI fluorescence area (DAPI-A) and **(b)** SSC-H *vs.* forward scatter height (FSC-H) showing all events (red: hiAMs, blue: debris, black: bare nuclei). **(c)** Plot of the hiAMs gated based on the SSC-H *vs.* DAPI-A scatter plot and **(d)** discrimination of added PBMCs (green) based on their significant lower FSC-H and SSC-H signals compared to hiAMs. **(e)** DNA histogram of the PBMC/hiAM mixture after removal of evident aggregates. **(f)** Representative graph of the ModFit LT analysis revealing the different hiAM populations.

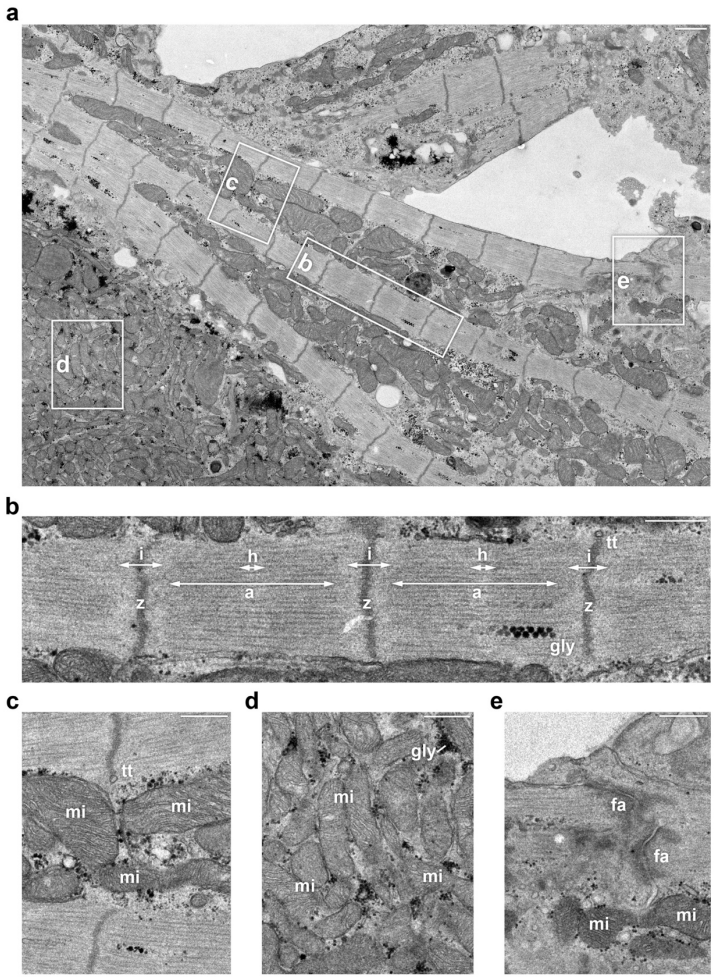


Supplemental Figure 3. Extended characterization of the hiAM phenotype during proliferation and after 12 days of differentiation. Proliferating and differentiated **(a)** hiAM-2.52 and **(b)** hiAM-2.90 were immunostained for Ki-67 (MKI67), SV40 LT, α-actinin 2 (ACTN2), cardiac muscle troponin T (TNNT2), the atrial and ventricular isoform of myosin regulatory light chain 2 (MYL7 and MYL2, respectively) and connexin 43 (GJA1). Scale bar, 25 µm. **(c)** Sarcomere length of hfAMs (n = 42 measurements from 14 images), hiAM-2.38 (n = 45 measurements from 15 images), hiAM-2.52 (n = measurements 15 from 5 images) and hiAM-2.90 (n = measurements 15 from 5 images) calculated based on z-line distance in cell layers stained for ACTN2. Mean shown, with error bars indicating standard deviation [SD]. *P < 0.05, **P < 0.01, one-way analysis of variance with Tukey *post-hoc* analysis. **(d)** Connexin 40 (GJA5) protein levels of hiAM-

2.38, -2.52 and -2.90 during proliferation (Prolif) and after differentiation (Diff). Lamin A/C (LMNA) is included as loading control. Ectopically expressed connexin 40 is included as positive/size control. See **Supplemental File 4** for uncropped blots.

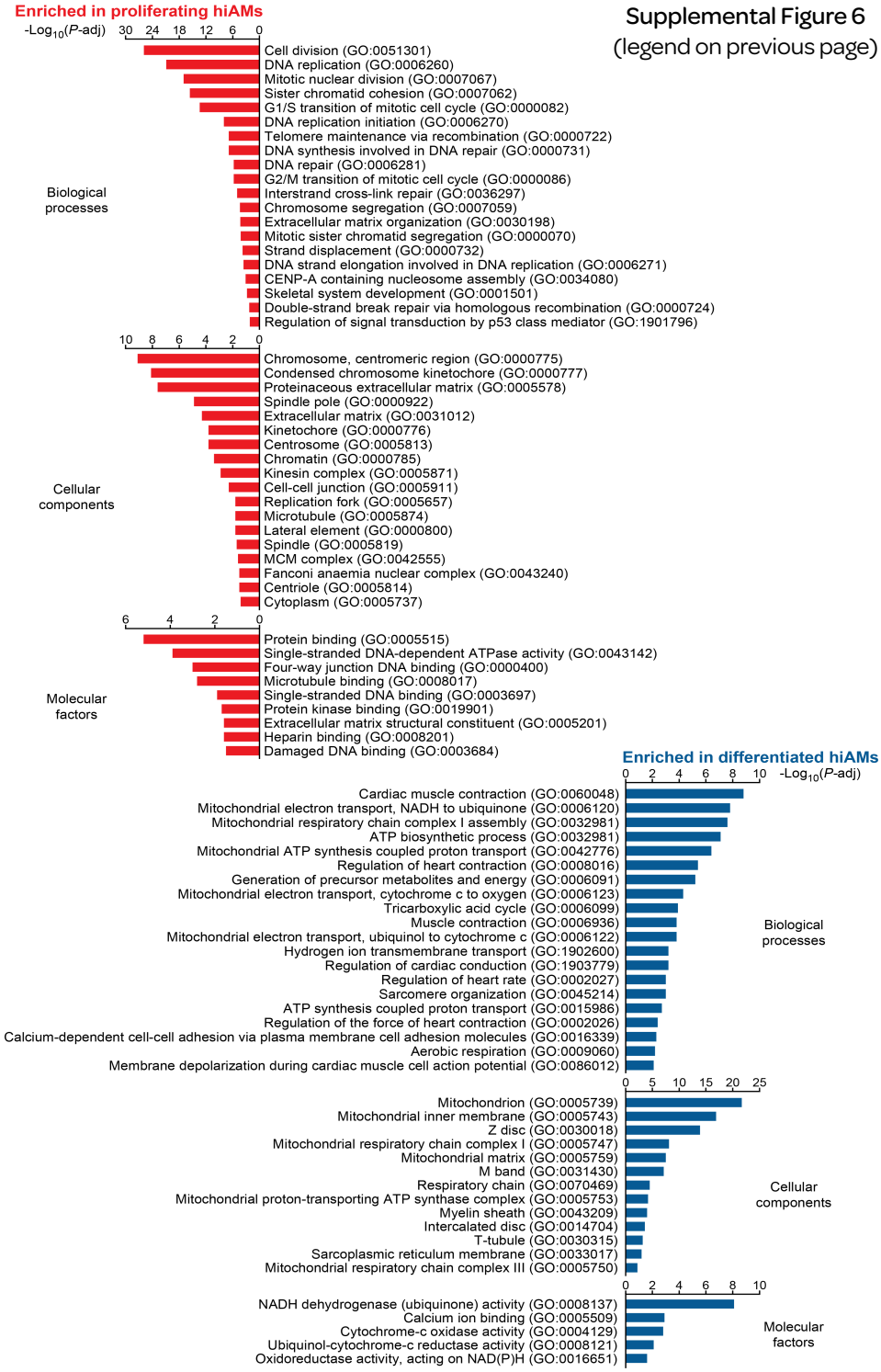


Supplemental Figure 4. Flow cytometric assessment of differentiated hiAM purity. **(a)** Representative side scatter area (SSC-A) *vs.* forward scatter area (FSC-A) plot showing all events. The red dotted line demarcates the hiAM population used for quantification. **(b)** Quantification of the proportion of differentiated hiAM-2.38, -2.52 and -2.90 staining positive for cardiac muscle troponin T (TNNT2) or α-actinin 2 (ACTN2).

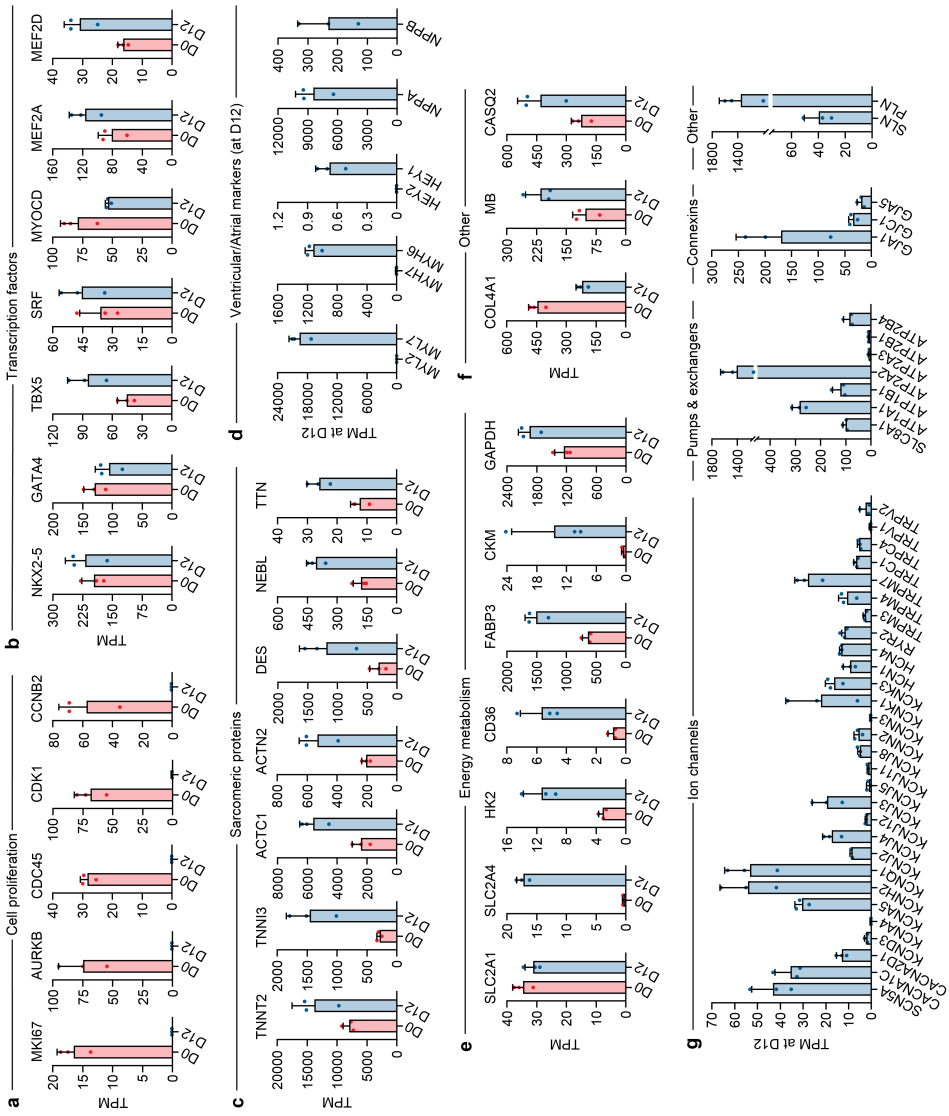


Supplemental Figure 5. Ultrastructural properties of differentiated hiAMs. **(a)** Transmission electron microscope image of differentiated hiAM-2.52. **(b)** Detailed view of sarcomeric organization (a, a-band. h, h-zone. i, i-band. z, z-line. gly, glycogen granules). The average sarcomere distance measured in overview **(a)** was 1.80 ± 0.11 µm. T-tubule-like structures (tt) were observed at the z-lines. **(c)** Mitochondria (mi) in between myofibrils. **(d)** Large cluster of perinuclear mitochondria and glycogen granules. **(e)** Intercalated disc connecting neighbouring hiAMs. fa, fascia adherens. **(a)** Scale bar, 1 µm. **(b-e)** Scale bar, 500 nm.

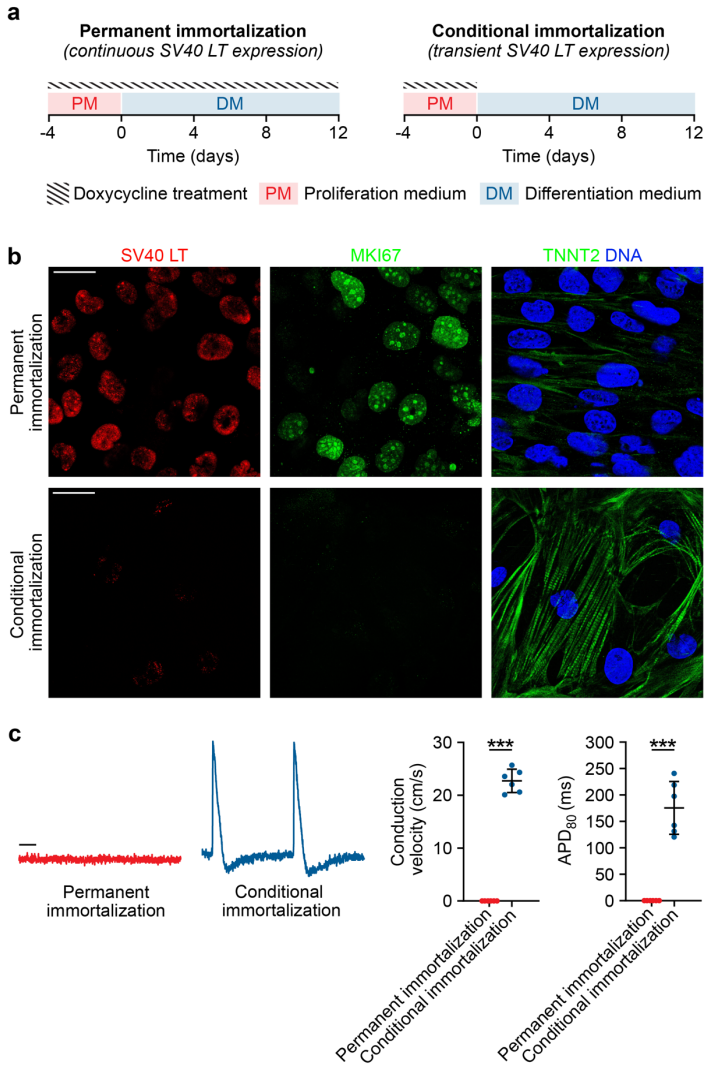
Supplemental Figure 6 (next page). Extended data on gene set enrichment analysis. Enriched GO terms (*P*-adjusted < 0.05) in proliferating hiAMs (left, red) and in differentiated hiAMs (blue, right).



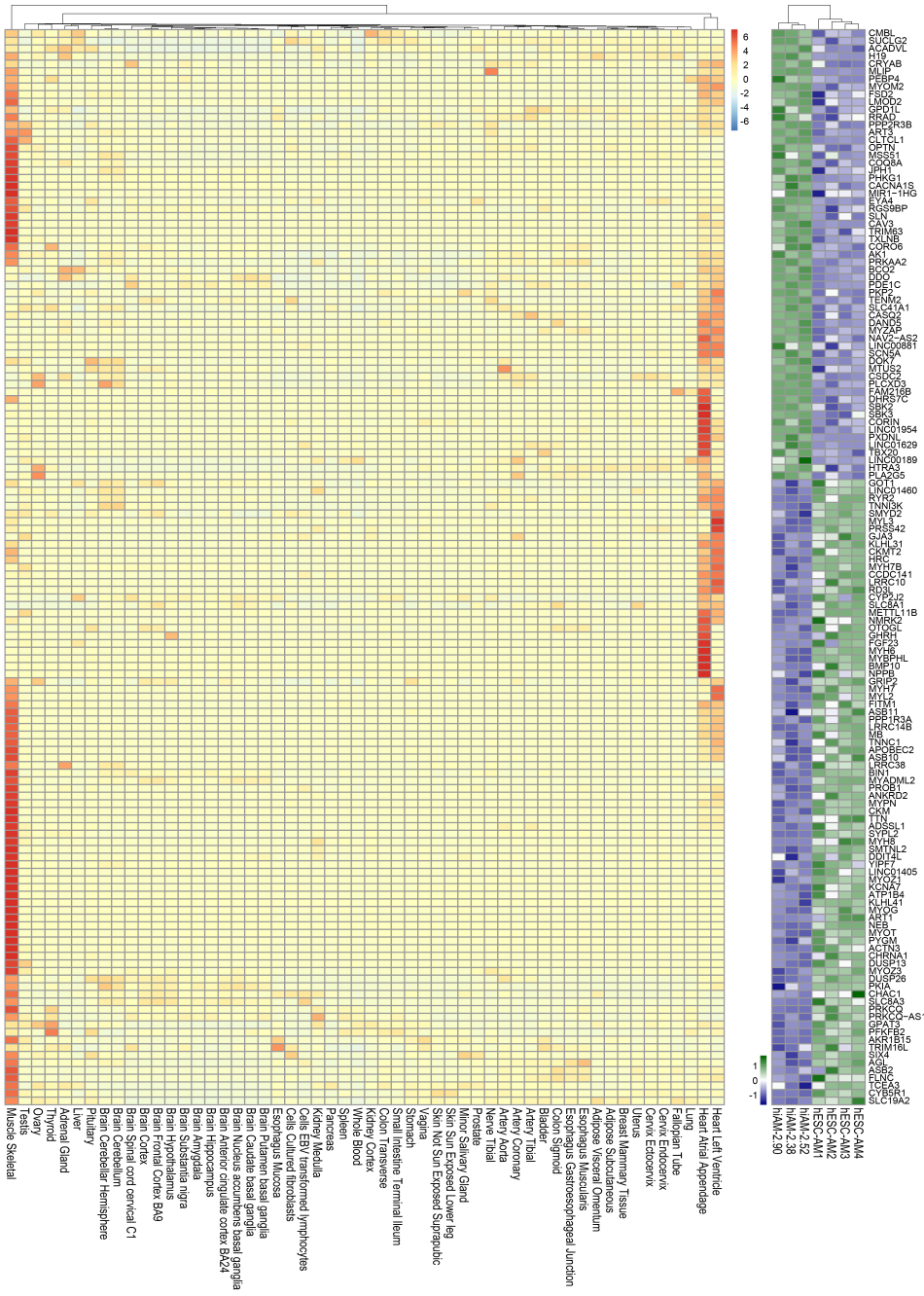
Supplemental Figure 6
(legend on previous page)



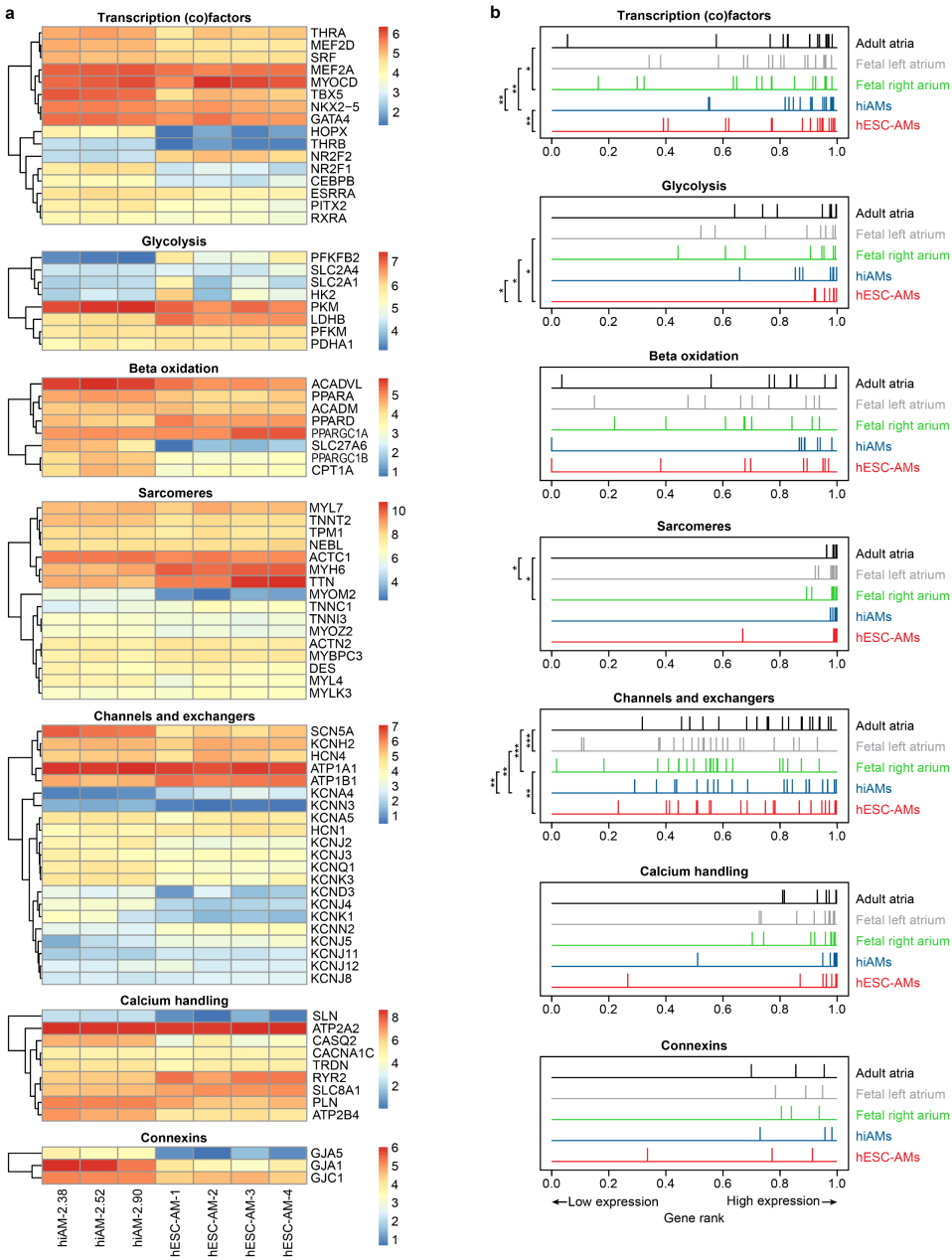
Supplemental Figure 7. Gene expression analysis by RNA-sequencing of hiAMs during proliferation (D0) and after differentiation (D12). Transcripts per million (TPM) are shown of genes **(a)** involved in cell proliferation, **(b)** encoding cardiac transcription factors, **(c)** coding for cardiac sarcomeric proteins, **(d)** preferentially expressed in atrial or ventricular cardiomyocytes, **(e)** involved in energy metabolism, and **(f)** encoding some other relevant genes. **(g)** TPM in differentiated hiAMs of genes involved in excitability, Ca^{2+} handling and electrical coupling. Bars represent mean gene expression levels in hiAM clones 2.38, 2.52 and 2.90 (n = 3 replicates per clone per time point). Error bars indicate SD. D0, zero days without dox. D12, twelve days without dox.



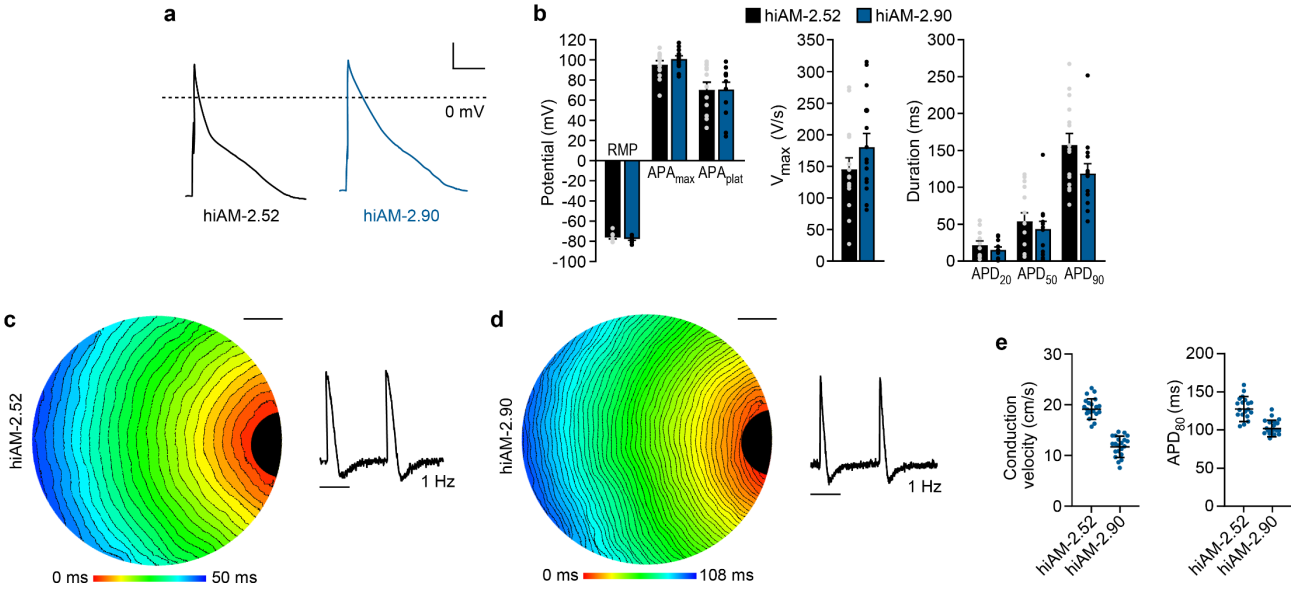
Supplemental Figure 8. Permanent cell immortalization vs. conditional cell immortalization. **(a)** Schematic overview of permanent immortalization (achieved through the continuous presence of dox) *vs.* conditional immortalization. In both cases, the proliferation medium was replaced by differentiation medium 12 days before analysis. **(b)** Immunofluorographs of hiAMs stained for Ki-67 (MKI67), SV40 LT and cardiac muscle troponin T (TNNT2) after 12 days of culture in differentiation medium. Scale bar, 25 µm. **(c)** Optical voltage mapping traces (left), CV and AP duration at 80% repolarization (APD_{80}) (right) after 12 days of culture in differentiation medium. Permanent LT expression precludes cardiomyogenic differentiation of hiAMs as evinced by the absence of excitable cells after 12 days of culture in differentiation medium. Scale bar, 200 ms. n = 6 layers from 2 independent differentiations. Mean shown, with error bars indicating SD. ***$P < 0.001$, unpaired t-test.



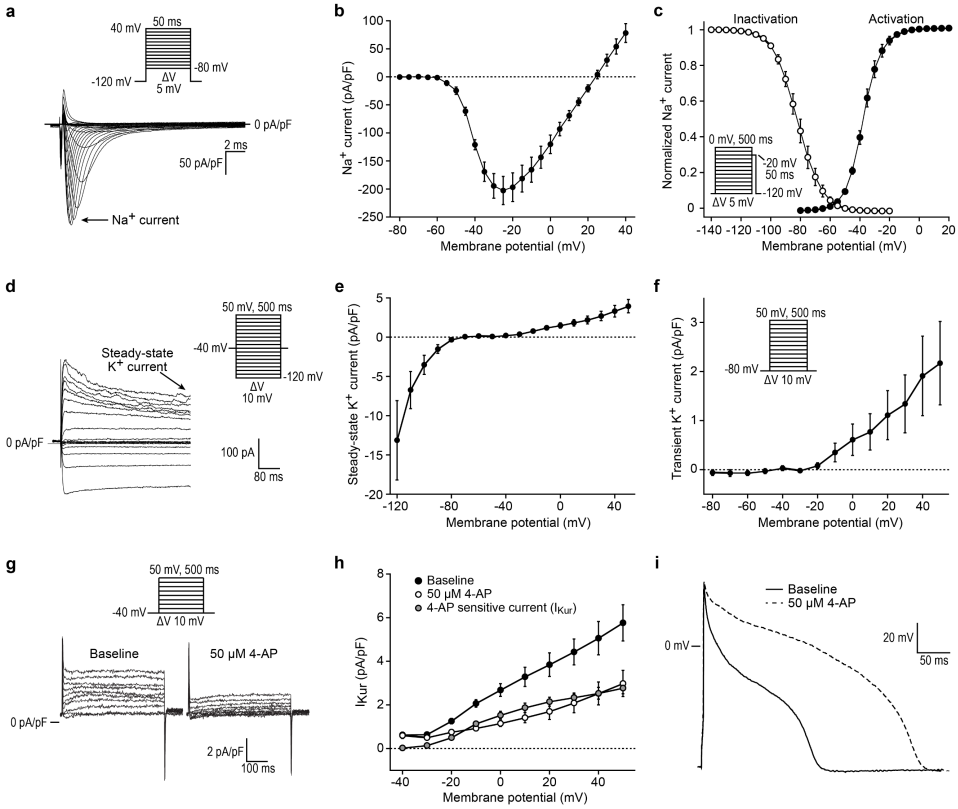
Supplemental Figure 9. Differential gene expression between hESC-AMs and hiAMs. Cluster of differentially expressed genes with striated muscle-specific expression. Expression levels shown in various human adult tissues (left) and in hiAMs and hESC-AMs (right). Scale bars indicate row-scaled and centred expression values. For better legibility of the figure (print version), visit doi.org/10.1038/s41551-021-00827-5



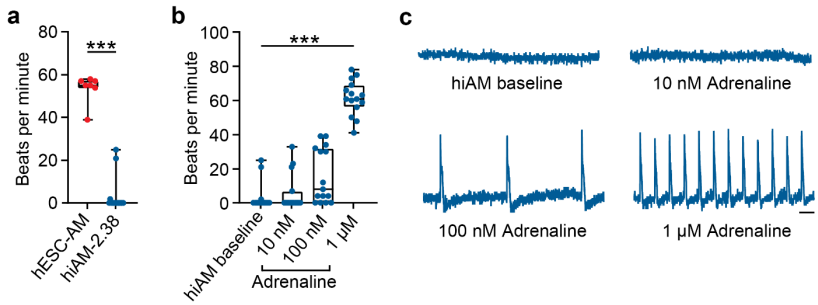
Supplemental Figure 10. Assessment of hiAM and hESC-AM maturity. **(a)** Expression of selected genes for comparison of the relative maturity of hiAMs and hESC-AMs. Scale bar indicates log-counts per million values. **(b)** Rank-based comparison of gene sets from **(a)** in human adult and foetal atria, differentiated hiAMs and hESC-AMs. **P* < 0.05, ***P* < 0.01, ****P* < 0.001, Wilcoxon signed-rank test.



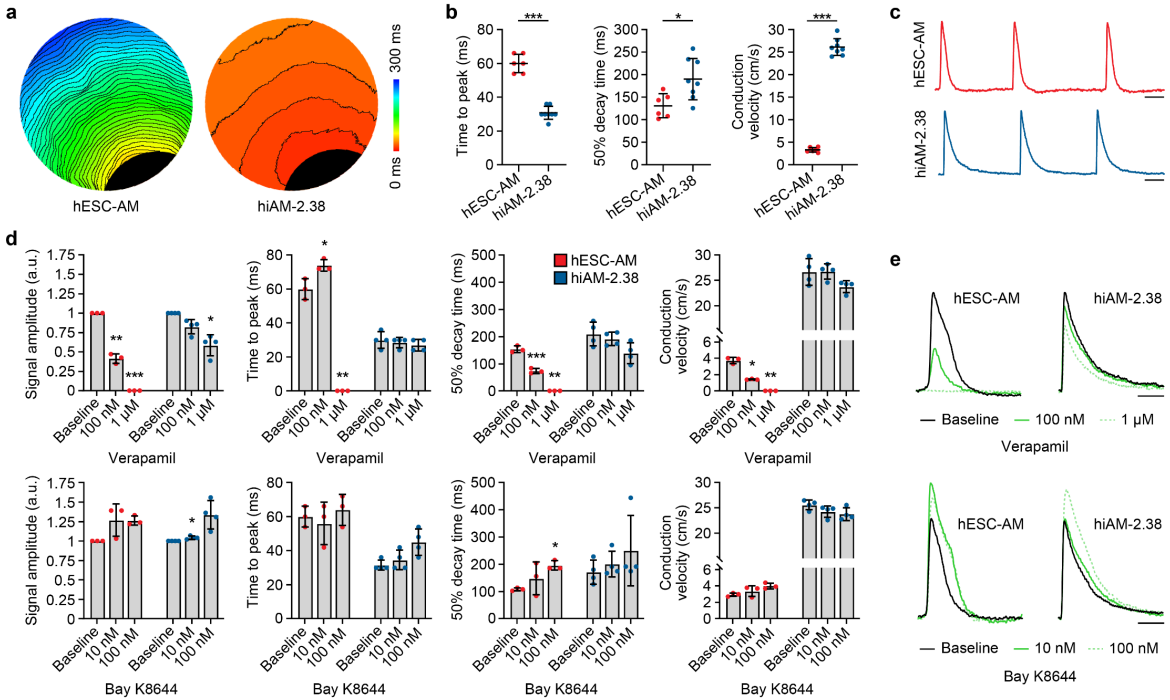
Supplemental Figure 11. Electrophysiological characterization of differentiated hiAM clones 2.52 and 2.90. **(a)** Representative AP traces and **(b)** mean AP parameters of single differentiated hiAM-2.52 (*n* = 13 cells from 3 independent differentiations) and single differentiated hiAM-2.90 (*n* = 14 cells from 3 independent differentiations) during 1-Hz electrical stimulation. Scale bars in **(a)** x = 50 ms, y = 20 mV. Dotted line in **(a)** indicates the zero mV level. RMP, resting membrane potential. APA_{max}, maximal AP amplitude. APA_{plat}, AP plateau amplitude. V_{max}, maximum AP upstroke velocity. $APD_{20/50/90}$, AP duration at 20, 50 and 90% of repolarization. Error bars indicate standard error of the mean (SEM). **(c, d)** Representative activation maps and optical voltage traces of differentiated **(c)** hiAM-2.52 and **(d)** hiAM-2.90 layers (24-well format). Isochrones, 2 ms. Scale bar of maps, 2 mm. Scale bar of traces, 500 ms. **(e)** Mean CV and APD_{80} in confluent layers of differentiated hiAM-2.52 (*n* = 19 layers from 4 independent differentiations) and hiAM-2.90 (*n* = 21 layers from 3 independent differentiations). Mean shown, with error bars indicating SD.



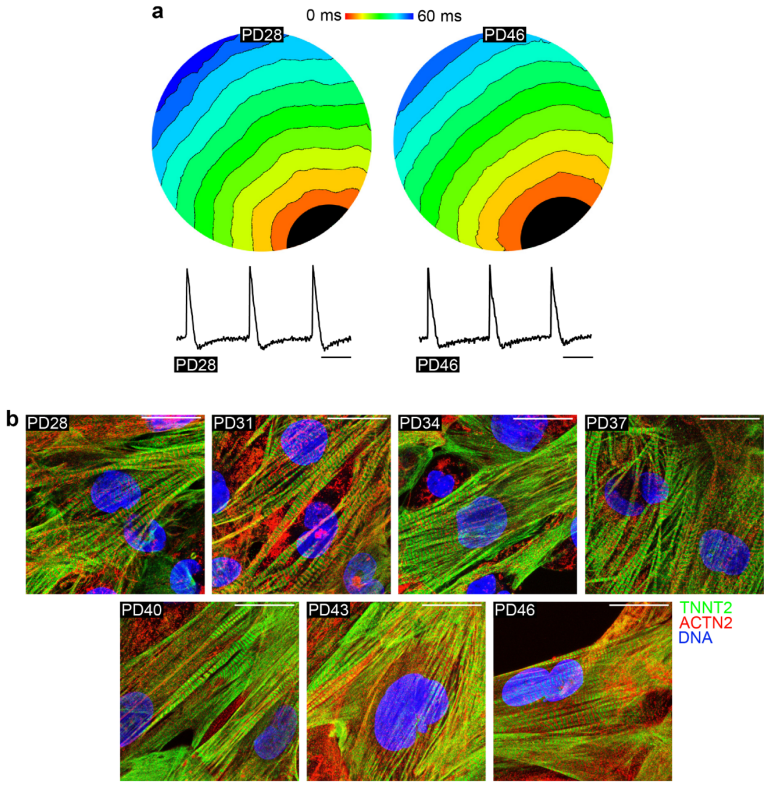
Supplemental Figure 12. Membrane currents in hiAM-2.38. **(a)** Voltage clamp protocol and typical examples of Na^+ currents. **(b)** Average current-voltage (I-V) relationship of the Na^+ current. **(c)** Voltage dependency of (in)activation. Inset, voltage clamp protocol used to measure voltage dependency of inactivation. $V_{1/2}$ was -37.1 ± 1.0 and -81.0 ± 1.8 mV for activation and inactivation, respectively. Slope factor k was 5.8 ± 0.6 and -5.9 ± 0.3 mV for activation and inactivation, respectively. **(b, c)** *n* = 9 cells from 3 independent differentiations. **(d)** Voltage clamp protocol and typical examples of steady-state K^+ currents. **(e)** Average I-V relationship of the steady-state current. *n* = 11 cells from 4 independent differentiations. **(f)** Average I-V relationship of the transient outward K^+ current. Inset, voltage clamp protocol used. *n* = 10 cells from 4 independent differentiations. **(g)** Voltage clamp protocol and typical examples of steady-state currents in absence and presence of 50 μM 4-aminopyridine (4-AP). **(h)** Average I-V relationship of the 4-AP-sensitive ultrarapid delayed rectifier K^+ current (I_{Kur}). *n* = 6 cells from 2 independent differentiations. **(i)** Typical example of the effects of I_{Kur} blockade on APs with 50 μM 4-AP. The average effects on APs are shown in Supplemental Table 4. **(b, c, e, f, h)** Mean shown, with error bars indicating SEM.



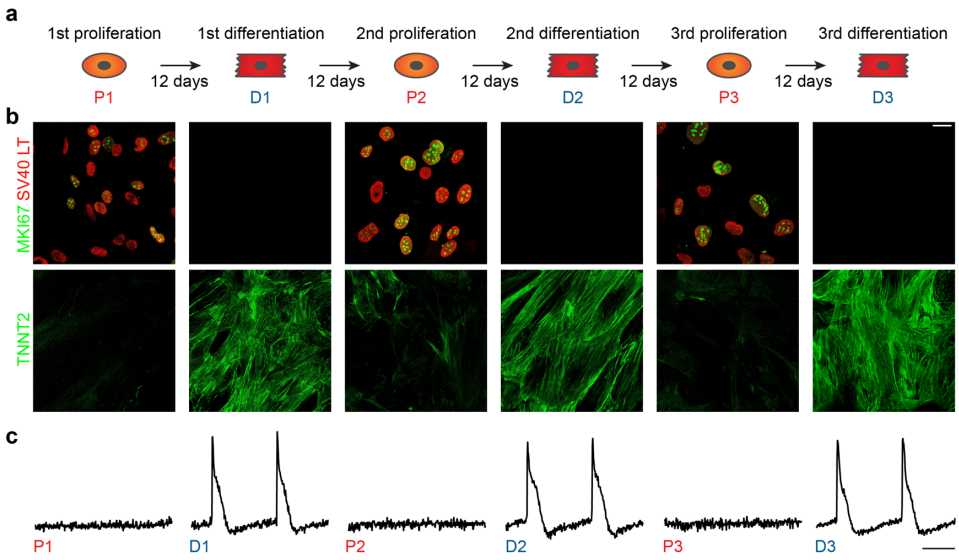
Supplemental Figure 13. Spontaneous activity of hESC-AM and hiAM layers. **(a)** Spontaneous beating rate of hESC-AM (red, *n* = 7 layers from 3 independent differentiations) and hiAM-2.38 (blue, *n* = 15 layers from 3 independent differentiations) layers. Beats per minutes defined as the number of APs measured by optical voltage or Ca^{2+} mapping per minute. ***$P < 0.001$, Mann-Whitney test. **(b)** Effect of an increasing concentration of adrenaline (Sigma-Aldrich, E4642) on the beating rate of hiAM-2.38 layers, revealing their chronotropic responsiveness to adrenoreceptor stimulation. *n* = 15 layers from 3 independent differentiations. ***$P < 0.001$, Friedman with Dunn *post-hoc* analysis comparing to baseline. **(a, b)** Median and quartiles are shown, error bars indicate minimum and maximum values. **(c)** Representative optical voltage traces of hiAM layers exposed to different adrenaline concentrations. Scale bar, 1 sec.



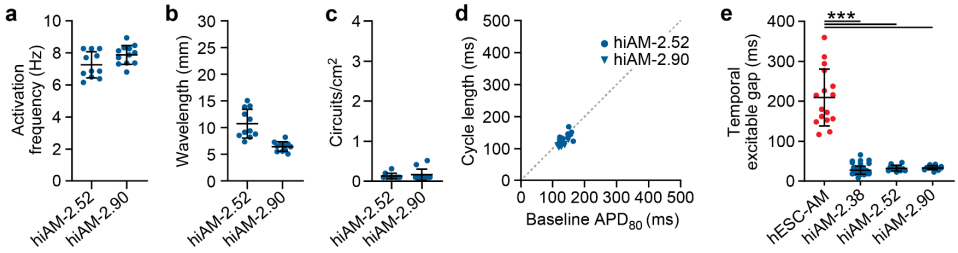
Supplemental Figure 14. Ca^{2+} transients of hESC-AMs and differentiated hiAMs. **(a)** Representative activation maps of hESC-AM and hiAM-2.38 layers (48-well format). Isochrones, 6 ms. **(b)** Mean time to peak, 50% decay time and CV of Ca^{2+} transients in hESC-AM (n = 6 layers from 2 independent differentiations) and hiAM-2.38 (n = 8 layers from 2 independent differentiations) layers. $P < 0.05$, ***$P <$ 0.001, unpaired t-test. Mean shown, with error bars indicating SD. **(c)** Representative optical Ca^{2+} traces. Scale bar, 500 ms. **(d)** Effect of L-type Ca^{2+} channel antagonist (verapamil) or agonist (Bay K8644) addition on Ca^{2+} transients in hESC-AMs (n = 3 layers from 2 independent differentiations) and hiAMs (n = 4 layers from 2 independent differentiations). a.u., arbitrary units. *$P < 0.05$, **$P < 0.01$, ***$P < 0.001$, repeated measures analysis of variance with Dunnett *post-hoc* analysis compared to baseline. Mean shown, with error bars indicating SD. **(e)** Representative optical Ca^{2+} traces in the absence and presence of verapamil and Bay K8644. Scale bar, 250 ms.



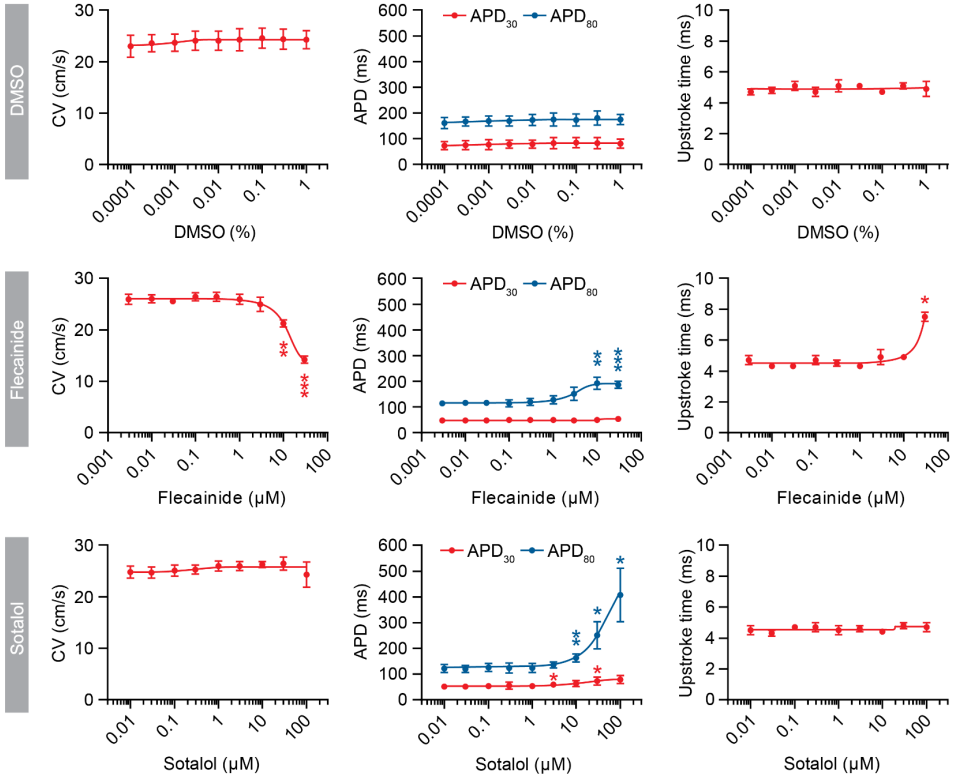
Supplemental Figure 15. Differentiation capacity of hiAMs at different PDs. **(a)** Representative activation map and optical voltage traces of differentiated hiAM-2.38 layer at PD 28 and at PD 46 (24-well format). Isochrones, 6 ms. Scale bar, 500 ms. **(b)** Immunostaining patterns of α-actinin 2 (ACTN2) and cardiac troponin T (TNNT2) of differentiated hiAMs at different PDs (from PD28 through PD46). Scale bar, 25 µm.



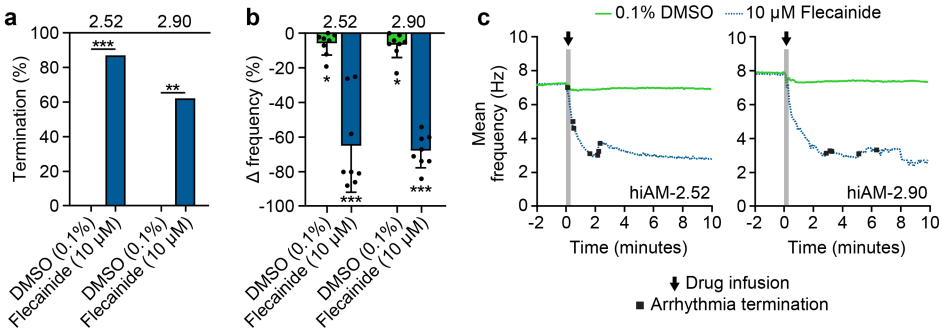
Supplemental Figure 16. Repeated switching of hiAMs between proliferation and differentiation. **(a)** Schematic overview of repeated switching of hiAM-2.38 between proliferation and differentiation. Each transition takes approximately 12 days. **(b)** Immunostaining patterns of SV40 LT, Ki-67 (MKI67) and cardiac muscle troponin T (TNNT2) showing full maintenance of cardiomyogenic differentiation ability during 3 successive cycles of hiAM-2.38 proliferation and differentiation. Scale bar, 25 µm. **(c)** Representative optical voltage traces of hiAM layers at the described time points, showing repeated loss and gain of excitability. Scale bar, 500 ms.



Supplemental Figure 17. Arrhythmia characteristics of differentiated hiAM-2.52 and -2.90 cultures. **(a)** Mean activation frequency, **(b)** wavelength and **(c)** arrhythmia complexity (*i.e.* the number of reentrant circuits per cm^2) of hiAM-2.52 and -2.90 cultures following induction of reentrant circuits. **(d)** Correlation between baseline APD_{80} and cycle length of induced reentrant circuits in hiAM-2.52 and -2.90 cultures. **(e)** Temporal excitable gap in arrhythmic hESC-AM and hiAM-2.38, -2.52 and -2.90 cultures. hESC-AM: n = 7 independent cultures, hiAM-2.38: n = 56 independent cultures. ***$P < 0.001$, one-way analysis of variance with Tukey *post-hoc* analysis. **(a-c, e)** Mean shown, with error bars indicating SD. **(a-e)** hiAM-2.52: n = 11 independent cultures, hiAM-2.90: n = 12 independent cultures.

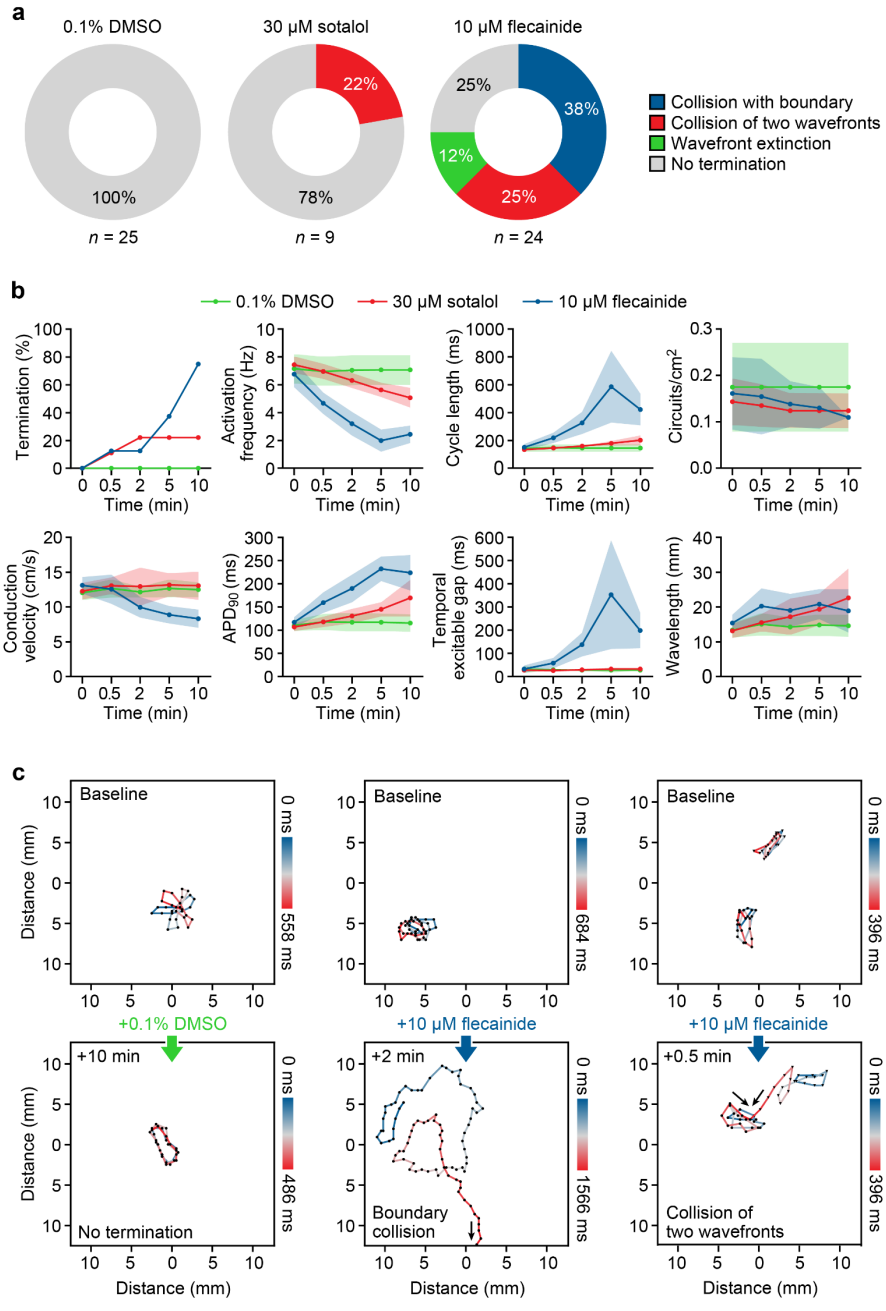


Supplemental Figure 18. Dose-dependent effects of flecainide and sotalol on differentiated hiAM cultures. Effects of DMSO (solvent/vehicle control), flecainide and sotalol at increasing concentrations on CV, AP duration at 30/80% repolarization ($APD_{30/80}$) and upstroke time in differentiated 2-cm^2 hiAM-2.38 cultures as measured by optical voltage mapping. Concentrations were increased until cultures were no longer excitable. n = 5 layers per compound for CV and APD, n = 3 layers for upstroke time. Mean shown, with error bars indicating SD. *P < 0.05, **P < 0.01, ***P < 0.001, repeated measures analysis of variance with Dunnett *post-hoc* analysis with the lowest concentrations serving as control (threshold P < 0.01 for *post-hoc* analyses).

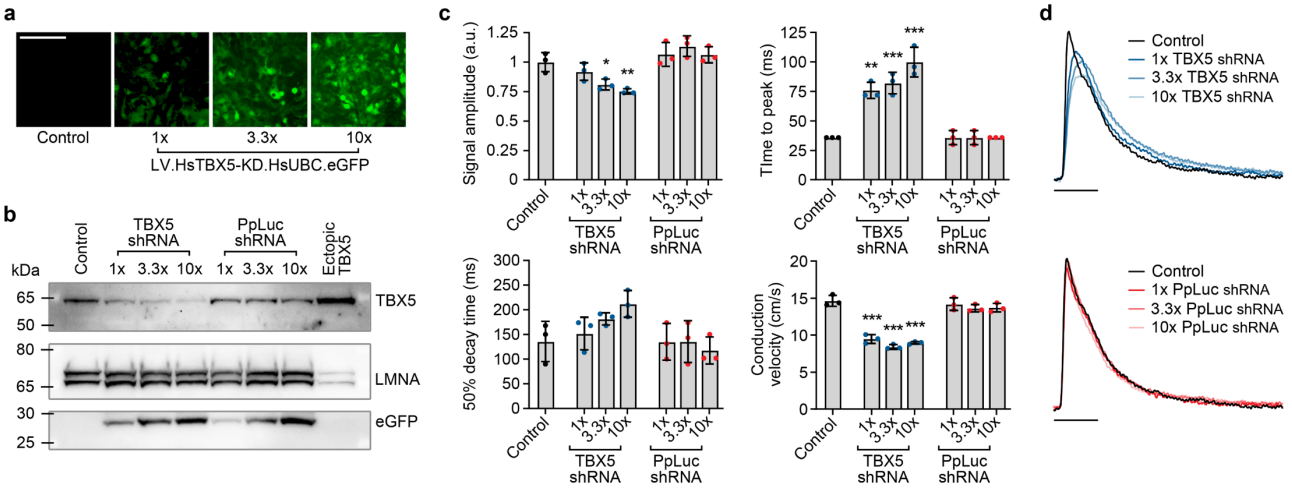


Supplemental Figure 19. Effects of flecainide on arrhythmic hiAM-2.52 and -2.90 cultures. **(a)** Rate of reentrant circuit termination and **(b)** change (Δ) in activation frequency in arrhythmic 10-cm^2 cultures of differentiated hiAM-2.52 and -2.90 at 10 min after infusion of 0.1% DMSO or 10 µM flecainide compared to baseline. Mean shown, with error bars indicating SD. **(c)** Continuous monitoring of mean activation frequency in arrhythmic hiAM- 2.52 and -2.90 cultures prior to and after infusion of 0.1% DMSO or 10 µM flecainide. **(a-c)** n = 8 for each compound and hiAM clone. *P<0.05, ***P < 0.001. **(a)** Chi-square test. **(b)** Paired t-test.

Supplemental Figure 20 (next page). Arrhythmia dynamics and termination following antiarrhythmic drug infusion. **(a)** Pie chart showing the frequency of arrhythmia termination and of the 3 main mechanisms causing arrhythmia termination using combined data from hiAM-2.38, -2.52 and -2.90. **(b)** Arrhythmia parameters measured at various time points prior to and following antiarrhythmic drug infusion. Number of hiAM-2.38 cultures with arrhythmic activity present at 0, 0.5, 2, 5, 10 min: 0.1% DMSO (8, 8, 8, 8, 8), 30 µM sotalol (9, 8, 7, 7, 7) and 10 µM flecainide (8, 7, 7, 5, 2). Mean shown, shaded area indicates SD. **(c)** Visualization of the position of the arrhythmia core in time. Left, infusion of 0.1% DMSO not resulting in arrhythmia termination. Middle, 10 µM flecainide infusion resulting in drifting and subsequent collision of the core with the boundary, thereby terminating arrhythmic activity. Right, 10 µM flecainide infusion resulting in collision and termination of 2 cores with opposite chirality. Time between points is 18 ms.



Supplemental Figure 20
(legend on previous page)



Supplemental Figure 21. Effect of TBX5 knockdown during hiAM differentiation on Ca^{2+} transients. **(a)** Immunofluorographs of differentiated hiAM-2.52 layers transduced with increased doses of the TBX5-specific shRNA-encoding LV. Scale bar, 200 µm. **(b)** TBX5 and eGFP levels in differentiated hiAMs expressing different amounts of TBX5-specific shRNAs and, as negative control, firefly luciferase (PpLuc)-specific shRNAs. LMNA is visualized as loading control. Ectopically expressed TBX5 is included as positive/size control. See **Supplemental File 4** for uncropped blots. **(c)** Ca^{2+} transient characteristics of differentiated hiAM layers ($n = 3$ per group) expressing different amounts of TBX5-specific and PpLuc-specific shRNAs. a.u., arbitrary units. Mean shown, with error bars indicating SD. *$P < 0.05$, **$P < 0.01$, ***$P < 0.001$, one-way analysis of variance with Dunnett *post-hoc* analysis comparing to the control condition. **(d)** Representative optical Ca^{2+} transients of hiAM layers in the different conditions. Scale bar, 250 ms.

Supplemental Table 1. Lentiviral integration sites.		
Clone	**Integration site**	**Region**
hiAM-2.38	chr3_39,185,198	CSRNP1 - Exon
	chr8_67,467,802	Non-coding area
	chr8_67,467,886	Non-coding area
	chrX_15,297,016	Non-coding area
hiAM-2.52	chr3_155,019,560	Non-coding area
	chr3_155,019,563	Non-coding area
	chr5_151,196,079	Non-coding area
	chr8_56,615,904	Non-coding area
	chr8_71,038,196	NCOA2 - Intron
hiAM-2.90	chr1_46,308,658	MAST2 - Intron
	chr7_94,588,214	PPP1R9A - Intron
	chr8_54,909,384	TCEA1 - Intron
	chr17_1,081,463	ABR - Intron
	chr19_4,724,095	Non-coding area
	chr19_44,735,866	ZNF227 - Intron

Supplemental Table 2. Ploidy of differentiated hiAMs.										
Clone	**Near-diploid**			**Aneuploid 1**			**Aneuploid 2**			
	%	DI	%CV	%	DI	%CV	%	DI	%CV	RCS
hiAM-2.38	5.2	0.9	5.3	77.7	1.7	4.4	17.1	3.3	4.0	2.9
hiAM-2.52	3.3	0.9	2.8	93.2	1.7	4.3	3.5	3.7	4.3	3.2
hiAM-2.90	12.0	0.9	5.3	81.4	1.8	5.3	6.6	3.4	4.2	3.2
%, percentage of total population. DI, DNA index. %CV, % coefficient of variation. RCS, reduced Chi-square of ModFit LT analysis.										

Supplemental Table 3. AP parameters of hfAMs, hiAMs and haAMs.

Parameter	hfAM (*n* = 6)	hiAM-2.38 (*n* = 39)	hiAM-2.52 (*n* = 13)	hiAM-2.90 (*n* = 14)	haAM (*n* = 9)
RMP (mV)	-74.5 (1.0)	-81.4 (0.7)***	-76.5 (1.2)	-77.9 (0.9)*	-78.3 (2.2)
APA_{max} (mV)	85.2 (6.0)	109.1 (1.8)***	95.4 (3.7)	101.0 (2.6)**	120.2 (3.3)
APA_{plat} (mV)	47.0 (4.0)	72.8 (4.0)*	70.5 (7.2)*	71.2 (6.5)*	58.4 (3.7)
V_{max} (V/s)	130 (28)	220 (19)	148 (21)	181 (22)	333 (33)
APD_{20} (ms)	6 (2)	13 (2)	24 (6)*	16 (4)	5 (2)
APD_{50} (ms)	37 (15)	46 (6)	58 (13)	44 (10)	27 (11)
APD_{90} (ms)	152 (27)	153 (11)	162 (17)	119 (13)	216 (36)

haAM, human adult AM. RMP, resting membrane potential. APA_{max}, maximal AP amplitude. APA_{plat}, AP plateau amplitude. V_{max}, maximum AP upstroke velocity. $APD_{20/50/90}$, action potential duration at 20%, 50% and 90% of repolarisation. Data presented as mean (SEM). *P < 0.05, **P < 0.01, ***P < 0.001, unpaired t-test comparing hiAMs to hfAMs.

Supplemental Table 4. Average effects of I_{Kur} blockade on hiAM-2.38 action potentials.

Parameter	Baseline (*n* = 6)	50 µM 4-AP (*n* = 6)	*P*-value
RMP (mV)	-80.1 (1.5)	-80.6 (1.5)	0.82
APA_{max} (mV)	111.3 (5.3)	118.0 (2.0)	0.17
APA_{plat} (mV)	83.1 (4.2)	110.1 (1.8)	< 0.001
V_{max} (V/s)	279.8 (32.4)	281.2 (31.9)	0.78
APD_{20} (ms)	18 (8)	86 (13)	< 0.001
APD_{50} (ms)	86 (9)	223 (18)	0.001
APD_{90} (ms)	206 (9)	296 (27)	0.01

RMP, resting membrane potential. APA_{max}, maximal AP amplitude. APA_{plat}, AP plateau amplitude. V_{max}, maximum AP upstroke velocity. $APD_{20/50/90}$, action potential duration at 20%, 50% and 90% of repolarisation. Data presented as mean (SEM). Paired t-test.

Supplemental Table 5. Antibodies.

Antigen	Host	Dilution	Supplier	Catalogue# (number)	
SV40 LT	Mouse	1:400 (ICC) 1:5,000 (WB)	Santa Cruz	sc-147	
MKI67	Rabbit	1:400 (ICC)	Abcam	ab15580	
ACTN2	Mouse	1:400 (ICC) 1:100 (FC)	Sigma-Aldrich	A7811	
TNNT2	Rabbit	1:400 (ICC) 1:100 (FC)	Abcam	ab45932	
MYL7	Rabbit	1:400 (ICC)	Abcam	ab127001	
MYL2	Mouse	1:50 (ICC)	Enzo	ALX-BC-1150-S-L001	
GJA1	Rabbit	1:400 (ICC)	Sigma-Aldrich	C6219	
NKX-2.5	Mouse	1:400 (ICC)	Santa Cruz	sc-376565	
GAPDH	Mouse	1:10,000 (WB)	Merck	MAB374	
TBX5	Goat	1:400 (WB)	Santa Cruz	sc-17866	
GJA5	Goat	1:400 (WB)	Santa Cruz	sc-20466	
eGFP	Rabbit	1:12,500 (WB)	Thermo Fisher	A11122	
LMNA	Rabbit	1:5,000 (WB)	Santa Cruz	sc-20681	
Antigen	**Host**	**Dilution**	**Supplier**	**Catalogue#**	**Conjugate**
Rabbit IgG (H+L)	Goat	1:50,000 (WB)	Abcam	ab97080	HRP
Goat IgG (H+L)	Donkey	1:5,000 (WB)	Santa Cruz	sc-2020	HRP
Mouse IgG (H+L)	Goat	1:10,000 (WB)	Abcam	ab97040	HRP
Mouse IgG (H+L)	Donkey	1:400 (ICC)	Thermo Fisher	A10037	Alexa Fluor 568
Rabbit IgG (H+L)	Donkey	1:400 (ICC) 1:200 (FC)	Thermo Fisher	A21206	Alexa Fluor 488
Mouse IgG (H+L)	Donkey	1:200 (FC)	Thermo Fisher	A21202	Alexa Fluor 488

ICC, immunocytochemistry. FC, flow cytometry. WB, western blot. HRP, horseradish peroxidase.

Supplemental Table 6. Primer pairs used for shRNA cloning.

Construct	Forward primer	Reverse primer
TBX5 shRNA	ccgg**GATACAAATTCGCAGATAATA**ctcgagTATTATCTGCGAATTTGTATCttttttg	aattcaaaaa**GATACAAATTCGCAGATAATA**ctcgagTATTATCTGCGAATTTGTATC
Ppluc shRNA	ccgg**CGCTGAGTACTTCGAAATGTC**ctcgagGACATTTCGAAGTACTCAGCGttttttg	aattcaaaaaC**GCTGAGTACTTCGAAATGTC**ctcgagGACATTTCGAAGTACTCAGCG

Sense (bold) and antisense sequences of the targeted genes are shown in capital letters.

Supplemental Video 1. Contractions of hfAMs and hiAMs. Spontaneous contractions in hfAM and hiAM-2.38 cultures. Scale bar, 1 mm. Video available at: doi.org/10.1038/s41551-021-00827-5

Supplemental Video 2. Optical voltage mapping of hESC-AM and hiAM layers. Optical voltage mapping recordings during 1-Hz electrical stimulation (white dots represent pacing electrode and electrical stimulation). Playback at 1/6 of real time speed. Scale bar, 2 mm. Video available at: doi.org/10.1038/s41551-021-00827-5

Supplemental Video 3. Induction of reentrant activity in hESC-AM and hiAM layers. Induction of reentrant activity through high frequency stimulation in hESC-AM and hiAM-2.38 layers (white dots represent pacing electrode and electrical stimulation). Playback at 1/3 of real time speed. Scale bar, 5 mm. Video available at: doi.org/10.1038/s41551-021-00827-5

Supplemental Video 4. hiAM arrhythmic activity with varying degrees of complexity. Three examples of atrial arrhythmias of different complexities as determined by the number of reentrant circuits present in the hiAM-2.38 layers following induction. Playback at 1/3 of real time speed. Scale bar, 1 cm. Video available at: doi.org/10.1038/s41551-021-00827-5

Supplemental Video 5. Effects of antiarrhythmic drugs on reentrant activity in hiAM layers. Effect of 0.1% DMSO, 30 μM sotalol and 10 μM flecainide on reentrant activity in hiAM layers after infusion. DMSO infusion has no effect on arrhythmic activity, whereas 30 μM sotalol reduces the activation frequency by 34% after 10 minutes. Flecainide (10 μM) infusion results in termination of arrhythmic activity, after which 1-Hz electrical stimulation results in normal conduction. Playback at 1/3 of real time speed. Scale bar, 5 mm. Video available at: doi.org/10.1038/s41551-021-00827-5

Supplemental Data File 1. Differentially expressed genes hiAM D0 vs D12. Data file available at: doi.org/10.1038/s41551-021-00827-5

Supplemental Data File 2. Differentially expressed genes hiAM vs hESC-AM. Data file available at: doi.org/10.1038/s41551-021-00827-5

Supplemental Data File 3. Individual (raw) data points and *P*-values. Data file available at: doi.org/10.1038/s41551-021-00827-5

Supplemental Data File 4: Uncropped western blots. Data file available at: doi.org/10.1038/s41551-021-00827-5

Chapter 6



Summary, discussion and future perspectives

Adapted from Cardiovasc Res. 2022;118:e105-e107.

Summary

Chapter 1 described the background of this thesis. Atrial fibrillation (AF), the most common cardiac arrhythmia, is an important contributor of morbidity, mortality and healthcare costs in the western world. It has been estimated that 1 in 3 Europeans will develop AF in their lifetimes, making it a key area of research. Presence of AF is characterised by rapid and chaotic electrical activation of the atria and is the result of a complex interaction of triggers, perpetuators and an atrial substrate. The pathophysiology behind the manifestation of AF remains a heavily studied topic, as the understanding of the multiform mechanisms leading to its initiation, maintenance and termination remains incomplete. The current treatment strategy for individuals with AF comprises a combination of stroke risk reduction, rate-control, symptom management and comorbidity treatment optimalization. These include several strategies for rhythm-control, such as antiarrhythmic drug therapy or ablation. Unfortunately, these treatment strategies are not effective in all patients and a portion of patients will remain symptomatic and/or progress to the persistent or long-standing persistent form of AF where restoration of sinus rhythm becomes more challenging.

Part one of this thesis focussed on rhythm-control through thoracoscopic ablation in symptomatic long-standing persistent AF. This strategy is particularly challenging given the presence of an extensive arrhythmogenic substrate in these patients. The ablation of this substrate requires the electrical isolation of additional atrial structures to the pulmonary veins, mainly the left atrial posterior wall and the left atrial appendage. Achieving durable isolation of these structures using endocardial ablation techniques only can be challenging. Surgical epicardial ablation through a median sternotomy is more effective but also highly invasive. Thoracoscopic epicardial ablation has gained popularity over the past two decades, by attempting to combine the best of both worlds. Here, limited data on (long-term) efficacy has been available in literature.

In **chapter 2**, we investigated to which degree the thoracoscopic ablation technique influences outcomes, by comparing the efficacy of two common thoracoscopic ablation tools for electrical isolation of the posterior left atrium. These two epicardial devices, a unidirectional nonclamping device and a bidirectional clamping device, are used to create the roof/inferior lesions of the "box" between the pulmonary veins. We found that acute intraoperative electrical isolation of the box compartment was significantly higher in the

clamping group than in the nonclamping group. After 1-year follow-up, 91% of the clamping group and 79% of the nonclamping group were in sinus rhythm (no statistically significant difference), whereas repeat catheter interventions were required in 10% of the clamping group and 21% of the nonclamping group (no statistically significant difference). Overall, we concluded that thoracoscopic ablation is effective in restoring sinus rhythm in long-standing persistent AF, and that clamping and nonclamping devices have no significantly different outcomes at short-term follow-up. More research is needed to assess whether outcomes remain comparable between the techniques at long-term follow-up.

In **chapter 3**, we assessed the long-term outcomes of thoracoscopic ablation using the clamping technique in symptomatic long-standing persistent atrial fibrillation, as this treatment is rapidly gaining popularity, while long-term follow-up data is remaining sparse. We found that freedom from atrial arrhythmias at 5 years was 50% following a single thoracoscopic procedure and 68% allowing endocardial touch-up procedures (performed in 1-in-5 patients). In this study, roughly half of the patients had continuous rhythm monitoring through an implantable loop recorder or pacemaker, allowing detailed assessment of recurrences. In these patients, the mean atrial fibrillation burden was reduced from 100% preoperatively to 0.1% at the end of the blanking period and 8% during the second year. Antiarrhythmic drug use decreased significantly from 49% preoperative to 14% at 5 years post-ablation. We concluded that thoracoscopic pulmonary vein and box isolation is effective in long-term restoration of sinus rhythm in long-standing persistent atrial fibrillation, especially when complemented by endocardial touch-up procedures.

Part two of this thesis focused on improving the access to well-differentiated human atrial cardiomyocytes with the goal of developing a clinically relevant in vitro model of AF. Traditionally, animal-based models have been employed to improve mechanistic insight into AF and to develop novel therapeutics. Current models range from fruit flies and zebrafish, to rodents and large domestic mammals, with the latter species showing the closest (although still limited) resemblance to human (patho)physiology. Even though the general consensus is that these animal models (at least on the short term) will maintain an important place in preclinical research, there is a need for more clinically relevant and standardized human in vitro models of AF. These differences in (patho)physiology between humans and animals, combined with increasing public opposition to animal testing, have resulted in a shift towards disease models based on human cells. Current sources of well-differentiated human

atrial myocytes (AMs) for such models are, however, limited. The poor availability of human atrial tissue, combined with the tendency of human adult cardiomyocytes to dedifferentiate in culture, makes primary human AMs unfavourable to work with. Advances in human pluripotent stem cell (hPSC) differentiation protocols have provided an alternative source of human AMs for in vitro modelling. However, in spite of their attractive features and unique applications, current hPSC-derived AMs (hPSC-AMs) are associated with laborious workflows, high phenotypic variation and overall immaturity.

In **chapter 4**, we characterized the electrophysiological properties of excised human atrial tissue and assessed whether this tissue could be used to create culturable cardiac tissue slices suitable for ex vivo electrophysiological studies. We found that more than 90% of the atrial tissues were excitable in their unsliced form, although the area of excitation varied. In the excitable appendages, the mean conduction velocity was 40 ± 14 cm/s and the average action potential duration measured 320 ± 106 ms at 80% of repolarisation. Generation of atrial tissue slices proceeded without complications from a technical stand-point in the majority of cases, however only 12% of attempts yielded clearly excitable atrial tissue slices upon optical voltage mapping. Culturing of these excitable atrial tissue slices using the liquid-air interface method was unsuccessful. Overall, we found a high rate of variability in the excitability of harvested atrial appendages and atrial tissue slices in this study. Further research is necessary to improve on the reliability of this promising preclinical research tool.

In **chapter 5**, we described a method for conditional cell immortalization, which we applied to create a new robust and scalable source of human AMs for in vitro research. Through conditional immortalization based on doxycycline-controlled expression of the early gene products of simian virus 40, human foetal AMs could be expanded at least one-quadrillion-fold and allowed to re-differentiate into fully functional AMs in a tightly controllable manner. The molecular, cellular and electrophysiological properties of these cells, which were named hiAMs (human immortalized atrial myocytes), closely resembled those of primary AMs. Noteworthy, these hiAMs displayed greater overall transcriptomic maturity and a more mature electrophysiological phenotype compared to hPSC-AMs. Using the hiAMs, we were able to create 10-cm2 confluent cell layers presenting activation frequencies of 7-8 Hz after induction of fibrillatory activity, which is consistent with the clinical manifestation of AF, and has previously not been possible using hPSC-AMs. Moreover, their arrhythmic activity could be terminated by infusion of anti-arrhythmic drugs

commonly used in clinical practice. Overall, the development of the hiAM lines provides proof-of-concept of a versatile method to produce, in a simple and rapid manner, massive numbers of authentic human cells for comprehensive disease modelling.

Discussion and future perspectives

Thoracoscopic ablation in long-standing persistent atrial fibrillation

While we concluded from **chapter 2** and **3** that thoracoscopic ablation is effective in restoration of sinus rhythm in long-standing persistent AF, it can be unclear to determine how the efficacy relates to other treatment modalities and exactly where the threshold for success lies. The 2024 HRS/EHRA/APHRS/LAHRS expert consensus statement on catheter and surgical ablation of atrial fibrillation (1) does provide recommendations on the reporting of efficacy data, including the advised endpoint of "absence of any atrial arrhythmia lasting more than 30 seconds". Despite these guidelines, comparison of the efficacy data to literature is complicated by heterogeneous study populations (comprising also paroxysmal and persistent AF), unclear reporting of antiarrhythmic drug use, and different rhythm monitoring intensity (ranging between incidental ECGs to frequent Holters, or even ILR implantation).

Using this endpoint and data from other observational studies reporting long-term (5+ years) outcomes following AF ablation as reference (**Table 1**), the long-term efficacy in our thoracoscopic ablation cohorts presented in **chapter 3** lies in-between the respective less- and more invasive catheter and surgical ablation. Still, a significant number of patients (up to half) have had a recurrence of AF (or other atrial tachyarrhythmia) ≥30 sec in the 5 years since their thoracoscopic ablation procedure. This probes the question; can such 50/50 outcome be considered successful?

While the freedom from any atrial arrhythmia ≥30 seconds is the recommended endpoint, the previously mentioned expert consensus does acknowledge that this metric likely does not correlate with symptom severity and is not associated with cardiovascular outcomes, thereby underestimating the efficacy of the ablation. Increasing evidence supports the reporting of AF burden to define ablation outcomes. Increased AF burden in general has been directly correlated to mortality, cardiovascular hospitalization and ischemic stroke (2). In the CASTLE-AF trial (3) (studying catheter ablation in patients with

AF and heart failure), AF burden reduction was correlated to decreased mortality and hospitalization, whereas the endpoint "presence of any AF recurrence ≥30 sec" was not predictive of these outcomes. Reduction of AF burden through ablation has also been associated with a quality-of-life improvement (4).

Table 1. Selected observational studies reporting long-term freedom (5+ years) from all atrial tachyarrhythmias ≥30 sec following long-standing persistent AF ablation.

Study	Lesion set of first procedure	Single	Multiple
Catheter ablation			
Tilz (2012) (5)	PVI (± CFAE/LA linear lesions)	20% at 5y‡	45% at 5y‡
Teunissen (2016) (6)	PVI	24% at 4.5y†	41% at 4.5y†
Winkle (2023) (7)	PVI (± CFAE/Box/CS/SCV/CTI)	30% at 5y† 18% at 10y†	43% at 5y† 32% at 10y†
Thoracoscopic ablation			
Kwon (2021) (8)	PVI+Box+GP+Marshall+LAAA	37% at 5y‡	
Harlaar (2022) (9)	PVI+Box+LAAA	50% at 5y‡	68% at 5y‡
Hybrid ablation			
Pannone (2023)* (10)	PVI+Box+PML (± LAAA/AML/CFAE/SVC/IVC/CTI)	46% at 5y†	
Surgical ablation			
Lapenna (2020) (11)	Cox-Maze IV	52% at 7y† 67% at 7y‡	
Ad (2017)* (12)	Cox-Maze III/IV	50% at 5y‡	

Single and multiple refers to the numbers of procedures performed (including touch-up).
PVI: pulmonary vein isolation, CFAE: complex fractionated atrial electrogram, LA: left atrium, Box: left atrial posterior wall, CS: coronary sinus, SCV: superior vena cava, ICV: inferior vena cava, CTI: cavotricuspid isthmus, GP: ganglionated plexi, LAAA: left atrial appendage amputation, PML: posterior mitral line, AML: anterior mitral line, AAD: antiarrhythmic drugs.
† Off-AAD, ‡ On-AAD, *Circa 20% of the population was persistent AF, 80% long-standing persistent AF

The target cut-off value for absolute or relative AF burden reduction, that also allows comparison between studies, still has to be determined. The burden outcome reported in **chapter 3**, showed that 94%, 77% and 65% of patients reached respectively a ≥75%, ≥95% and ≥99% burden reduction during the first 2 years after ablation. Recently, the medium-term data was published of the

CASA-AF trial (13), which compared the efficacy, safety and cost-effectiveness of thoracoscopic surgical ablation and catheter ablation for long-standing persistent AF. Interestingly, between these two treatment modalities, the efficacy was not significantly different. The number of patients with a ≥75% AF burden reduction at 2-year follow-up following thoracoscopic ablation was around 63%, which is markedly lower than the 94% we showed in our study (**chapter 3**). Why thoracoscopic ablation performed so poorly in this study in unclear, although the difference could be partly explained by the fact that in the CASA-AF study only off-AAD outcomes are reported (14), as well as the difference in thoracoscopic ablation technique applied, as discussed in **chapter 2**.

Another treatment strategy, hybrid ablation, has gained interest over the recent years, particularly for treating long-standing persistent AF, by combining thoracoscopic ablation and catheter ablation to attempt to improve the efficacy of either technique alone. The randomized CEASE-AF study (15) recently showed superiority of hybrid ablation over catheter ablation only. In this study, the endocardial ablation was however performed 3-6 months post-thoracoscopic ablation. The question arises whether such a combined strategy results in overtreating patients, as we showed in **chapter 3** that 50% of patients were free from AF recurrences at 5-year follow-up after just thoracoscopic ablation alone. Application of endocardial touch-up procedures only in case of recurrence (in 21% of patients), further improved the outcome from 50% to 68% freedom at 5-year follow-up. Therefore, it might be worth considering to only perform additional catheter ablation after thoracoscopic ablation in case of recurrence, to prevent overtreating. This is further supported by the recent meta-analysis conducted by Aerts et al. (16) compared thoracoscopic ablation and hybrid ablation in patients with various types of atrial fibrillation (AF). The study found that the addition of an endocardial ablation procedure in all patients, increased the 5-year freedom from AF from 47% to 64%, with no significant difference between a one-stage or two-stage strategy. This implies that only 1-in-6 patients will experience an improvement in long-term efficacy after hybrid ablation versus thoracoscopic ablation alone. Given that waiting lists for catheter ablation in paroxysmal AF are currently extensive, it can be argued that such resources might be more effectively allocated elsewhere. Still, more research is needed into selecting the right patient for the right ablation modality, as thoracoscopic ablation alone may already overtreat patients, given that 20–25% pulmonary vein isolation-alone responders have been reported for endocardial ablation in long-standing persistent AF (**Table 1**).

The AF ablation field remains under continuous development with novel ablation devices and energy delivery techniques, such as most recently the introduction of pulsed field ablation (17). This new ablation technology uses electroporation as opposed to thermal energy and is presumed to have increased specificity for targeting cardiomyocytes, resulting in comparable success rates with lower complication rates. The first post-approval studies reporting these data seem to support these conclusions (18, 19). These ongoing innovations in ablation technology, together with better patient selection and better rhythm monitoring strategies have the potential to improve the efficacy of AF ablation and provide better perspectives for symptomatic AF patients.

Human in vitro models of atrial fibrillation

Coinciding with the publication of chapter 5, the European Society of Cardiology Working Group on Myocardial Function and the European Society of Cardiology Working Group on Cellular Biology of the Heart published a consensus document providing an extensive overview of animal-based disease models and animal-free innovations across cardiovascular research (20). The document notes that a cell-based model of paroxysmal AF has not yet been developed. This probes the question, which elements are required for a cellular system to be regarded as an in vitro model of AF?

While a model serves as a simplified representation of a system or phenomenon, it can still exhibit varying degrees of complexity. The most basic in vitro models of AF would constitute the inducibility of a self-perpetuating electrical activation in an atrial cellular medium. These examples do exist in literature and can be based on either animal-derived, immortalized or pluripotent stem cell induced cardiomyocytes, as shown in **Table 2**.

Comparing the average activation frequencies of the induced arrhythmic activity, it shows that existing models either display relative slow (1.5-3.4 Hz) or fast (14.1-18.9 Hz) frequencies compared to the 6-8 Hz observed in human AF. This is usually (respectively) a result of a relatively slow conduction velocity (mainly due to an immature phenotype) or a short action potential duration (normal in rodent cardiomyocytes). The model based on human conditionally immortalized atrial myocytes (hiAMs) we described in **chapter 5** displays clinically relevant characteristics, with an average activation frequency around 7.5 Hz. Additionally, these cultures exhibit responses to antiarrhythmic drugs that closely mirror the effects seen in human atrial arrhythmias, further underscoring their clinical significance.

Table 2. Selected *in vitro* studies reporting re-entrant electrical activity in atrial cultures.

Study	Cells (origin)	Electrophysiological Properties	Activation Frequency#
Native			
Bingen et al. (21)	Native AMs (rat)	APD80 56 ± 13 ms CV 23.8 ± 2.5 cm/s	14.1 ± 7.4 Hz
Permanently Immortalized			
Houston et al. (22)	HL-1 clone 6 (mouse)	APD90 42 ± 9 ms† CV 4.5 ± 0.2 cm/s†	2.7 ± 1.0 Hz
Hong et al. (23)	HL-1 (mouse)	APD not reported CV ± 2.5 cm/s	± 3 Hz
Climent et al. (24)	HL-1 (mouse)	APD not reported CV ± 2-3 cm/s	3.1 ± 0.2 Hz
Conditionally Immortalized			
Liu et al. (25)	iAM-1 (rat)	APD80 54 ± 5 ms CV 20.8 ± 1.8 cm/s	18.9 ± 1.3 Hz
Harlaar et al. (26)	hiAM-2.38 (human)	APD80 136 ± 12 ms CV 24.4 ± 2.3 cm/s	7.5 ± 1.0 Hz
Pluripotent Stem Cells			
Laksman et al. (27)	ESC-derived (human) ± 80% atrial-like CMs*	APD90 206 ± 73 ms CV 5.4 ± 1.3 cm/s	3.2 ± 0.3 Hz
Harlaar et al. (26)	ESC-derived (human) ± 100% atrial-like CMs*	APD80 121 ± 41 ms CV 2.1 ± 0.4 cm/s	3.0 ± 0.8 Hz
Goldfracht et al. (28)	ESC-derived (human) ± 80% atrial-like CMs*	APD90 230 ± 5 ms CV 4.1 ± 0.2 cm/s	2.3-2.6 Hz‡
Shiti et al. (29)	iPSC-derived (human) ± 70% atrial-like CMs*	APD80 190 ± 37 ms CV 5.2 ± 3.2 cm/s	3.4 ± 0.5 Hz
Casini et al. (30)	iPSC-derived (human) Unknown % atrial-like CMs	APD90 183 ± 68 ms CV not reported	1.5 ± 0.3 Hz

AM: atrial myocyte, CM: cardiomyocyte, CV: conduction velocity, APD80/90: action potential duration at 80/90% repolarization, ESC: embryonic stem cell, iPSC: induced pluripotent stem cell.
Reference activation frequency in AF patients is 6 to 8 Hz, depending on AF type (31-33).
† The paper references to Dias et al. (34) for corresponding electrophysiological properties.
‡ Based on the examples given in Figure 4, as no average data is reported.
* Number of atrial like cells is estimated by taking into account the efficiency of differentiation and atrial/ventricular phenotype.

While the model introduced in **chapter 5** does represent a significant advancement in the in vitro modelling of AF, it remains a considerable simplification of the complex, multifactorial nature of AF in humans. A more sophisticated in vitro model would integrate the various factors that contribute to the occurrence of AF in certain patients but not in others. These models would encompass both a trigger and a substrate that enable the initiation and maintenance of an arrhythmia, which would not exist in their absence. Working towards such more advanced 2D in vitro models of AF, the human immortalized atrial myocytes using the immortalization technology described in **chapter 5** do provide a solid basis. Triggers could be introduced through the promotion of enhanced automaticity or delayed afterdepolarizations, possibly by tweaking ion channels influencing resting membrane potentials, upregulating pacemaker channel genes and/or altering calcium handling (in a part) of the atrial population. Mimicking the diseased atrial substrate could be achieved by including human fibroblasts and stimulating matrix production. The overall culture size could be scaled to sizes comparable to the human atria. Together, such changes could be the first steps on improving on the complexity of the 2D in vitro AF model.

Hypothesizing about even more intricate human atrial disease models, the immortalization technology described in **chapter 5** could also be applied to the other human cardiac cell types that are present in- and around the heart, by for instance combining it with the culturable cardiac tissue slices described in **chapter 4**. The generation of a large number of human cardiac cell lines using this immortalization technique, together with (future) advances in 3D tissue engineering technology, could help pave the way towards the creation of complex human heterocellular cardiac models with high translational value, a concept shown in **Figure 1**.

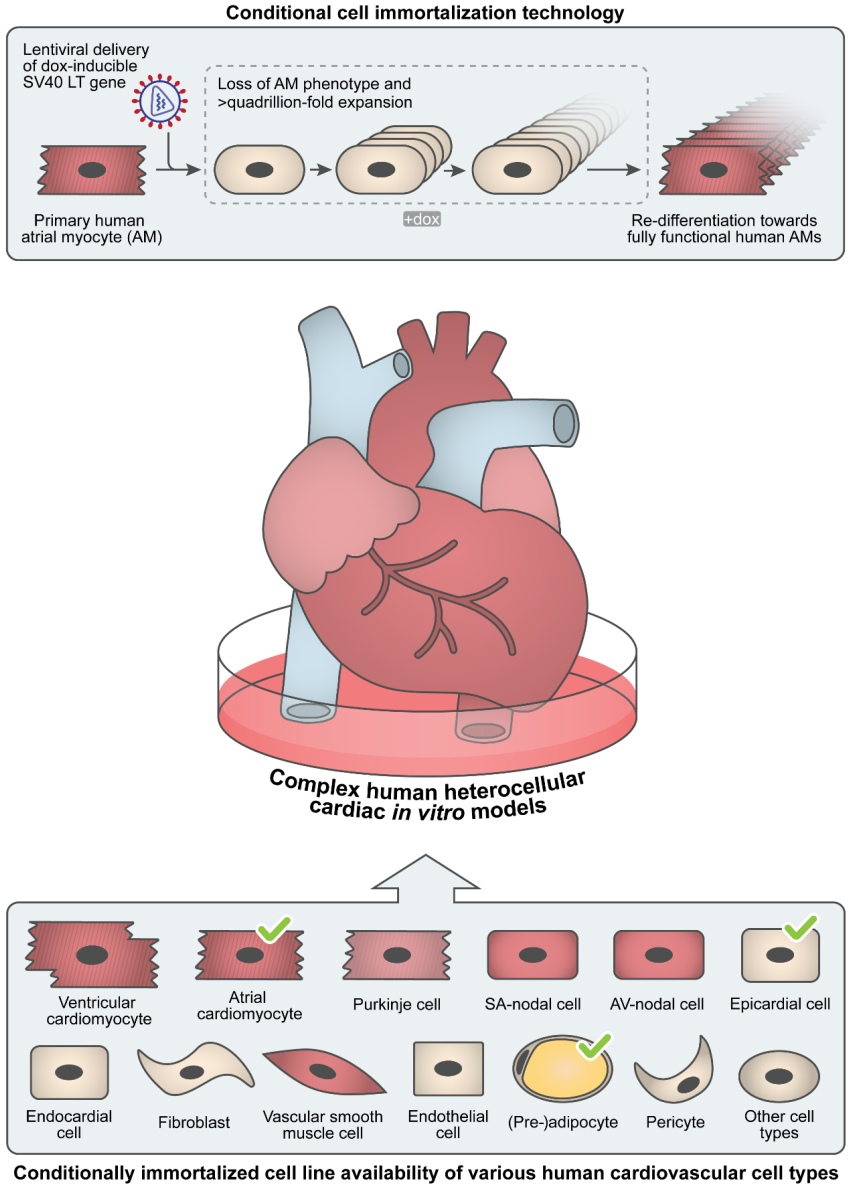


Figure 1. Upper panel, schematic overview of the generation of conditionally immortalized human atrial myocytes (AMs) by transduction of primary human AMs with a lentiviral vector conferring doxycycline (dox)-inducible expression of the simian virus 40 (SV40) large T (LT) gene. Lower panel, generation of human cardiovascular cell types using conditional immortalization technology for the creation of complex human heterocellular cardiac models. Currently, conditionally immortalized lines of human atrial cardiomyocytes (35), human epicardial cells (36) and human preadipocytes (37) have been generated.

References

1. Tzeis S, Gerstenfeld EP, Kalman J, Saad EB, Sepehri Shamloo A, Andrade JG, et al. 2024 European Heart Rhythm Association/Heart Rhythm Society/Asia Pacific Heart Rhythm Society/Latin American Heart Rhythm Society expert consensus statement on catheter and surgical ablation of atrial fibrillation. Europace. 2024;26(4).

2. Chew DS, Li Z, Steinberg BA, O'Brien EC, Pritchard J, Bunch TJ, et al. Arrhythmic Burden and the Risk of Cardiovascular Outcomes in Patients With Paroxysmal Atrial Fibrillation and Cardiac Implanted Electronic Devices. Circ Arrhythm Electrophysiol. 2022;15(2):e010304.

3. Marrouche NF, Brachmann J, Andresen D et al. Catheter Ablation for Atrial Fibrillation with Heart Failure. N Engl J Med. 2018;378(5):417-27.

4. Blomstrom-Lundqvist C, Gizurarson S, Schwieler J, Jensen SM, Bergfeldt L, Kenneback G, et al. Effect of Catheter Ablation vs Antiarrhythmic Medication on Quality of Life in Patients With Atrial Fibrillation: The CAPTAF Randomized Clinical Trial. JAMA. 2019;321(11):1059-68.

5. Tilz RR, Rillig A, Thum AM, Arya A, Wohlmuth P, Metzner A, et al. Catheter ablation of long-standing persistent atrial fibrillation: 5-year outcomes of the Hamburg Sequential Ablation Strategy. J Am Coll Cardiol. 2012;60(19):1921-9.

6. Teunissen C, Kassenberg W, van der Heijden JF, Hassink RJ, van Driel VJHM, Zuithoff NPA, et al. Five-year efficacy of pulmonary vein antrum isolation as a primary ablation strategy for atrial fibrillation: a single-centre cohort study. Europace. 2016;18(9):1335-42.

7. Winkle RA, Mead H, Engel G, Salcedo J, Brodt C, Barberini P, et al. Very long term outcomes of atrial fibrillation ablation. Heart Rhythm. 2023;20(5):680-8.

8. Kwon HJ, Jeong DS, Park SJ, Park KM, Kim JS, On YK. Long-term outcome of totally thoracoscopic surgical ablation in atrial fibrillation: A single-center experience. Int J Cardiol Heart Vasc. 2021;36:100861.

9. Harlaar N, Oudeman MA, Trines SA, de Ruiter GS, Mertens BJ, Khan M, et al. Long-term follow-up of thoracoscopic ablation in long-standing persistent atrial fibrillation. Interact Cardiov Th. 2022;34(6):990-8.

10. Pannone L, Mouram S, Della Rocca DG, Sorgente A, Monaco C, Del Monte A, et al. Hybrid atrial fibrillation ablation: long-term outcomes from a single-centre 10-year experience. Europace. 2023;25(5).

11. Lapenna E, De Bonis M, Giambuzzi I, Del Forno B, Ruggeri S, Cireddu M, et al. Long-term Outcomes of Stand-Alone Maze IV for Persistent or Long-standing Persistent Atrial Fibrillation. Ann Thorac Surg. 2020;109(1):124-31.

12. Ad N, Holmes SD, Friehling T. Minimally Invasive Stand-Alone Cox Maze Procedure for Persistent and Long-Standing Persistent Atrial Fibrillation: Perioperative Safety and 5-Year Outcomes. Circ Arrhythm Electrophysiol. 2017;10(11).

13. Boyalla V, Haldar S, Khan H, Kralj-Hans I, Banya W, Lord J, et al. Long-term clinical outcomes and cost-effectiveness of catheter vs thoracoscopic surgical ablation in long-standing persistent atrial fibrillation using continuous cardiac monitoring: CASA-AF randomized controlled trial. Heart Rhythm. 2024.

14. Khan HR, Kralj-Hans I, Haldar S, Bahrami T, Clague J, De Souza A, et al. Catheter Ablation versus Thoracoscopic Surgical Ablation in Long Standing Persistent Atrial Fibrillation (CASA-AF): study protocol for a randomised controlled trial. Trials. 2018;19(1):117.

15. Doll N, Weimar T, Kosior DA, Bulava A, Mokracek A, Monnig G, et al. Efficacy and safety of hybrid epicardial and endocardial ablation versus endocardial ablation in patients with persistent and longstanding persistent atrial fibrillation: a randomised, controlled trial. EClinicalMedicine. 2023;61:102052.

16. Aerts L, Kawczynski MJ, Bidar E, Luermans JGL, Chaldoupi SM, La Meir M, et al. Short- and long-term outcomes in isolated vs. hybrid thoracoscopic ablation in patients with atrial fibrillation: a systematic review and reconstructed individual patient data meta-analysis. Europace. 2024;26(10).

17. Maizels L, Kalman JM. Pulsed-field ablation: a revolution in atrial fibrillation therapy. Nat Rev Cardiol. 2024;21(8):519-20.

18. Reddy VY, Gerstenfeld EP, Natale A, Whang W, Cuoco FA, Patel C, et al. Pulsed Field or Conventional Thermal Ablation for Paroxysmal Atrial Fibrillation. N Engl J Med. 2023;389(18):1660-71.

19. Ekanem E, Neuzil P, Reichlin T, Kautzner J, van der Voort P, Jais P, et al. Safety of pulsed field ablation in more than 17,000 patients with atrial fibrillation in the MANIFEST-17K study. Nat Med. 2024;30(7):2020-+.

20. van der Velden J, Asselbergs FW, Bakkers J, Batkai S, Bertrand L, Bezzina CR, et al. Animal models and animal-free innovations for cardiovascular research: current status and routes to be explored. Consensus document of the ESC Working Group on Myocardial Function and the ESC Working Group Cellular Biology of the Heart. Cardiovasc Res. 2022;118(15):3016-51.

21. Bingen BO, Neshati Z, Askar SF, Kazbanov IV, Ypey DL, Panfilov AV, et al. Atrium-specific Kir3.x determines inducibility, dynamics, and termination of fibrillation by regulating restitution-driven alternans. Circulation. 2013;128(25):2732-44.

22. Houston C, Tzortzis KN, Roney C, Saglietto A, Pitcher DS, Cantwell CD, et al. Characterisation of re-entrant circuit (or rotational activity) in vitro using the HL1-6 myocyte cell line. J Mol Cell Cardiol. 2018;119:155-64.

23. Hong JH, Choi JH, Kim TY, Lee KJ. Spiral reentry waves in confluent layer of HL-1 cardiomyocyte cell lines. Biochem Biophys Res Commun. 2008;377(4):1269-73.

24. Climent AM, Guillem MS, Fuentes L et al. Role of atrial tissue remodeling on rotor dynamics: an in vitro study. Am J Physiol Heart Circ Physiol. 2015;309(11):H1964-73.

25. Liu J, Volkers L, Jangsangthong W, Bart CI, Engels MC, Zhou G, et al. Generation and primary characterization of iAM-1, a versatile new line of conditionally immortalized atrial

myocytes with preserved cardiomyogenic differentiation capacity. Cardiovasc Res. 2018;114(14):1848-59.

26. Harlaar N, Dekker SO, Zhang J, Snabel RR, Veldkamp MW, Verkerk AO, et al. Conditional immortalization of human atrial myocytes for the generation of in vitro models of atrial fibrillation. Nat Biomed Eng. 2022;6(4):389-402.

27. Laksman Z, Wauchop M, Lin E, Protze S, Lee J, Yang W, et al. Modeling Atrial Fibrillation using Human Embryonic Stem Cell-Derived Atrial Tissue. Sci Rep. 2017;7(1):5268.

28. Goldfracht I, Protze S, Shiti A, Setter N, Gruber A, Shaheen N, et al. Generating ring-shaped engineered heart tissues from ventricular and atrial human pluripotent stem cell-derived cardiomyocytes. Nat Commun. 2020;11(1):75.

29. Shiti A, Arbil G, Shaheen N, Huber I, Setter N, Gepstein L. Utilizing human induced pluripotent stem cells to study atrial arrhythmias in the short QT syndrome. J Mol Cell Cardiol. 2023;183:42-53.

30. Casini M, Santos CF, Emig R, Peyronnet R, Ravens U, Oviedo IO, et al. In vitro model of atrial fibrillation: investigating the initiation and maintenance mechanisms of atrial remodeling using hiPSC-derived atrial cardiomyocytes. Eur Heart J. 2023;44.

31. Sanders P, Berenfeld O, Hocini M, Jais P, Vaidyanathan R, Hsu LF, et al. Spectral analysis identifies sites of high-frequency activity maintaining atrial fibrillation in humans. Circulation. 2005;112(6):789-97.

32. Schuessler RB, Kay MW, Melby SJ, Branham BH, Boineau JP, Damiano RJ, Jr. Spatial and temporal stability of the dominant frequency of activation in human atrial fibrillation. J Electrocardiol. 2006;39(4 Suppl):S7-12.

33. Yoshida K, Ulfarsson M, Oral H, Crawford T, Good E, Jongnarangsin K, et al. Left atrial pressure and dominant frequency of atrial fibrillation in humans. Heart Rhythm. 2011;8(2):181-7.

34. Dias P, Desplantez T, El-Harasis MA, Chowdhury RA, Ullrich ND, Cabestrero de Diego A, et al. Characterisation of connexin expression and electrophysiological properties in stable clones of the HL-1 myocyte cell line. PLoS One. 2014;9(2):e90266.

35. Harlaar N, Dekker SO, Zhang J, Snabel RR, Veldkamp MW, Verkerk AO, et al. Conditional immortalization of human atrial myocytes for the generation of in vitro models of atrial fibrillation. Nat Biomed Eng. 2022;6(4):389-402.

36. Ge Y, Smits AM, Liu J, Zhang J, van Brakel TJ, Goumans MJTH, et al. Generation, Characterization, and Application of Inducible Proliferative Adult Human Epicardium-Derived Cells. Cells-Basel. 2021;10(8).

37. Liu J, Kuipers EN, Sips HCM, Dorleijn JC, van Dam AD, Christodoulides C, et al. Conditionally immortalized brown preadipocytes can switch between proliferative and differentiated states. Bba-Mol Cell Biol L. 2019;1864(12).



Appendices

Nederlandse Samenvatting

Hoofdstuk 1 beschreef de achtergrond van dit proefschrift. Atriumfibrilleren (AF), de meest voorkomende hartritmestoornis, is een belangrijke veroorzaker van morbiditeit, mortaliteit en zorgkosten in de westerse wereld. Naar schatting zal 1 op de 3 Europeanen in de loop van hun leven AF ontwikkelen, wat het tot een belangrijk onderzoeksgebied maakt. De aanwezigheid van AF wordt gekenmerkt door snelle en chaotische elektrische activatie van de atria en is het resultaat van een complexe interactie tussen triggers, onderhoudende factoren en een atriaal substraat. De pathofysiologie achter het ontstaan van AF blijft een intensief bestudeerd onderwerp, waarbij het inzicht in de multiforme mechanismen die leiden tot initiatie, instandhouding en beëindiging onvolledig blijft. De huidige behandelstrategie bij patiënten met AF omvat een combinatie van het reduceren van het risico op een beroerte, frequentiecontrole, symptoombehandeling en optimalisatie van comorbiditeiten. Dit omvat tevens strategieën voor ritmecontrole, zoals anti-aritmische medicamenteuze therapie of ablatie. Helaas zijn deze behandelstrategieën niet bij alle patiënten effectief, en een deel van de patiënten blijft symptomatisch en/of ontwikkelt persisterend of langdurig persisterend AF, waarbij het herstel van sinusritme uitdagender wordt.

Deel één van dit proefschrift richtte zich op ritmecontrole door middel van thoracoscopische ablatie bij symptomatisch langdurig persisterend AF. Deze strategie is bijzonder uitdagend gezien de aanwezigheid van een uitgebreid aritmogeen substraat bij deze patiënten. De ablatie van dit substraat vereist de elektrische isolatie van additionele atriale structuren naast de longvenen, met name de posterieure wand van het linker atrium en het linker hartoor. Het bereiken van duurzame isolatie van deze structuren met uitsluitend endocardiale ablatie kan moeilijk zijn. Chirurgische epicardiale ablatie via een mediane sternotomie is effectiever, maar ook zeer invasief. Thoracoscopische epicardiale ablatie heeft in de afgelopen twee decennia aan populariteit gewonnen doordat het de voordelen van beide benaderingen tracht te combineren. Echter, in de literatuur zijn slechts beperkte gegevens beschikbaar over (lange termijn) effectiviteit.

In **hoofdstuk 2** onderzochten wij in welke mate de gebruikte thoracoscopische ablatietechniek de uitkomsten beïnvloedt, door de effectiviteit van twee gangbare thoracoscopische ablatietools voor elektrische isolatie van het posterieure linker atrium te vergelijken. Deze twee epicardiale systemen, een unidirectioneel niet-clampend device en een bidirectioneel clampend device,

worden gebruikt voor het creëren van de dak- en bodemlaesies van de zogenoemde "box" tussen de longvenen. Wij vonden dat acute intraoperatieve elektrische isolatie van het box-compartiment significant vaker werd bereikt in de clamp-groep dan in de niet-clamp-groep. Na één jaar follow-up waren respectievelijk 91% van de patiënten in de clamp-groep en 79% in de niet-clamp-groep in sinusritme (geen statistisch significant verschil), terwijl herhaalde katheterinterventies nodig waren bij respectievelijk 10% en 21% van de patiënten (eveneens geen statistisch significant verschil). Al met al concludeerden wij dat thoracoscopische ablatie effectief is in het herstellen van sinusritme bij langdurig persisterend AF, en dat clampende en niet-clampende devices op korte termijn geen significant verschillende uitkomsten geven. Meer onderzoek is nodig om te beoordelen of deze resultaten op de lange termijn vergelijkbaar zijn.

In **hoofdstuk 3** onderzochten wij de langetermijnuitkomsten van thoracoscopische ablatie met de clamp-techniek bij symptomatisch langdurig persisterend AF, aangezien deze behandeling snel aan populariteit wint, terwijl langetermijngegevens schaars blijven. Wij vonden dat de aritmie-vrije overleving na 5 jaar 50% bedroeg na een enkele thoracoscopische procedure en 68% wanneer aanvullende endocardiale “touch-up”-procedures werden toegestaan (uitgevoerd bij 1 op de 5 patiënten). In deze studie had ongeveer de helft van de patiënten continue ritmemonitoring door middel van een implanteerbare loop-recorder of pacemaker, wat een gedetailleerde beoordeling van recidieven mogelijk maakte. Bij deze patiënten daalde de gemiddelde AF-belasting van 100% preoperatief tot 0,1% aan het einde van de blankingperiode en 8% gedurende het tweede jaar. Het gebruik van anti-aritmische medicatie nam significant af van 49% preoperatief tot 14% vijf jaar na ablatie. Wij concludeerden dat thoracoscopische longvenen- en box-isolatie effectief is in het langdurig herstellen van sinusritme bij langdurig persisterend AF, in het bijzonder wanneer dit wordt aangevuld met endocardiale touch-up-procedures.

Deel twee van dit proefschrift richtte zich op het verbeteren van de beschikbaarheid van goed gedifferentieerde humane atriale cardiomyocyten met als doel het ontwikkelen van een klinisch relevant *in vitro* model van AF. Traditioneel zijn met name diermodellen gebruikt om mechanistisch inzicht in AF te verkrijgen en nieuwe therapieën te ontwikkelen. Deze modellen variëren van fruitvliegen en zebravissen tot knaagdieren en grotere zoogdieren, waarbij de laatste de grootste (zij het nog steeds beperkte) gelijkenis vertonen met de humane (patho)fysiologie. Hoewel de algemene consensus is dat deze

diermodellen (ten minste op de korte termijn) een belangrijke rol in preklinisch onderzoek zullen behouden, bestaat er behoefte aan klinisch relevantere en gestandaardiseerde humane in vitro modellen van AF. De verschillen in (patho)fysiologie tussen mens en dier, gecombineerd met toenemende maatschappelijke weerstand tegen dierproeven, hebben geleid tot een verschuiving richting ziektemodellen gebaseerd op humane cellen. Huidige bronnen van goed gedifferentieerde humane atriale myocyten (AM's) voor dergelijke modellen zijn echter beperkt. De slechte beschikbaarheid van humaan atriumweefsel, in combinatie met de neiging van volwassen humane cardiomyocyten om in kweek te dedifferentiëren, maakt primaire humane AM's ongunstig om mee te werken. Ontwikkelingen in differentiatieprotocollen van humane pluripotente stamcellen (hPSC) hebben een alternatief geboden voor humane AM's voor *in vitro* modellering. Ondanks hun aantrekkelijke eigenschappen en unieke toepassingen gaan huidige hPSC-afgeleide AM's (hPSC-AM's) echter gepaard met arbeidsintensieve werkprocessen, hoge fenotypische variatie en algehele onvolwassenheid.

In **hoofdstuk 4** karakteriseerden wij de elektrofysiologische eigenschappen van geëxcideerd humaan atriumweefsel en onderzochten of dit weefsel gebruikt kon worden om kweekbare hartweefselplakjes te creëren die geschikt zijn voor *ex vivo* elektrofysiologische studies. Wij vonden dat meer dan 90% van het atriumweefsel in ongesneden vorm exciteerbaar was, hoewel het gebied van excitatie varieerde. In de exciteerbare hartoren bedroeg de gemiddelde geleidingssnelheid 40 ± 14 cm/s en de gemiddelde actiepotentiaalduur 320 ± 106 ms bij 80% repolarisatie. Het vervaardigen van atriumweefselplakjes verliep technisch probleemloos in de meerderheid van de gevallen, maar slechts 12% van de pogingen leverde duidelijk exciteerbare atriumweefselplakjes op bij optical voltage mapping. Het kweken van deze exciteerbare weefselplakjes met de liquid-air interface methode was niet succesvol. Al met al vonden wij een hoge mate van variabiliteit in de exciteerbaarheid van de verkregen hartoren en atriumweefselplakjes in deze studie. Verdere onderzoeken zijn noodzakelijk om de betrouwbaarheid van dit veelbelovende preklinische onderzoeksinstrument te verbeteren.

In **hoofdstuk 5** beschreven wij een methode voor conditionele celimmortalisatie, die wij toepasten om een nieuwe robuuste en schaalbare bron van humane AM's voor *in vitro* onderzoek te creëren. Door conditionele immortaliseringsmethoden gebaseerd op doxycycline-gereguleerde expressie van de vroege genproducten van het simian virus 40, konden humane foetale AM's minimaal tot de orde van een quadriljoenvoud worden uitgebreid en

vervolgens in een strak controleerbare manier her-differentiëren tot volledig functionele AM's. De moleculaire, cellulaire en elektrofysiologische eigenschappen van deze cellen, die hiAM's (human immortalized atrial myocytes) werden genoemd, vertoonden een sterke overeenkomst met die van primaire AM's. Opmerkelijk was dat deze hiAM's een grotere transcriptomische maturiteit en een meer volwassen elektrofysiologisch fenotype vertoonden dan hPSC-AM's. Met behulp van hiAM's konden wij confluerende cellagen van 10 cm^2 genereren met activatiefrequenties van 7–8 Hz na inductie van fibrillatoire activiteit, wat overeenkomt met de klinische manifestatie van AF en wat voorheen niet mogelijk was met hPSC-AM's. Bovendien kon hun aritmische activiteit worden beëindigd door toediening van anti-aritmische medicatie die gangbaar is in de klinische praktijk. Al met al biedt de ontwikkeling van de hiAM-lijnen een proof-of-concept van een veelzijdige methode om op eenvoudige en snelle wijze enorme aantallen authentieke humane cellen te produceren voor uitgebreid ziektemodellering.

List of publications

Full Publications

Majumder R, De Coster T, Kudryashova N, Verkerk AO, Kazbanov IV, Ördög B, **Harlaar N**, Wilders R, de Vries AA, Ypey DL, Panfilov AV, Pijnappels DA. Self-restoration of cardiac excitation rhythm by anti-arrhythmic ion channel gating. Elife. 2020;9:e55921.

Harlaar N, Verberkmoes NJ, van der Voort PH, Trines SA, Verstraeten SE, Mertens BJA, Klautz RJM, Braun J, van Brakel TJ. Clamping versus nonclamping thoracoscopic box ablation in long-standing persistent atrial fibrillation. J Thorac Cardiovasc Surg. 2020;160:399-405.

Harlaar N, Dekker SO, Zhang J, Snabel RR, Veldkamp MW, Verkerk AO, Fabres CC, Schwach V, Lerink LJS, Rivaud MR, Mulder AA, Corver WE, Goumans MJTH, Dobrev D, Klautz RJM, Schalij MJ, Veenstra GJC, Passier R, van Brakel TJ, Pijnappels DA, de Vries AAF. Conditional immortalization of human atrial myocytes for the generation of in vitro models of atrial fibrillation. Nat Biomed Eng. 2022;6:389-402.

Harlaar N, Oudeman MA, Trines SA, de Ruiter GS, Mertens BJ, Khan M, Klautz RJM, Zeppenfeld K, Tjon A, Braun J, van Brakel TJ. Long-term follow-up of thoracoscopic ablation in long-standing persistent AF. Interact Cardiovasc Thorac Surg. 2022;34:990-998.

Nyns ECA, Portero V, Deng S, Jin T, **Harlaar N**, Bart CI, van Brakel TJ, Palmen M, Hjortnaes J, Ramkisoensing AA, Zhang GQ, Poelma RH, Ördög B, de Vries AAF, Pijnappels DA. Light transmittance in human atrial tissue and transthoracic illumination in rats support translatability of optogenetic cardioversion of AF. J Intern Med. 2023;294:347-357.

Letters

Harlaar N, Pijnappels DA, de Vries AAF. Conditional immortalization of human cardiomyocytes for translational in vitro modeling of cardiovascular disease. Cardiovasc Res. 2022;118:e105-e107.

Selected peer-reviewed abstracts

Harlaar N, Liu J, Volkers L, Ramkisoensing AA, Schalij MJ, Klautz RJM, van Brakel TJ, Pijnappels DA, de Vries AAF. Massive expansion of native human atrial cardiomyocytes through immortogenetics: generation of the hiAM cell lines. Eur. Heart J. 2019:40;ehz748.0187

Harlaar N, Oudeman MAP, Trines SA, de Ruiter GS, Khan M, Zeppenfeld K, Tjon A, Braun J, van Brakel TJ. Long-term follow-up of thoracoscopic ablation for long-standing persistent atrial fibrillation. Eur. Heart J. 2020:41;ehaa946.0625

Harlaar N, Dekker SO, Zhang J, Schalij MJ, Klautz RJM, van Brakel TJ, Pijnappels DA, de Vries AAF. Modelling of atrial fibrillation at physiologically relevant scales enabled by massive expansion of native human atrial cardiomyocytes. EP Europace. 2021:23; euab116.553.

List of abbreviations

Alphabetical order

4-AP, 4-aminopyridine

AAD, antiarrhythmic drug

AF, atrial fibrillation

AFL, atrial flutter

AM, atrial myocyte

AP, action potential

APA_{max}, maximal AP amplitude

APA_{plat}, AP plateau amplitude

APD, action potential duration

$APD_{20/50/80/90}$, action potential duration at 20, 50, 80 and 90% of repolarization

AT, atrial tachycardia

Box, left atrial posterior wall

bp, base pairs

BP, biological process

BSA, bovine serum albumin

CC, cellular component

CFAE, complex fractionated atrial electrograms

CHA_2DS_2-VASc score, congestive heart failure, hypertension, age, diabetes, stroke, vascular disease and sex score

CHA_2DS_2-VA score, congestive heart failure, hypertension, age, diabetes, stroke and vascular disease score

CI, confidence interval

CL, cycle length

CPM, counts per million

CS, coronary sinus

CTI, cavotricuspid isthmus

CV, conduction velocity

DEG, differentially expressed gene

DI, DNA index

DMEM, Dulbecco's modified Eagle's medium

DMSO, dimethylsulfoxide

dox, doxycycline

FBS, foetal bovine serum

FC, flow cytometry

FDR, false discovery rate

FSC, forward scatter

GO, gene ontology

haAM, human adult atrial myocyte

hESC-AM, human embryonic stem cell derived atrial myocyte

hESC, human embryonic stem cell

hfAM, human foetal atrial myocyte

hiAM, human immortalized atrial myocyte

hiPSC, human induced pluripotent stem cell

hPSC-AM, human pluripotent stem cell derived atrial myocyte

hPSC, human pluripotent stem cell

HR, hazard ratio

HRP, horseradish peroxidase

IAS, interatrial septum

ICC, immunocytochemistry

ICD, implantable cardioverter defibrillator

ICR, interquartile range

ILR, implantable loop recorder

LA, left atrium

LAA, left atrial appendage

LAAI, left atrial appendage isolation

LAVI, left atrial volume index

LPV, left pulmonary veins

LSPAF, long-standing persistent atrial fibrillation

LT, large T

LUMC, Leiden University Medical Center

LV, lentiviral vector

MI, mitral isthmus

MTS, modified Tyrode's solution

NDS, normal donkey serum

OR, odds ratio

PBMC, peripheral blood mononuclear cell

PBS, phosphate-buffered saline

PC, principal component

PD, population doubling

PV, pulmonary vein

RA, right atrium

RAA, right atrial appendage

RCS, reduced Chi-square

RF, radiofrequency

RMP, resting membrane potential

RPV, right pulmonary veins

RT, room temperature

SD, standard deviation

SE, standard error

SEM, standard error of the mean

shRNA, short hairpin RNA

SR, sinus rhythm

SSC, side scatter

SV40, simian virus 40

SVT, supraventricular tachycardia

T3, triiodo-L-thyronine

TIA, transient ischemic attack

TPM, transcripts per million

VCS, vena cava superior

V_{max}, maximum AP upstroke velocity

WB, western blot

List of contributing authors

Alphabetical order

Thomas J. van Brakel, Department of Cardiothoracic Surgery, Leiden University Medical Center, Leiden, The Netherlands.

Jerry Braun, Department of Cardiothoracic Surgery, Leiden University Medical Center, Leiden, The Netherlands.

Carla Cofiño Fabres, Applied Stem Cell Technologies, University of Twente, Enschede, The Netherlands.

Willem E. Corver, Department of Pathology, Leiden University Medical Center, Leiden, The Netherlands.

Sven O. Dekker, Laboratory of Experimental Cardiology, Leiden University Medical Center, Leiden, The Netherlands.

Dobromir Dobrev, Institute of Pharmacology, University Duisburg-Essen, Essen, Germany.

Marie José T. H. Goumans, Department of Cell and Chemical Biology, Leiden University Medical Center, Leiden, The Netherlands.

Muchtair Khan, Department of Cardiology, OLVG, Amsterdam, The Netherlands.

Robert J. M. Klautz, Department of Cardiothoracic Surgery, Leiden University Medical Center, Leiden, The Netherlands.

Lente J. S. Lerink, Laboratory of Experimental Cardiology, Leiden University Medical Center, Leiden, The Netherlands.

Bart J. A. Mertens, Department of Biomedical Data Sciences, Leiden University Medical Center, Leiden, The Netherlands.

Aat A. Mulder, Department of Cell and Chemical Biology, Leiden University Medical Center, Leiden, The Netherlands.

Maurice A. Oudeman, Department of Cardiothoracic Surgery, OLVG, Amsterdam, The Netherlands.

Robert Passier, Applied Stem Cell Technologies, University of Twente, Enschede, The Netherlands.

Daniël A. Pijnappels, Laboratory of Experimental Cardiology, Leiden University Medical Center, Leiden, The Netherlands.

Mathilde R. Rivaud, Department of Clinical and Experimental Cardiology, Amsterdam UMC, Amsterdam, The Netherlands.

Gijsbert S. de Ruiter, Department of Cardiology, OLVG, Amsterdam, The Netherlands.

Martin J. Schalij, Department of Cardiology, Leiden University Medical Center, Leiden, The Netherlands.

Verena Schwach, Applied Stem Cell Technologies, University of Twente, Enschede, The Netherlands.

Rebecca R. Snabel, Department of Molecular Developmental Biology, Radboud University, Nijmegen, The Netherlands.

Andrew Tjon, Department of Cardiothoracic Surgery, OLVG, Amsterdam, The Netherlands.

Serge A. Trines, Department of Cardiology, Leiden University Medical Center, Leiden, The Netherlands.

Gert Jan C. Veenstra, Department of Molecular Developmental Biology, Radboud University, Nijmegen, The Netherlands.

Marieke W. Veldkamp, Department of Clinical and Experimental Cardiology, Amsterdam UMC, Amsterdam, The Netherlands.

Niels J. Verberkmoes, Department of Cardiothoracic Surgery, Catharina Hospital Eindhoven, Eindhoven, The Netherlands.

Arie O. Verkerk, Department of Clinical and Experimental Cardiology, Amsterdam UMC, Amsterdam, The Netherlands.

Stefan E. Verstraeten, Department of Cardiothoracic Surgery, Catharina Hospital Eindhoven, Eindhoven, The Netherlands.

Pepijn H. van der Voort, Department of Cardiology, Catharina Hospital Eindhoven, Eindhoven, The Netherlands.

Antoine A. F. de Vries, Laboratory of Experimental Cardiology, Leiden University Medical Center, Leiden, The Netherlands.

Katja Zeppenfeld, Department of Cardiology, Leiden University Medical Center, Leiden, The Netherlands.

Juan Zhang, Laboratory of Experimental Cardiology, Leiden University Medical Center, Leiden, The Netherlands.

Dankwoord

Het voltooien van dit proefschrift is geen individuele prestatie maar het resultaat van een gezamenlijke inspanning. Mijn dank gaat uit naar allen die met hun steun, expertise en vriendschap dit mogelijk maakten.

Daniël, bedankt voor jouw continue steun en begeleiding sinds ik als 19-jarige geneeskundestudent het lab binnenkwam, een tijd die mij niet alleen gevormd heeft, maar waar ik ook met enorm veel plezier op terug kijk. Twan, de hoeveelheid kennis waar je over beschikt is net zo ongelimiteerd als jouw enthousiasme, dank voor je inzet en motivatie die dit proefschrift tot een succes hebben gemaakt. Thomas, dank voor de fijne begeleiding en je betrokkenheid. Je bent voor mij als jonge dokter een voorbeeld van de goede combinatie van clinicus en onderzoeker.

Aan alle collega's van het Laboratorium Experimentele Cardiologie, de afdelingen Hartziekten en Thoraxchirurgie van het LUMC en de afdeling Cardiologie van het Alrijne, die ik de afgelopen jaren heb leren kennen: hartelijk dank voor de fijne samenwerking en de vele waardevolle momenten, zowel binnen als buiten het ziekenhuis. Cindy, Minka en Juan, dank voor jullie ondersteuning en vooral ook jullie gezelligheid. Sven, bedankt voor je eindeloze inzet. Het was niet alleen ontzettend plezierig, maar ook cruciaal voor onze overwinning op het (academische) slagveld.

Emile, met zekerheid kan ik zeggen dat mijn tijd in het lab er heel anders had uitgezien zonder jouw aanwezigheid. Dank voor de goede vriendschap, de mooie momenten binnen het lab en daarbuiten, en vooral ook de gezonde rivaliteit die dit proefschrift mede mogelijk heeft gemaakt.

Angelos en Rogier, ik ben enorm blij dat ik samen met jullie ook dit traject heb kunnen doorlopen. Dank voor de waardevolle vriendschap. Ik kijk uit naar een mooie toekomst van ons Verloskundig, Oogheelkundig en Cardiologisch verband.

Tot slot wil ik mijn diepe dank uitspreken aan mijn familie en dierbaren. Papa, Mama, Romy en Isabelle, mijn dank aan jullie is de allergrootste, voor jullie onvoorwaardelijke liefde en steun die mij de vrijheid gaf mijn dromen te volgen. Opa, u bent een voorbeeld voor mij, ik ben enorm blij dat u mijn promotie nog kan meemaken. Lieve Isabel, de afronding van dit proefschrift had ongetwijfeld nog langer op zich laten wachten zonder jou, dankjewel dat je altijd het beste in mij naar boven haalt, ik kijk uit naar een mooie toekomst samen.

Curriculum Vitae

Niels Harlaar was born on August 8, 1995 in Alkmaar. He obtained his atheneum diploma *cum laude* in 2013 at the Jac. P. Thijsse College in Castricum, after which he started medical training that same year at Leiden University. During his second year, he was selected to participate in the MD/PhD-program of the Leiden University Honours College, for which he joined the Laboratory of Experimental Cardiology under the supervision of prof. dr. D.A. Pijnappels and dr. A.A.F. de Vries. After obtaining his Bachelor degree *cum laude* in 2016, he decided to turn this line of research into a full-time PhD program, now also involving the Department of Cardiothoracic Surgery with the additional guidance of dr. T.J. van Brakel. For this research, he obtained a PhD-fellowship from the LUMC Executive Board as a part of the MD/PhD-program. The results obtained during his PhD training are described in this thesis. During his training he won several awards, including the Young Investigator Award at EHRA 2021 and the Hugo van Poelgeest award from Stichting Proefdiervrij. He finished his medical training in 2023 and became a Cardiology resident at the Leiden University Medical Centre in 2025 (supervisor dr. Trines), currently in the pre-Cardiology phase in Internal Medicine at the Alrijne Ziekenhuis (supervisor dr. L. Hardi).

Selected grants and awards

2022 - Winner Hugo van Poelgeest Award (Stichting Proefdiervrij)

2021 - Winner Young Investigator Award (EHRA congress)

2019 - PhD-fellowship (LUMC Executive Board)

2019 - Best oral presentation (Rembrandt Symposium, Noordwijkerhout)

2019 - Travel grant (EHRA congress, Lisbon)

2019 - Highest rated abstract award (NVT spring congress, Utrecht)

2019 - Basic science travel grant (ESC congress, Paris)

2019 - Finalist Young Investigator Award competition (CES/HRS, San Francisco)

2018 - Basic science travel grant (ESC congress, Munich)

2015 - MD/PhD program starting grant (LUMC)